Low-frequency and macro-Raman analysis of respirable dosage forms and their sampling with a low flow rate single-nozzle cascade impactor

by

Hui Wang

A thesis submitted in partial fulfillment of the requirements for the degree of

Master of Science

Department of Mechanical Engineering
University of Alberta

Abstract

Applications of Raman spectroscopy to respirable dosage forms are explored in this thesis. First, a high performance Raman system enabling low-frequency Raman signal detection is described and used for pharmaceutical sample analysis. Applications to species identification and solid state differentiation are presented, including solid phase identification and differentiation of glycopyrronium bromide and formoterol fumarate in pharmaceutical powders, and identification of active pharmaceutical ingredients, *e.g.*, salmeterol xinafoate, fluticasone propionate, mometasone furoate, and salbutamol sulphate, as well as excipients, *e.g.*, amino acids, in different formulations, are presented. For the first time, low-frequency shift Raman spectra of mannitol polymorphs were measured and used for solid phase identification. Unambiguous identification of two similar bronchodilator metered dose inhalers, Ventolin® HFA and Airomir®, was accomplished. The low-frequency shift Raman signals can be used for the analysis of crystallinity of small samples (< 5 mg) of respiratory dosage forms in a multi-component formulation matrix containing less than 3% by weight of the component of interest.

Second, quantitative macro-Raman spectroscopy was applied to the analysis of bulk compositions of pharmaceutical drug powders. A custom designed dispersive macro-Raman instrument with a large sample volume of 0.16 μL was utilized to quantitatively evaluate the composition of multi-component powder samples extracted from commercial products. A Monte-Carlo model was developed to predict the minimum sample volume required for representative sampling from heterogeneous samples with variable particle size distributions and compositions. For typical carrier-free respirable powder samples the required minimum sample volume was on the order of 10^{-4} μL to

achieve representative sampling with less than 3% relative error. However, dosage forms containing non-respirable carriers, *e.g*., lactose, required sample volume on the order of microliter for representative measurements. Error analysis of the experimental results showed good agreement with the error predicted by the simulation.

Finally, a low volume flow rate single-nozzle impactor was designed and manufactured for the collection of aerosols in the respirable range for subsequent macro-Raman characterization. The impactor utilized standard scanning electron microscopy stubs as the impaction plate, allowing easy removal and sample analysis. The impactor was designed to operate at a volume flow rate of 0.5 L/min, and included multiple stages to allow aerodynamic diameter measurements in the range from 0.6 μm to 10 μm. Preliminary tests showed satisfactory performance of the new impactor, which was capable of collecting a single dose (300μg) of respirable particulate drugs actuated from a commercial pressurized metered dose inhaler.

Preface

Chapter 2 of this thesis has been published as Wang, H., Boraey, M. A., Williams, L., Lechuga-Ballesteros, D., and Vehring, R. (2014). "Low-frequency shift dispersive Raman spectroscopy for the analysis of respirable dosage forms". *International Journal of Pharmaceutics*, 469(1), 197-205. I was responsible for experimental design, data collection, analysis, and manuscript composition. M. A. Boraey assisted with part of the data collection and contributed to the manuscript edits. L. Williams provided essential samples used in the paper and contributed to manuscript edits. D. Lechuga-Ballesteros provided advice regarding concept development and contributed to manuscript edits. R. Vehring was the supervisory author who built the initial experimental setup, and was involved with concept formation, discussion of results, and manuscript composition.

Chapter 3 of this thesis is a submitted paper manuscript named "Quantitative Macro-Raman Spectroscopy on Microparticle-based Pharmaceutical Dosage Forms" in the name of Wang, H., Williams, L., Hoe, S., Lechuga-Ballesteros, D., and Vehring, R. I was responsible for experimental design, modeling, data collection, analysis, and manuscript composition. L. Williams assisted with part of the data collection and contributed to the manuscript edits. S. Hoe assisted with selection of samples used in the paper and contributed to the manuscript edits. D. Lechuga-Ballesteros assisted with part of the data collection and contributed to manuscript edits. R. Vehring was the supervisory author, and was involved with concept formation, discussion of results, and manuscript composition.

Acknowledgment

My deepest gratitude goes first to Dr. Reinhard Vehring, who patiently guided me through my past two years of graduate study. You have always been a source of ideas and solutions whenever I turn to you for advice. For countless times, you led me through the barriers of research with your expertise, generosity, and optimistic attitude towards both work and life. Your high standard for writing was initially shocking but turned out to be such a useful lesson to me. Thank you for putting your trust on me. I would have never thought about finishing my first period of graduate study abroad so smoothly without your guidance and persistent help.

I must also give my thanks to the colleagues in Particle Engineering research group. It is my honor to have been given the chance to work with so many great guys in such a top-level group. Mohammed, you are the one full of wisdom and the one who led me into my current research area step by step, best luck to you and your family in your new page of life. James, you are always the mature and thoughtful one with the most practical solutions to even the most complicated problems, and as an engineer I have always been taking you as a role model. Alberto, you are one of the key elements to make our research life so enjoyable, and I feel so lucky to have you as not only a colleague but also a friend. David, our expert in managing and organizing, thank you for making everything so organized and also taking over the endless measurements from me while I was preparing this thesis.

It is also the assistance from Department of Mechanical Engineering's office support staff, electronics shop, and machine shop that makes the completion of this thesis happen.

Special thanks go to Richard Groulx, Gail Dowler, and Rick Conrad. You are the strongest backup forces to all of us mechanical engineers.

In addition, my family members and friends have been the constant motivations for me to go further with my education. Dad, your encouragement and support are the most important stimulations to me whenever and wherever I am. Mom, you are, and will always be, the concern through all my life, and none of this will happen without your dedication. My elder sister, Seven, you are the only reason that I dared to come such far away to Canada without worrying too much about our aged parents, and I give my sincerest wishes to your coming new phase of life. Jacie, thank you for constantly providing me with ideas from the perspective of a materials and chemical engineer, most importantly, you are the source of happiness for the hours when the office and lab lights are off.

Last but not the least, resources and funding generously provided by Pearl Therapeutics Inc., National Resource Council Canada, National Institute for Technology and University of Alberta are gratefully acknowledged. Your support made this all possible.

Table of Contents

List of Tables

List of Figures

Chapter 1: Introduction

Raman spectroscopy is a technique that detects inelastically scattered monochromatic excitation light photons by materials of interest and correlates the acquired spectra with corresponding molecular structures. As a well-developed technique, Raman spectroscopy has been extensively applied in various research areas including biomedical, pharmaceutical, chemistry, materials, mechanical, physics, etc. (De Wolf, 1996; Malard et al., 2009; Malinovsky and Sokolov, 1986; Morris and Matousek, 2010; Parker, 1983; Pelletier, 1999; Weber and Merlin, 2000) for diverse applications. Raman spectroscopy is actually a family of techniques, and may be further divided into dispersive Raman (Dao, 2006), Fourier transform (FT) Raman (Hendra et al., 1991), Raman microscopy (Andrew, 2006), resonance Raman (Carey, 1982), stimulated Raman (Bloembergen, 1967), surface enhanced Raman (Campion and Kambhampati, 1998), tip enhanced Raman (Stöckle et al., 2000). Among them, the three most widely used branches are dispersive, FT, and micro Raman. A comparison of these three techniques is presented in Table 1.1.

Table 1.1 Comparison between different Raman techniques: dispersive Raman, FT-Raman, and micro-Raman

	Dispersive Raman	FT-Raman	Micro-Raman (dispersive or FT)
Advantages	• Simple instrumentation • Adaptable for wide range of excitation source • Large room for customization	• Fluorescence minimization • Applicable to colored samples • Larger radiation throughput than that of monochromators imposed by narrow slits	• Micro-scale analysis with high spatial resolution (~0.5μm) • Two-dimensional mapping of surface component distribution • Confocal 3-dimensional imaging

Disadvantages	• Associated fluorescence with visible excitation source	• Potential broad band absorption by aqueous samples • Low Raman scattering cross section • Interference by thermal emission of heated samples • Low detector response	• Long acquisition time • Relatively poor spectral quality • Low instrument collection efficiency
Key Component	• Spectrograph	• Michelson interferometer	• Microscope

Despite the wide applications of Raman spectroscopy to pharmaceutical research, there haven't been many reports on the applications of its low-frequency spectra. Low-frequency Raman spectra contain abundant structural information related to the solid states of pharmaceutical molecules. Also because solid states stability of drugs is crucial during the shelf-life of products, low-frequency Raman has the potential to become a routinely utilized tool in pharmaceutical product development and stability assessment. Due to instrumental limitations, the low-frequency Raman spectra (10-200cm^{-1}) used to be very difficult to record. Double and even triple monochromators were traditionally used to extend the lower limit of Raman spectrum closer to the laser line, with a resultant sacrifice of spectral quality. With the introduction of ultra-narrow notch filters, low-frequency Raman spectra can now be easily detected. This has enabled extensive utilization of low-frequency Raman for analysis of pharmaceutical samples.

A custom designed and assembled dispersive Raman system enabling the detection of low-frequency Raman spectra close to 10cm^{-1} in wavenumber shift is introduced in Chapter 2. The capabilities of recorded low-frequency signals for differentiating solid

states are presented. The results of this chapter include successful identification of various active pharmaceutical ingredients, component identification in multi-component mixtures, amorphous-crystalline component identification and differentiation in pharmaceutical powders, unambiguous polymorph differentiation, and authentication of finished commercial products. The indication is that low-frequency Raman is very suited to the analysis of solid pharmaceutical dosage forms.

The above discussion is mainly on qualitative analysis using low-frequency Raman. In the area of quantitative Raman analysis of pharmaceutical samples, recent research has emphasized micrometer-scale imaging of component distributions in powders, tablets, etc., with industrial applications still mostly limited to the quantification of bulk materials. However, there are still problems to be solved in the area of quantitative Raman analysis of macroscopic bulk samples. Measured compositions may deviate from corresponding nominal values due to non-representative sampling, and such deviations in many cases may be the primary source of measurement error in quantitative application cases (Campbell Roberts et al., 2002; Rantanen et al., 2005; Strachan et al., 2007). Different sampling techniques have been proposed to diminish the quantification errors caused by sample heterogeneity (Bell et al., 2004; Johansson et al., 2005). A rigorous investigation of the sample volume needed for representative analysis will be very helpful in determining the reliability of quantification results.

Such a discussion on the required minimum sample volume for representative Raman quantification of micro-particle based powder samples is presented in Chapter 3. A Monte-Carlo simulation model is used to predict the required minimum sample volume. The model will be helpful for developing new sampling techniques or even building new

Raman instruments. The results of this chapter will also be instructive in interpretation of Raman quantification errors.

One of the simulation results in Chapter 3 indicates that thousands and even millions of particles are typically required for representative quantification of typical solid respirable dosage forms for bulk composition. Thus, instead of measuring individual particles, respirable pharmaceutical particles in the form of aerosols need to be accumulated as powder samples for quantitative Raman characterization. To this end, a new inertial impactor for aerosol collection is introduced in Chapter 4. The low flow rate single-nozzle impactor is uniquely suited to direct sampling of aerosols for Raman characterization.

This thesis aims to provide a broad exploration of the characterization capabilities of low frequency Raman and macro-Raman spectroscopy in the context of pharmaceutical samples, with an emphasis on respirable particulate dosage forms. The thesis is presented in a mixed format and includes work that has been published as research articles and additional work that has yet to be published.

Chapter 2: Low-frequency Shift Dispersive Raman Spectroscopy for the Analysis of Respirable Dosage Forms

A similar version of this chapter has been published as: Hui Wang, Mohammed A. Boraey, Lisa Williams, David Lechuga-Ballesteros, and Reinhard Vehring. "Low-frequency Shift Dispersive Raman Spectroscopy for the Analysis of Respirable Dosage Forms." *International Journal of Pharmaceutics* 469 (1). **2014**: 197-205.

2.1. Introduction

Chemical and solid phase identification of particulate solid dosage forms is frequently required during the pharmaceutical development process and for the testing of finished products, including those already on the market. Particulate dosage forms are widely used in oral and parenteral drug delivery. Powders in the respirable size range are a necessity for drug delivery to the lung. To guarantee the quality of such pharmaceutical products, identity testing of raw materials, and monitoring of chemical and solid phase changes during manufacture, storage, and usage is required (Costantino et al., 1998; Hubert et al., 2011; Zhang et al., 2004).

Identification and verification of finished products is also sometimes needed because of concerns regarding counterfeit and substandard pharmaceutical products in circulation (Deisingh, 2005; Martino et al., 2010; Newton et al., 2006). Pharmaceutical products without active ingredient or having incorrect composition have caused and will continue to cause a severe public health threat (Aldhous, 2005; Kelesidis et al., 2007; Reidenberg and Conner, 2001).

Identification of solid phases is particularly important for inhalable dosage forms. Typical inhalable powders are blends of micronized or spray dried active pharmaceutical ingredients and are often sensitive to environmental conditions, especially moisture (Ahlneck and Zografi, 1990; Hancock and Zografi, 1994). The interactions between drugs and excipients can also affect the potency of the medicine (Jackson et al., 2000; Masuda et al., 2012). Due to the high specific surface area of respirable aerosol particles and the frequently partially or fully amorphous nature of the components, respirable powders may undergo solid phase transformations.

Various phase transitions between different solid forms can occur (Willart and Descamps, 2008; Wunderlich, 1999). Of primary concern for respirable dosage forms are amorphous to crystalline and polymorphic inter-conversions. It has been demonstrated that different solid phases of excipients and active pharmaceutical ingredients in respirable formulations can have different pharmaceutical and therapeutic performance (Hancock and Zografi, 1997; Huang and Tong, 2004; Vippagunta et al., 2001b). Even a small fraction of crystalline-amorphous inter-conversions can have a significant impact on the drug performance (York, 1983). Therefore, quality testing should include detection of the solid phase of critical formulation components.

Many analytical techniques sensitive to solid phase transitions of pharmaceutical products have been described (Newman and Byrn, 2003), including calorimetry (Clas et al., 1999; O'Neill and Gaisford, 2011), spectroscopy (Brittain et al., 1993; Bugay, 2001; Heinz et al., 2009), x-ray diffraction (Brittain, 2001), and vapor sorption (Mackin et al., 2002), etc. Usually, these testing techniques are used together with other methods to comprehensively characterize pharmaceutical products both statically and dynamically

(Hickey et al., 2007a, b; Newman and Byrn, 2003). Among these techniques, terahertz spectroscopy has been gaining popularity for pharmaceutical applications (Zeitler et al., 2007). Terahertz spectroscopy uses far-infrared radiation to induce intermolecular low energy vibrations in the solid of interests. It is a fast, non-destructive technique that has been successfully applied to the analysis of solid phases, especially crystallinity and polymorphism (Strachan et al., 2004). In comparison to traditional Raman technology, terahertz spectroscopy uses lower power and shorter recording time, minimizing sample loading effects (Beard et al., 2002; Heinz et al., 2009). Also, using radiation in the far-infrared region avoids interference from fluorescence, which can be problematic in Raman spectroscopy with visible excitation. However, the current terahertz spectroscopy instruments can only cover the spectral range of about 2-130 cm^{-1} (Taday and Newnham, 2004), *i.e.*, cannot access information from transitions with larger energy difference, *e.g.*, most intramolecular vibrations.

Raman spectroscopy has been proven to be an appropriate method for counterfeit tablet testing (de Veij et al., 2007; Witkowski, 2005). It has several advantages in this context: (1) simple or no sample preparation is required; (2) non-invasive analysis; (3) applicable to aqueous systems or systems with varying water content (Fini, 2004; Vankeirsbilck et al., 2002a; Wartewig and Neubert, 2005b).

Raman spectroscopy has the potential to identify most pharmaceutical excipients and active pharmaceutical ingredients, because organic molecules are generally Raman active. Also, it is sensitive to the changes in the molecular packing in the solid phase of the measured molecules. Raman spectra of organic compounds mainly reflect two classes of transitions between different energy states: Firstly, internal vibrational modes that are

caused by different types of intramolecular vibrations or rotations, creating a unique fingerprint for each type of molecule in the sample. The energy associated with these intramolecular vibrations is relatively high, giving rise to Raman lines that are significantly shifted from the laser frequency, *i.e.*, the excitation frequency. Expressed in wavenumber shift, the internal modes most commonly used for compound identification appear between about 150 and 1800 cm^{-1}, the so-called fingerprint region. Some information about the solid phase of the sample can be derived from the fingerprint region, because intramolecular vibrations are often affected by the local chemical environment of the molecules, *i.e.*, the relationship to neighboring molecules. Secondly, external vibrational modes, which are also known as lattice vibrational modes or phonon modes, are caused by intermolecular vibrations (Hedoux et al., 2011b). Analysis of intermolecular vibrations provides a direct measure of crystal structure and level of disorder. Hence, it is a powerful technique for analyzing solid phases. As intermolecular forces are weaker than intramolecular forces, Raman lines associated with external vibrational modes typically appear in the low-frequency shift range of less than 150 cm^{-1}. Different solid phases of the same substance are due to differences in the three dimensional arrangements of molecules, which in the Raman spectrum are manifested with higher contrast in intermolecular vibrational bands than intramolecular motions.

Assignments of low-wavenumber Raman signals of active pharmaceutical ingredients have been studied with the assistance of quantum mechanical calculation based on density function theory (Ayala, 2007). A discussion about the feasibility of applying low-frequency Raman spectroscopy to analyze crystalline-amorphous transition has been performed on indomethacin (Hédoux et al., 2009). A precise and low-frequency shift

Raman-based method of determining small fractions of a crystallized component within an amorphous matrix was also introduced. Low-frequency shift (<100cm^{-1}) Raman mapping of polymorph was introduced by Hubert and shown to be capable of precise analysis of local solid phase transitions within a pharmaceutical tablet (Hubert et al., 2011). Low-frequency shift Raman spectroscopy (50cm^{-1}-450cm^{-1}) has also been used to study the mechanism of pressure- and heat-induced denaturation of lysozyme (Hedoux et al., 2011c). To our knowledge, low frequency shift Raman spectroscopy has not been applied to respirable pharmaceutical dosage forms.

Respirable particles or their substructures typically have dimensions on the order of the excitation and scattered wavelengths involved in Raman scattering. This causes inhomogeneous internal radiation fields in the particles and may lead to frequency dependent distortion of the spectra, including morphology-dependent resonance effects (Davis and Schweiger, 2002). This phenomenon has also been discussed extensively in the literature (Aardahl et al., 1996; Schweiger, 1990, 1991). Resonance effects depend on particle size, refractive index, and wavelengths and are difficult to predict for arbitrarily shaped particles, but they tend to average out when measuring a large number of particles with different particle size (Chan et al., 1991; Vehring et al., 1998). Hence, in the work presented here, instead of analyzing individual particles we have chosen to use a small powder sample mass to reduce the effects of particle size and shape. Consequently, the information derived from these measurements is representative of the bulk powder, not of individual particles or particle substructures, *e.g.*, surface or core.

Most Raman instruments used for pharmaceutical applications are either Fourier transform Raman systems or single-stage dispersive Raman systems. Neither of them is

capable of measuring frequency shifts that are very close to the laser line. This limitation is particularly severe for respirable particles which scatter the excitation wavelength very strongly due to their particulate nature. Hence, additional laser line rejection filters are generally necessary in this case. The rejection filters used in traditional dispersive Raman systems have a relatively large band width, which leads to rejection of the Raman signals in the low-frequency shift range together with the laser line (Chen et al., 2012; Vehring, 2005). The difficulties of detecting low-frequency signals have limited its application. Monochromators are commonly used as filters to reject the excitation frequency, but this configuration reduces instrumental efficiency. Usually, low frequency shift Raman spectra are recorded using double (Deschamps et al., 2012; Hedoux et al., 2011a) or triple (Ayala, 2007; Ivanda et al., 2007) monochromators. In such cases, Raman signals as close as $10cm^{-1}$ to the elastically scattered light could be recorded. Recently, however, ultra-narrow band laser rejection filters have become available that allow measurements closer than $10cm^{-1}$ to the laser line (Moser and Havermeyer, 2009). In the work presented here, we have combined ultra-narrow band notch filters with traditional dispersive Raman setup to test the feasibility of this approach for the solid state analysis of respirable powders.

2.2. Materials and methods

2.2.1. Materials

Most of the samples measured in this study are active ingredients of respirable dosage forms indicated for asthma and chronic obstructive pulmonary disease (COPD). Crystalline raw materials included salbutamol sulphate (SS, 944/059, Neuland Laboratories Ltd., Andhra Pradesh, India), micronized fluticasone propionate (FP, 05 ST

75M HQ 00047 02, Hovione, Loures, Portugal), micronized mometasone furoate anhydrous (MF, 05ST51M.HQ00051, Hovione, Loures, Portugal), salmeterol xinafoate (SX, P-1M-2, Inke S.A., Barcelona, Spain), glycopyrronium bromide (GP, 77146U001, PCAS Oy, Turku, Finland), and formoterol fumarate dihydrate (FF, P-8, Inke S.A., Barcelona, Spain. All raw materials were recrystallized by dissolving them in ethanol followed by slow solvent evaporation at room temperature. They were measured when the crystals were completely dried.

Amorphous GP and amorphous FF were also prepared by spray drying. The feed solution for amorphous GP was prepared by dissolving raw glycopyrrolate (glycopyrronium bromide) in purified water (WFI). The solution was stirred with a stir bar during spray drying. Methanol was used for preparation of the spray drying feedstock of amorphous FF. Both spray drying processes used an inlet temperature of 50°C, an outlet temperature of 42.5°C, and a feedstock flow rate of 5 mL/min.

Four D-amino acids, *i.e.*, D-Leucine (D-Leu), D-Methionine (D-Met), D-Tyrosine (D-Tyr), D-Tryptophan (D-Trp) and trehalose dihydrate were used in this paper to prepare multi-component powders via spray drying. Weighted solids were transferred to a glass bottle with water added. A resultant clear solution was achieved after electromagnetic stirring for two hours at 700 rpm and a temperature of 35°C. The inlet and outlet temperature were set to be 90°C and 45°C, respectively, during the spray drying process with a feed flow rate of 3mL/min.

Three polymorphic forms of mannitol were produced and studied. β-mannitol was tested directly using the commercially available D-mannitol (SLBH1429V, Sigma-Aldrich Corp., St. Louis, MO, USA). The other two forms were prepared using the

method of slow solvent evaporation. Acetone, ethanol and water were mixed in a volume ratio of 5:5:2. During electromagnetic stirring at 50°C, mannitol was added to the mixed solvent until saturation. The solution was then cooled to room temperature to crystallize out α-mannitol (Xie et al., 2008). The δ-form was achieved by drying an aqueous D-mannitol solution at room temperature. The resultant crystals were measured after they were completely dried.

The contents of two commercial pressurized metered dose inhalers (MDI), Airomir® (DIN 02232570, Medicis Canada Ltd., Toronto, Ontario, Canada) and Ventolin® (DIN 02241497, GlaxoSmithKline Inc., Mississauga, Ontario, Canada), were analyzed. Both products contain salbutamol sulphate suspended in pressurized norflurane (HFA-134a) propellant. Airomir® also contains 11% (w/w) ethanol and a trace amount of oleic acid. Powders were extracted from frozen MDI aluminum cans and dried in a vacuum chamber. Three repeat measurements were conducted for powders from the same canister and three canisters for each brand were measured.

2.2.2. Raman instrument

The schematic diagram of the dispersive Raman instrument is shown in Figure 2.1. This Raman system can be classified into three parts: the excitation system (1-4), the sample interaction system (5-11) and the signal collection system (12-23).

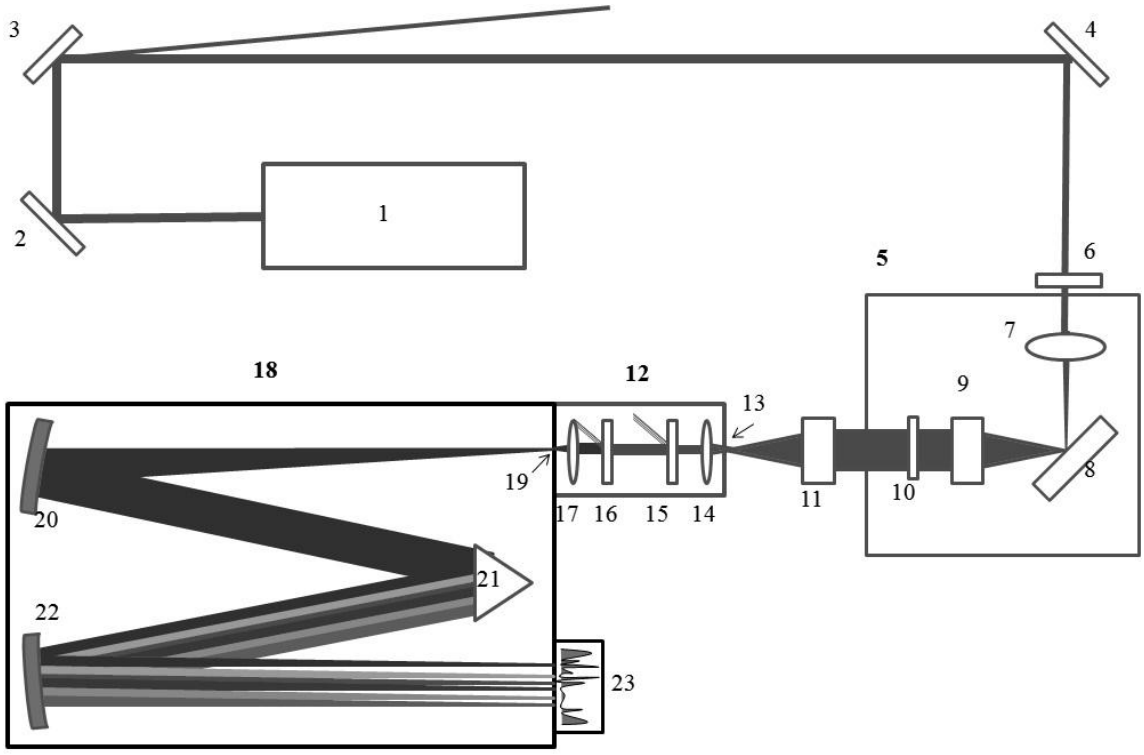

Figure 2.1. Schematic diagram of the Raman setup: (1) laser; (2, 4) highly reflective mirrors; (3) laser emission filter; (5) sample chamber; (6) neutral density filter; (7) focusing lens; (8) sample holder; (9,11,14,17) collection lenses; (10,15,16) ultra-narrow band notch filters; (12) modified filter stage; (13) entrance slit; (18) spectrograph; (19) middle slit; (20,22) collimating mirrors; (21) grating turret; (23) CCD sensor.

An argon ion laser (Innova 70-4, Coherent, Inc., CA, USA) was used in the setup and operated at a wavelength of 514.5 nm in TEM_{00} mode with a nominal maximum output power of 1700mW and a line width of 10 GHz (~0.3 cm^{-1}). An Amplified Spontaneous Emission filter (#114-ER297-002, Ondax Inc., USA) was used to suppress the broad band spontaneous emission from the laser cavity.

Before entering the sample chamber the laser powder was optionally attenuated using a non-reflective neutral density filter (#63-395, Edmund Optics Inc., USA), *e.g.*, to avoid

sample overheating. A convex lens was used to focus the laser into a small cavity of an aluminum sample holder. The conical cavity had a base diameter of 1mm which corresponded to a volume of less than 0.2μL, *i.e.*, a typical sample mass of about 200 μg. The sample holder was mounted on translational stages (M-460P-XYZ, Newport) for alignment. The opening angle of the conical cavity was selected to allow multiple reflections of the laser off sample and cavity wall, which increased the Raman signal from the cavity and made it more homogeneous. Scattered light, both elastic and inelastic, was collected by a collection lens (#RMS10×, Thorlab, Newton, New Jersey, USA) with focal length of 18 mm and numerical aperture of 0.25 at an angle of 90°. A color video camera (#PVM, Sony Corp., Tokyo, Japan) was used to monitor the relative position of sample and laser focus.

The collimated, scattered light was then projected onto a pre-filter (#114-ER297-001, Ondax Inc., USA.) and focused onto the entrance slit (#SP-716, Acton Research Corp., MA, USA) of a filter stage by a microscope objective (#RMS4×, Thorlab, Newton, New Jersey, USA). Two identical ultra-narrow band filters (#114-ER297-001, Ondax Inc., USA.) were mounted inside the filter stage (#NFC-446-040, Acton Research Corp., MA, USA) to further reject elastic scattering. Each of the filters had a nominal optical density >4 centered at 514.5nm and a full width half maximum bandwidth less than 20 cm^{-1}. The typical transmission efficiency in the passband was 0.65.

The entrance slit of the spectrograph (SpectraPro-500i, Acton Research Corp., MA, USA) became a middle slit after mounting of the additional filter stage. The spectrograph was a single stage Czerny-Turner type with focal length of 500 mm, accuracy of ± 0.2 nm and repeatability of ±0.05 nm. A grating turret with three different gratings was

assembled in the spectrograph. A ruled grating with groove density of 1200 g/mm was used in this study and was able to achieve a linear dispersion of about 1.5 nm/mm at 514.5nm.

The sensor was a cryogenically cooled CCD detector (LN/CCD-400EHR-G1, Princeton Instruments, Inc., USA) with front illuminated, deep depleted array architecture. The sensor had a format of 1340×400 pixel with pixel size of 20μm×20μm and was controlled by a CCD camera controller (ST-133, #7355-0017, Princeton Instruments, Inc.). The sensor covered a spectral range of about 1400 cm^{-1} for each measurement.

2.2.2.1. Calibration

The calibration of Raman systems includes two main parameters: intensity and wavelength. Investigators have summarized different procedures for Raman calibration (Hutsebaut et al., 2005; Tedesco and Davis, 1999). Intensity calibration corrects for any spectrum shape distortion caused by variations of the instruments spectral response. The techniques to derive and correct the response function of instrument have been described in detail before (McCreery, 2005; Ray and McCreery, 1997). The techniques rely on comparing the spectrum of a well characterized broadband light source with the measured spectrum to derive an efficiency function.

Spectrograph wavelength calibration determines the extent of matching between sensor pixels and Raman shifts, and it can be classified into absolute and relative calibration. A commonly used absolute wavelength calibration method is introducing instrument independent wavenumber standards (Hutsebaut et al., 2005). In this work, atomic emission lines of a modified He-Ne laser were used as absolute standards to

calibrate the setup. This was done by drilling a hole in the laser housing to gain access to the plasma emissions which are then scattered by the sample. Emission lines scattered by the sample can be recorded by the sensor and appear as signals for calibration (Vehring, 2005).

A relative calibration was accomplished in this paper by using the position of Rayleigh scattering which appears as a sharp peak exactly at 0 cm^{-1} in a well calibrated system. Due to the attenuation of the filters, the laser power was increased until the laser peak was detectable. Then, fine spectrum adjustments were conducted during data processing to match the Rayleigh peak with the origin.

For the calibration of the low frequency shift region, a new method was developed which takes advantage of the symmetry of Stokes and anti-Stokes scattering (Ferraro and Nakamoto, 1994). Because molecules can bi-directionally transit between two energy levels, Raman lines on two sides of the laser line are created that have the same absolute Raman shift. Due to the higher population density of molecules in the lower vibrational energy levels, the intensities of the Stokes peaks are stronger than those of the anti-Stokes peaks. In the nitrogen spectrum shown in Figure 2.2, we selected two pairs of corresponding peaks, indicated by arrows, and shifted the whole spectrum until the peaks were exactly symmetric with respect to the zero position.

2.2.2.2. Instrument validation

Resolution and sensitivity of the new instrument was tested by measuring the rotational spectrum of nitrogen. During this test the sample chamber was filled with nitrogen and the sample holder was removed, the laser was operated at full power without attenuation and the exposure time was 150 s. The measured rotational Raman spectrum of

nitrogen at conditions of 24°C and RH < 3% is shown in Figure 2.2. The measurable rotational lines closest to the center position are -12.0 cm^{-1} and 20.0 cm^{-1} on the anti-Stokes and Stokes side respectively. With sufficient integration time, a high signal-to-noise ratio can be achieved such that even the weak rotational lines above 200 cm^{-1} can be clearly detected.

Based on the underlying theory of diatomic molecular spectroscopy (Hoskins, 1975), the rotational spectrum of nitrogen at 24°C was simulated over the range of -250 cm^{-1} to 250 cm^{-1}. The theoretical calculation agrees well with reported spectrum (Lofthus and Krupenie, 1977) and is plotted together with the measured spectrum in Figure 2.2 with theoretical peak intensities indicated by triangles. The nitrogen spectrum contains sharp peaks equally spaced by 7.95 ± 0.05 cm^{-1} and the intensities vary in an alternating pattern. Peak positions and intensities of the measured spectrum matched well with the results of simulation.

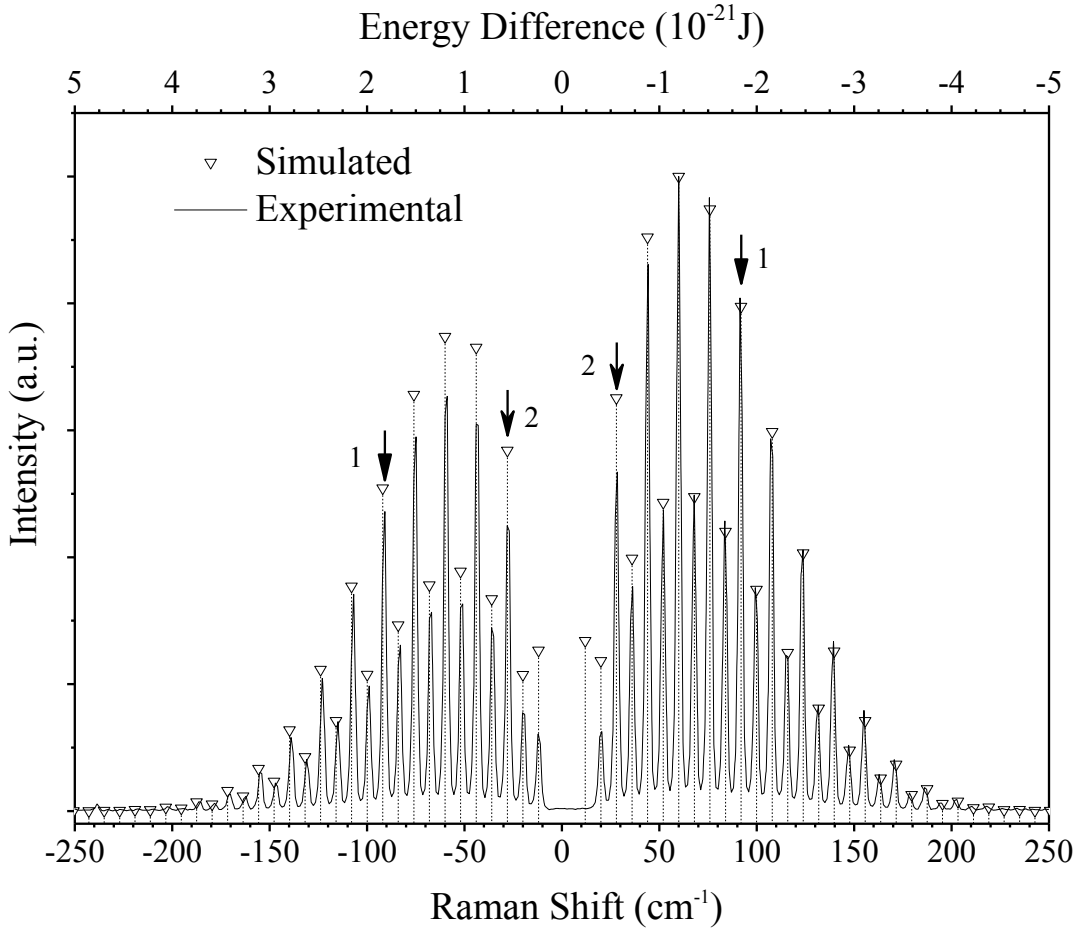

Figure 2.2. Measured and simulated (24°C) N_2 rotational Stokes and Anti-Stokes Raman spectrum (-250cm^{-1} to 250cm^{-1})

The minimum measurable mass for N_2 can be approximated by considering the N_2 mass in the cylindrical scattering volume. The diameter of the scattering volume can be approximated by the focal diameter, which is 40μm (Dickey and Scott, 2002). The height of the cylinder can be calculated by the optical magnification and detector height and is 0.6 mm in this case. The N_2 mass in this scattering volume was approximately 0.88 ng.

Mismatches between the peak intensities of simulated and experimental results are present as shown in Figure 2.2. This was mainly caused by the variation of the

transmission efficiency of the ultra-narrow band rejection filters over wavelength. The transmission function of the Raman instrument near the laser line can be derived by comparing the simulated spectrum of nitrogen with the measured one. As there are no rotational peaks in the range of -12 cm^{-1} to 12 cm^{-1}, the transmission curve for this range was similarly derived by analyzing the measured spectrum of a broad band light source. The resultant transmission curve, which represents the efficiency of the whole Raman instrument including the sensor, is shown in Figure 2.3. The fluctuation of transmission efficiency outside the rejection area and the shape of the rejection band were in agreement with the transmission characteristics of typical reflective volume holographic filters (Moser and Havermeyer, 2009). Figure 2.2 and Figure 2.3 show that the rejection band was shifted towards the Stokes side by adjusting the filter angles relative to the optical axis. This was done to maximize rejection of the laser line in the Stokes low frequency shift region, which was used primarily in the work presented here.

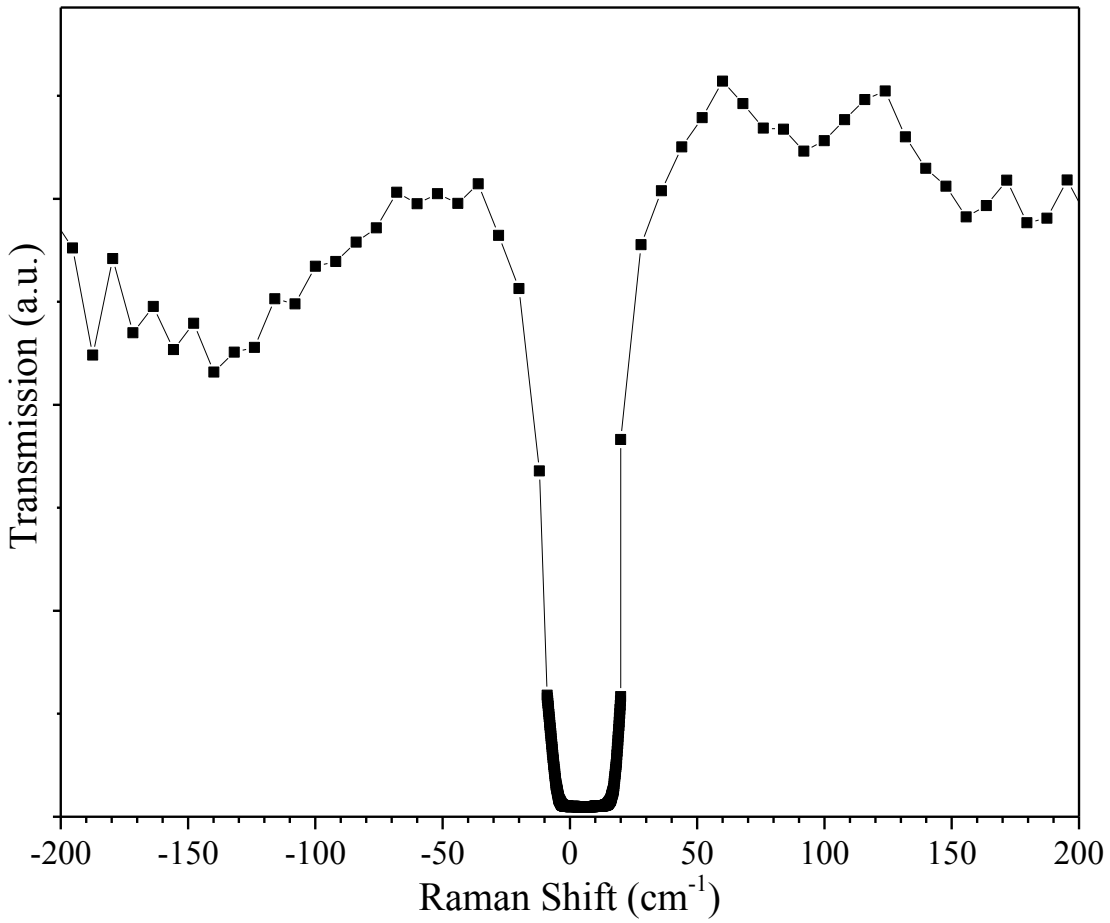

Figure 2.3. Transmission curve of the Raman instrument in the low frequency shift region, derived by comparing the measured N_2 spectrum with a theoretical simulation. Variations of transmittance are in agreement with properties of typical holographic notch filters.

2.2.3. Methods

Samples were first loaded into the sample holder and then kept under a dry air or nitrogen atmosphere during the measurement. All measurements were conducted under similar conditions of 22°C and RH < 3%. Depending on the sample, exposure times ranged from 30 s to 200 s for signal-to-noise ratios larger than 100 on major Raman

peaks. Before further processing, the numerical resolution of the recorded spectra was increased by a linear interpolation process. This interpolation fixed the measured spectra into an equidistant grid with a spacing of 0.1 cm^{-1} between each two neighboring data points, thus allowing for higher precision when shifting spectra, *e.g.*, during calibration or deconvolution of multi-component systems. The original spectral resolution of the Raman system was about 1 cm^{-1}/pixel at 514.5nm laser using a 1200g/mm-groove density grating and middle slit setting of 20 μm.

When analyzing multi-component systems, a deconvolution process was used to determine the contributions of each component. The measured raw and normalized reference spectra of individual components were denoted S and $S_{i,norm}$, respectively. The contributions of each component were subtracted from the raw spectrum by deconvolution according to (Vehring, 2005):

$$S=B+\sum I_i S_{i,norm}(\Delta\nu + b_i) \quad (2.1)$$

B indicates the background of the mixture which is usually approximated as a linear function of Raman shift. I_i is the intensity factor for component i, which is semi-quantitatively related to the mass fraction of component i. Reference spectra were adjusted as needed by a small frequency shift, b_i, to minimize the residual spectrum. The deconvolution was performed by iteratively minimizing the residuals for each component.

2.3. Results and discussion

2.3.1. Identification and differentiation of pharmaceutical actives and excipients

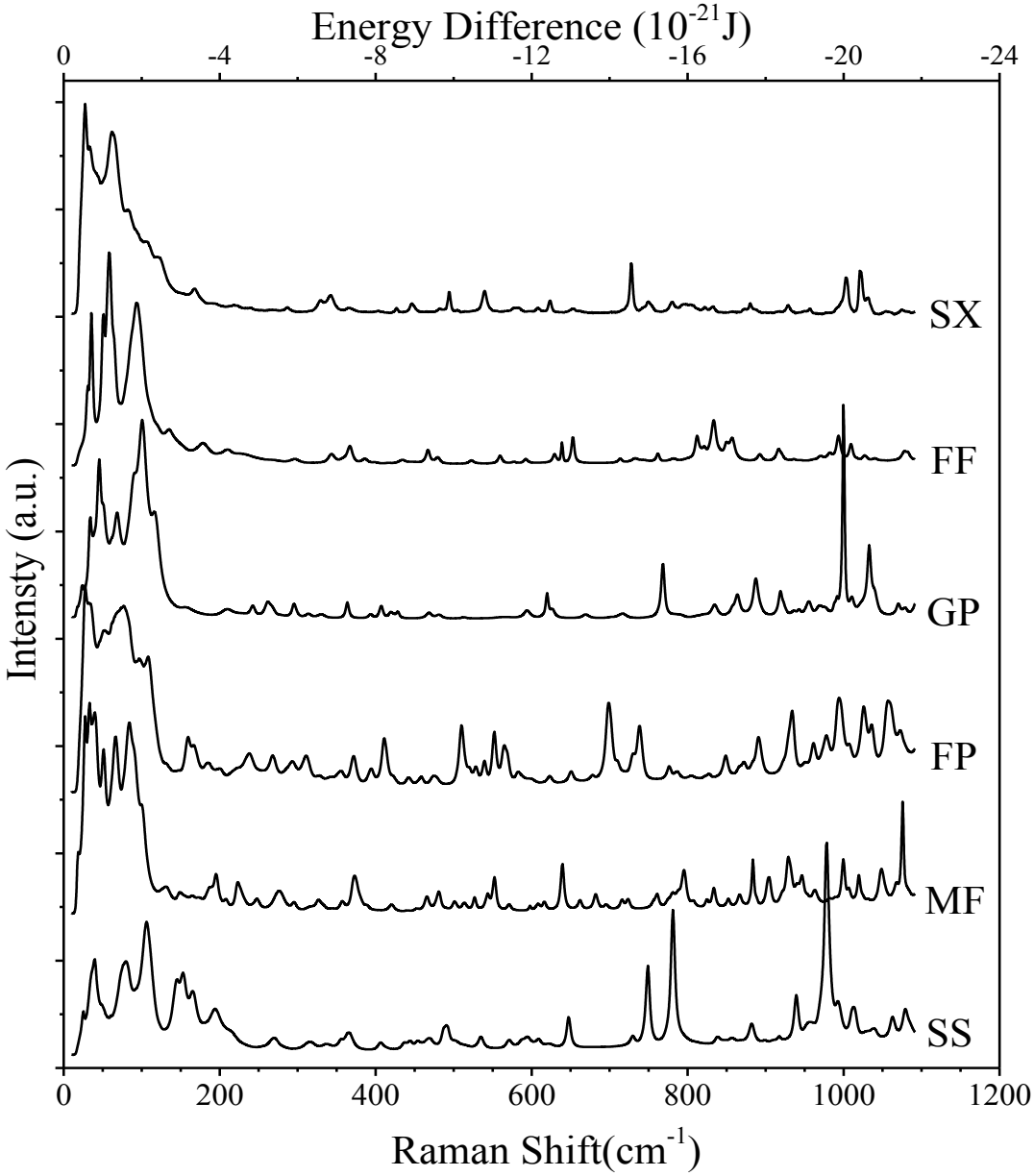

Figure 2.4. Raman spectra of different crystalline respirable dosage forms (salmeterol xinafoate, SX, formoterol fumarate, FF, glycopyrronium bromide, GP, fluticasone propionate, FP, mometasone furoate, MF, and salbutamol sulphate, SS) in the low frequency shift (0 to 200 cm^{-1}) and fingerprint regions.

Raman spectra of several respirable pharmaceutical compounds used for the treatment of asthma or COPD are shown in Figure 2.4. All samples were measured successfully and the lattice modes of the crystalline materials are visible. The fingerprint regions of the spectra are in agreement with those previously reported (Rogueda et al., 2011). These spectra show distinct differences along the whole spectra, in both the low-frequency shift phonon region and the higher frequency shift fingerprint region, with signals in the low-frequency shift region having higher intensities and contrasts. Due to the different characteristic spectra for different ingredients, unambiguous identification of active ingredients is feasible.

2.3.2. Differentiation of solid phases

2.3.2.1. Crystalline and amorphous

Raman spectra of glycopyrronium bromide and formoterol fumarate in crystalline and amorphous phases are presented in Figure 2.5 and Figure 2.6 respectively. In the fingerprint region, several peaks show significant line broadening in the spectra of the amorphous samples relative to the sharp peaks in the spectra of amorphous material. In the low-frequency region, differences between the samples are more distinct. Sharp and strong phonon peaks corresponding to lattice vibrations are dominant for the crystalline samples. However for the amorphous sample, the low-frequency shift spectrum consists of a single broad band peak in the same region as the phonon peaks.

The broadening effect in the fingerprint range is caused by the greater disorder of molecules in the amorphous state (Hedoux et al., 2011b). The spectral differences in the fingerprint region between amorphous and crystalline samples are relatively small in comparison to the spectral differences observed in the low-frequency shift region. Raman active peaks in the low frequency shift region reflect the symmetry properties of the

crystal lattice, and thus provide structural information about the crystal (Ferraro and Nakamoto, 1994). However, for the amorphous sample, the low-frequency shift Raman spectrum consists of a single broad band peak in the same region as the phonon peaks, which corresponds to the envelope of the phonon peaks of the crystalline counterpart. The clear differences between amorphous and crystalline spectra in the low-frequency shift region facilitate unambiguous identification and differentiation of amorphous and crystalline forms of the same material.

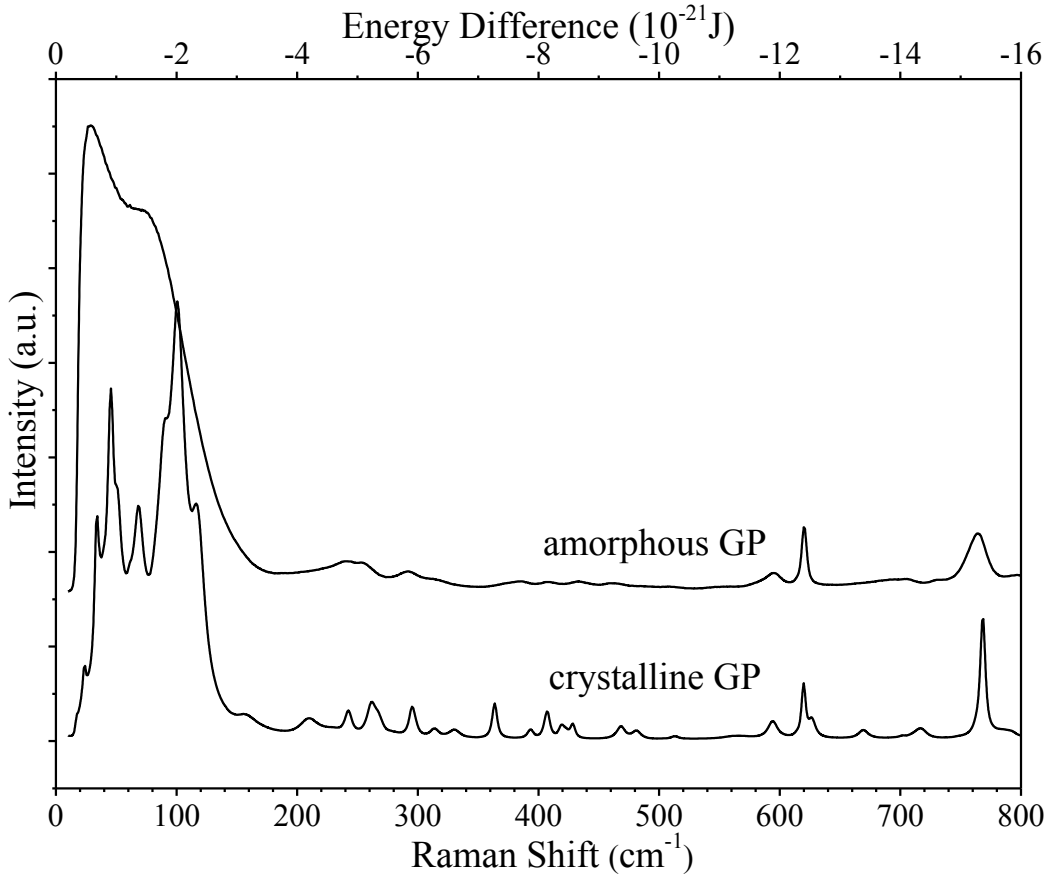

Figure 2.5. Raman spectra for crystalline and amorphous glycopyrronium bromide ($10cm^{-1}$ to $800cm^{-1}$)

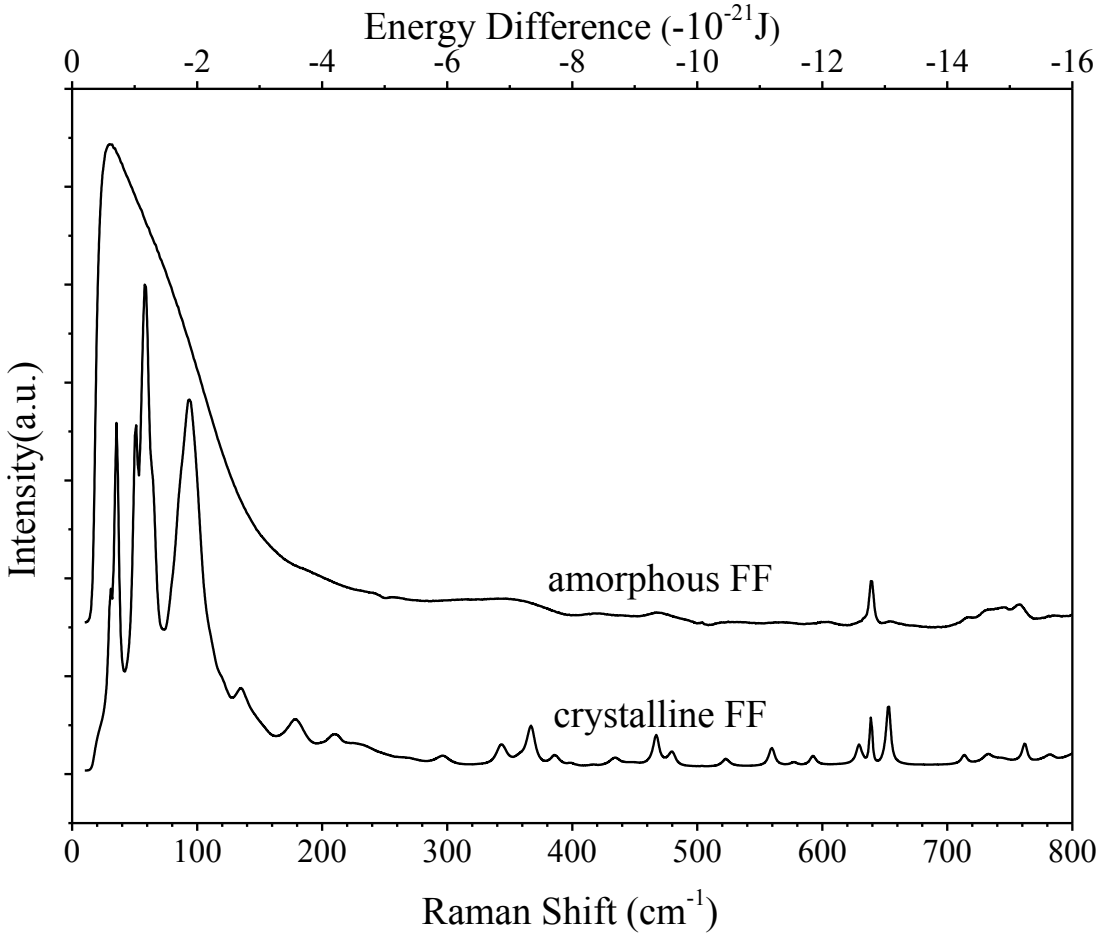

Figure 2.6. Raman spectra for crystalline and amorphous formoterol fumarate ($10cm^{-1}$ to $800cm^{-1}$)

2.3.2.2. Multi-component systems

The test system for this application was a D-amino acid – trehalose multi-excipient formulation currently investigated for respiratory delivery in cystic fibrosis indications (Hoe et al., 2014). Each component in a multi-component system has its characteristic Raman peaks, thus the components can often be identified in multi-component systems by deconvolution. The D-tryptophan sample used in this study was found to exhibit interfering residual fluorescence when excited at a wavelength of 514.5 nm. Hence, a suitable reference spectrum could not be recorded for this component. For this reason the

spectral contribution of D-tryptophan was not identified but rather treated as background. The spectrum of the spray dried mixture of Trehalose, D-Leu, D-Met, D-Tyr, and D-Trp with a mass fraction of 60%, 30%, 3.3%, 3.3% and 3.3%, respectively, and the results of the deconvolution are shown in Figure 2.7. Both low-frequency and fingerprint range spectra were used for accurate deconvolution. Trehalose and D-methionine were identified to be amorphous because the lattice modes associated with their crystalline phases were absent in the low frequency shift region. The sum of the deconvoluted components superimposes well with the measured spectrum. Due to the high sensitivity of the instrument, the air spectrum was also taken into account in the deconvolution. The results show that the components exist in different solid phases in the respirable powder formulation. This example shows that identification of the solid phase of components in pharmaceutical multi-component systems by low-frequency shift Raman spectroscopy is possible, even if these components are present in low concentrations and in different solid phases.

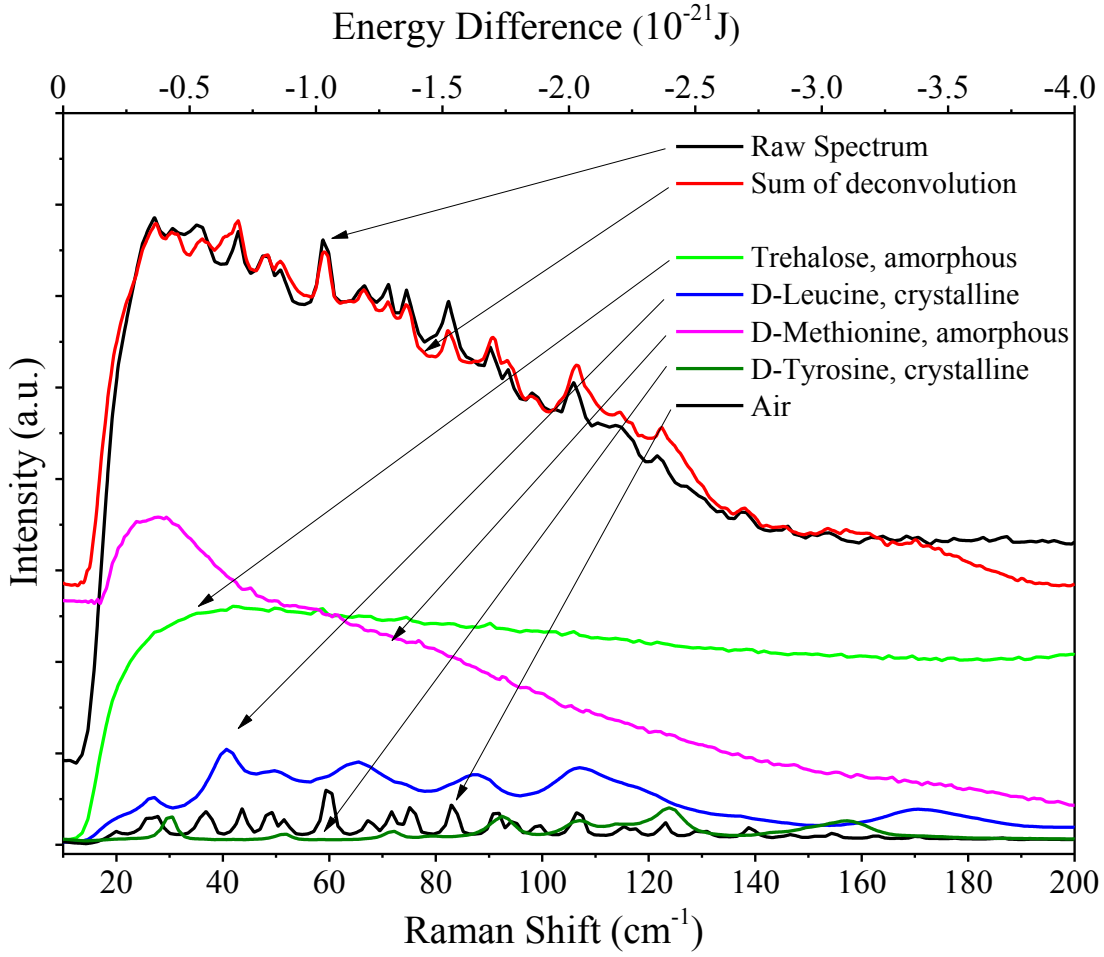

Figure 2.7. Solid phase identification in multi-component mixtures: Trehalose (60%wt), D-Leucine (30%wt), D-Methionine (3.3%wt), D-Tyrosine (3.3%wt), D-Tryptophan

2.3.2.3. Identification of polymorphs

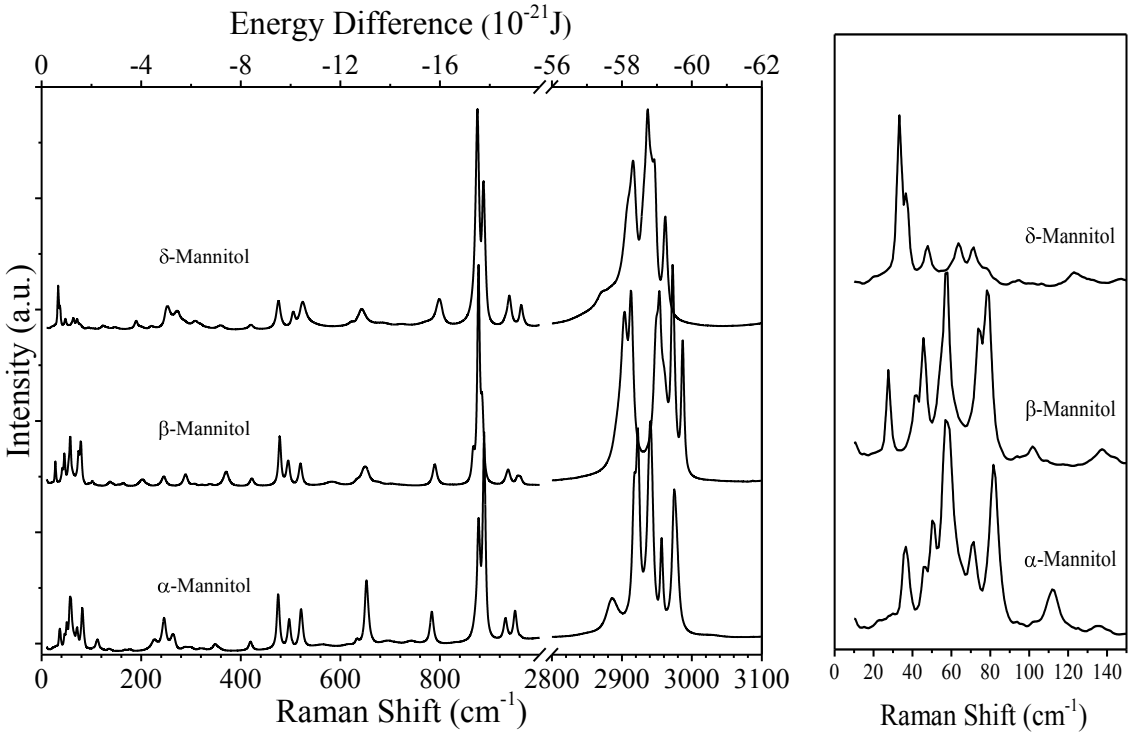

Figure 2.8. Raman spectra of the three polymorphs of mannitol ($10cm^{-1}$ to $1000cm^{-1}$, $2800cm^{-1}$ to $3100cm^{-1}$): α-mannitol, β-mannitol and δ-mannitol. To the right is an enlargement of the low-frequency shift spectral region.

Respiratory mannitol (Li et al., 2014) was proved to be suitable for the treatment of diseases like mucociliary dysfunction (Daviskas et al., 2005), cystic fibrosis (Robinson et al., 1999), etc. Spectra of three mannitol polymorphs are shown in Figure 2.8 with magnified spectra of their low-frequency lattice modes. The spectral region around 2950 cm^{-1} which corresponds to C-H bond stretching vibration has been used before to identify different mannitol polymorphs (Burger et al., 2000; Campbell Roberts et al., 2002; Xie et al., 2008). The fingerprint region also has spectral differences suitable for identification

of the mannitol polymorphs (Chan et al., 2004; Vehring, 2005). The magnified low-frequency shift spectra in Figure 2.8 show clear lattice modes that can verify the crystalline phase of the samples. The distinct spectral differences reflect the different crystal structures for the mannitol polymorphs.

2.3.3. Identification of Finished Dosage Forms

To test the ability of the method to identify finished commercial inhalation products, two salbutamol sulphate MDI, Ventolin® and Airomir®, were measured and analyzed. First, the reproducibility of the method was verified by comparing the results of repeated independent measurements. In Figure 2.9, three spectra of Ventolin® taken from the powder extracted from the same inhaler and their average spectrum are displayed. It is apparent that they superimpose well with each other. The spectral difference, which is expressed as percentage of the highest peak intensity, between measured spectra and the average spectrum are shown below. Signal differences for repeated measurements from the same inhalers are below 3% along the whole spectral range. This test was repeated for three different Ventolin® inhalers with similar level of reproducibility.

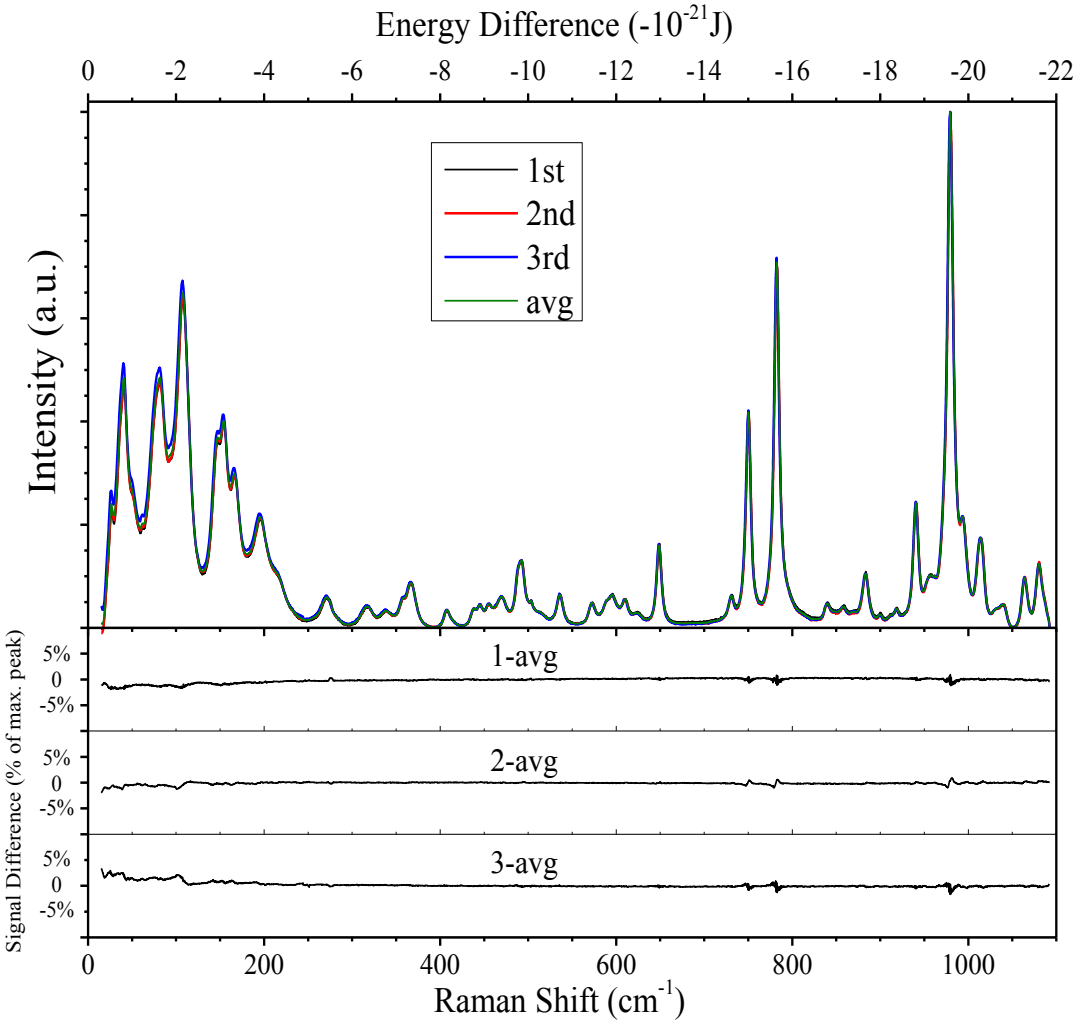

Figure 2.9. Spectral comparison of repeated measurements of Ventolin® and spectral differences in percentage of the highest peak intensity

Dry powders from two different commercial brands of inhalers were measured to test if they could be identified. Spectra of powders extracted from Ventolin® and Airomir® inhalers and their difference spectrum are shown in Figure 2.10. Spectral differences between the two brands were much larger than between repeated measurements of the same inhaler. The low frequency shift region indicated that both inhalers contained crystalline salbutamol sulphate as expected. The largest differences between the products was found in the spectral region displayed in Figure 2.10, indicated by black arrows, and

can be assigned to oleic acid peaks (De Gelder et al., 2007; Mendes et al., 2003; Tandon et al., 2000) at Raman shifts of around 1300 cm^{-1}, 1450 cm^{-1}, 1650 cm^{-1} and 2900 cm^{-1}. The difference is indicative of a trace amount of oleic acid in Airomir®, which agrees with the information in the package insert. Because even very similar legitimate products can be differentiated with this technique, rapid identification of products with incorrect ingredients is feasible.

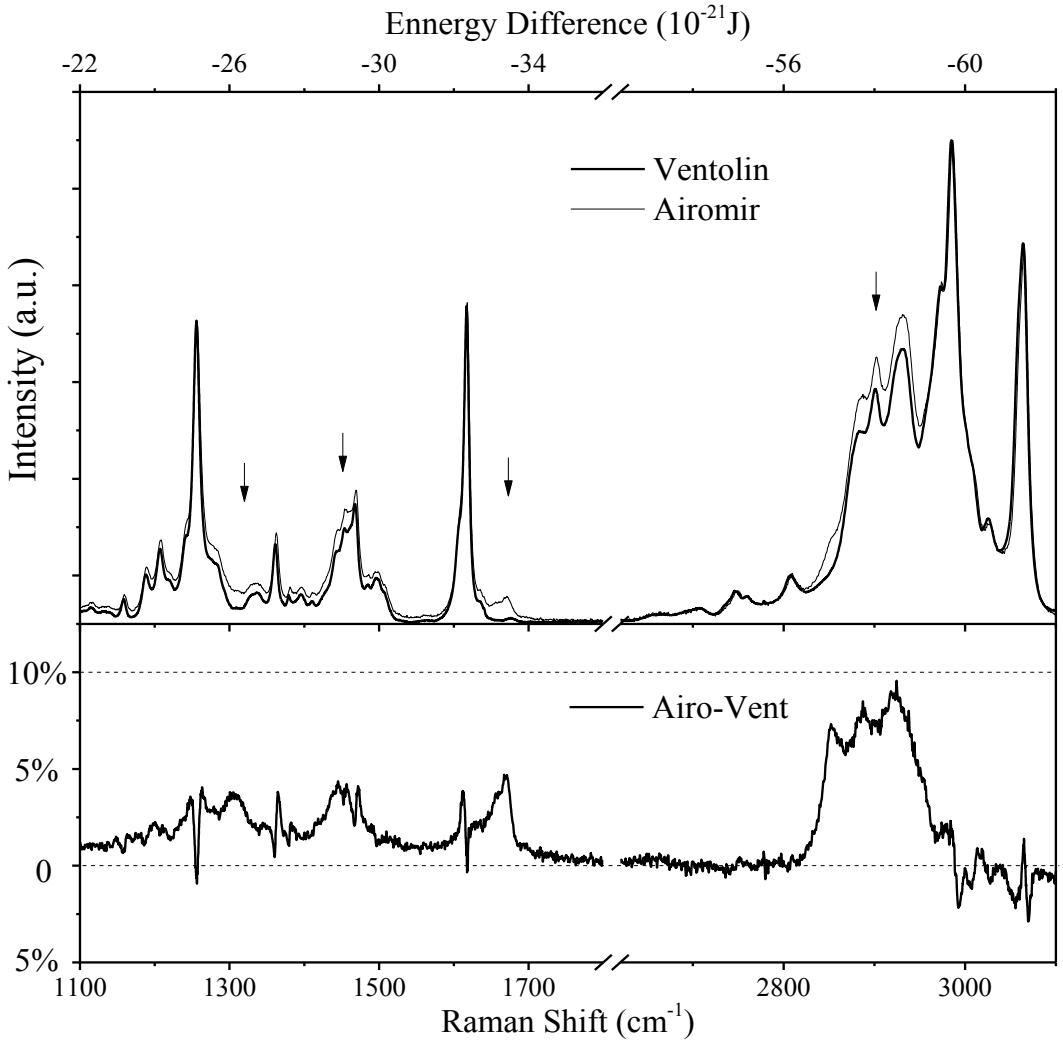

Figure 2.10. Spectral comparison between Ventolin® and Airomir® and spectral differences in percentage of the highest peak intensity

2.4. Conclusions

In this paper, we describe a high-performance Raman spectrometer together with its applications for the analysis of respirable dosage forms. The capabilities of identifying different materials and solid phases in single and multi-component systems make it a suitable and powerful instrument for applications in the pharmaceutical development process and for detecting counterfeit and substandard drugs. Also, using the low-frequency shift Raman signals for the analysis of solid state is shown to be advantageous compared to traditional Raman analysis using spectral regions with Raman shifts larger than 200 cm^{-1} because of the clearer and stronger signals in the low frequency shift region. Further advantages include small sample mass and good reproducibility. However, some samples may require excitation with a different laser, *e.g.*, in the near infrared region, to avoid interference from sample fluorescence or possible sample overheating during fluorescence bleaching.

2.5. References

Aardahl, C.L., Foss, W.R., Davis, E.J., 1996. The Effects of Optical Resonances on Raman Analysis of Liquid Aerosols. *Journal of Aerosol Science* 27, 1015-1033.

Ahlneck, C., Zografi, G., 1990. The Molecular Basis of Moisture Effects on the Physical and Chemical Stability of Drugs in the Solid State. *International Journal of Pharmaceutics* 62, 87-95.

Aldhous, P., 2005. Counterfeit Pharmaceuticals: Murder by Medicine. *Nature* 434, 132-136.

Ayala, A.P., 2007. Polymorphism in Drugs Investigated by Low Wavenumber Raman Scattering. *Vibrational Spectroscopy* 45, 112-116.

Beard, M.C., Turner, G.M., Schmuttenmaer, C.A., 2002. Terahertz Spectroscopy. *Journal of Physical Chemistry B* 106, 7146-7159.

Brittain, H.G., 2001. X-Ray Diffraction Iii: Pharmaceutical Applications of X-Ray Powder Diffraction. *Pharmaceutical Technology* 25(3), 142-150.

Brittain, H.G., Morris, K.R., Bugay, D.E., Thakur, A.B., Serajuddin, A., 1993. Solid-State Nmr and Ir for the Analysis of Pharmaceutical Solids: Polymorphs of Fosinopril Sodium. *Journal of Pharmaceutical and Biomedical Analysis* 11, 1063-1069.

Bugay, D.E., 2001. Characterization of the Solid-State: Spectroscopic Techniques. *Advanced Drug Delivery Reviews* 48, 43-65.

Burger, A., Henck, J.O., Hetz, S., Rollinger, J.M., Weissnicht, A.A., Stoettner, H., 2000. Energy/ Temperature Diagram and Compression Behavior of the Polymorphs of D-Mannitol. *Journal of Pharmaceutical Sciences* 89, 457-468.

Campbell Roberts, S.N., Williams, A.C., Grimsey, I.M., Booth, S.W., 2002. Quantitative Analysis of Mannitol Polymorphs. Ft-Raman Spectroscopy. *Journal of Pharmaceutical and Biomedical Analysis* 28, 1135-1147.

Chan, C.K., Flagan, R.C., Seinfeld, J.H., 1991. Resonance Structures in Elastic and Raman Scattering from Microspheres. *Applied Optics* 30(4), 459-467.

Chan, H.K., Clark, A.R., Feeley, J.C., Kuo, M.-C., Lehrman, S.R., Pikal-Cleland, K., Miller, D.P., Vehring, R., Lechuga-Ballesteros, D., 2004. Physical Stability of Salmon Calcitonin Spray-Dried Powders for Inhalation. *Journal of Pharmaceutical Sciences* 93, 792-804.

Chen, Z.P., Li, L.M., Jin, J.W., Nordon, A., Littlejohn, D., Yang, J., Yu, R.Q., 2012. Quantitative Analysis of Powder Mixtures by Raman Spectrometry: The Influence of Particle Size and Its Correction. *Analytical Chemistry* 84(9), 4088-4094.

Clas, S.D., Dalton, C.R., Hancock, B.C., 1999. Differential Scanning Calorimetry: Applications in Drug Development. *Pharmaceutical Science & Technology Today* 2, 311-320.

Costantino, H.R., Carrasquillo, K.G., Cordero, R.A., Mumenthaler, M., Hsu, C.C., Griebenow, K., 1998. Effect of Excipients on the Stability and Structure of Lyophilized Recombinant Human Growth Hormone. *Journal of Pharmaceutical Sciences* 87, 1412-1420.

Davis, E.J., Schweiger, G., 2002. The Airborne Microparticle: Its Physics, Chemistry, Optics, and Transport Phenomena. Springer.

Daviskas, E., Anderson, S.D., Gomes, K., Briffa, P., Cochrane, B., Chan, H., Young, I.H., Rubin, B.K., 2005. Inhaled Mannitol for the Treatment of Mucociliary Dysfunction in Patients with Bronchiectasis: Effect on Lung Function, Health Status and Sputum. *Respirology* 10, 46-56.

De Gelder, J., De Gussem, K., Vandenabeele, P., Moens, L., 2007. Reference Database of Raman Spectra of Biological Molecules. *Journal of Raman Spectroscopy* 38, 1133-1147.

de Veij, M., Vandenabeele, P., Hall, K.A., Fernandez, F.M., Green, M.D., White, N.J., Dondorp, A.M., Newton, P.N., Moens, L., 2007. Fast Detection and Identification of Counterfeit Antimalarial Tablets by Raman Spectroscopy. *Journal of Raman Spectroscopy* 38, 181-187.

Deisingh, A.K., 2005. Pharmaceutical Counterfeiting. *Analyst* 130, 271-279.

Deschamps, T., Martinet, C., de Ligny, D., Bruneel, J.L., Champagnon, B., 2012. Low-Frequency Raman Scattering under High Pressure in Diamond Anvil Cell: Experimental Protocol and Application to Geo_2 and Sio_2 Boson Peaks. *Journal of Non-Crystalline Solids* 358, 3156-3160.

Dickey, Fred M., Scott C. Holswade, eds. Laser beam shaping: theory and techniques. CRC Press, 2002.

Ferraro, J.R., Nakamoto, K., 1994. Introductory Raman Spectroscopy. Academic Press, pp. 1-90.

Fini, G., 2004. Applications of Raman Spectroscopy to Pharmacy. *Journal of Raman Spectroscopy* 35, 335-337.

Hancock, B.C., Zografi, G., 1994. The Relationship between the Glass Transition Temperature and the Water Content of Amorphous Pharmaceutical Solids. *Pharmaceutical Research* 11, 471-477.

Hancock, B.C., Zografi, G., 1997. Characteristics and Significance of the Amorphous State in Pharmaceutical Systems. *Journal of Pharmaceutical Sciences* 86, 1-12.

Hedoux, A., Decroix, A.A., Guinet, Y., Paccou, L., Derollez, P., Descamps, M., 2011a. Low-and High-Frequency Raman Investigations on Caffeine: Polymorphism, Disorder and Phase Transformation. *The Journal of Physical Chemistry B* 115, 5746-5753.

Hedoux, A., Guinet, Y., Descamps, M., 2011b. The Contribution of Raman Spectroscopy to the Analysis of Phase Transformations in Pharmaceutical Compounds. *International Journal of Pharmaceutics* 417, 17-31.

Hedoux, A., Guinet, Y., Paccou, L., 2011c. Analysis of the Mechanism of Lysozyme Pressure Denaturation from Raman Spectroscopy Investigations, and Comparison with Thermal Denaturation. *The Journal of Physical Chemistry B* 115, 6740-6748.

Hédoux, A., Paccou, L., Guinet, Y., Willart, J.F., Descamps, M., 2009. Using the Low-Frequency Raman Spectroscopy to Analyze the Crystallization of Amorphous Indomethacin. *European Journal of Pharmaceutical Sciences* 38, 156-164.

Heinz, A., Strachan, C.J., Gordon, K.C., Rades, T., 2009. Analysis of Solid-State Transformations of Pharmaceutical Compounds Using Vibrational Spectroscopy. *Journal of Pharmacy and Pharmacology* 61, 971-988.

Hickey, A.J., Mansour, H.M., Telko, M.J., Xu, Z., Smyth, H.D.C., Mulder, T., McLean, R., Langridge, J., Papadopoulos, D., 2007a. Physical Characterization of Component Particles Included in Dry Powder Inhalers. I. Strategy Review and Static Characteristics. *Journal of Pharmaceutical Sciences* 96, 1282-1301.

Hickey, A.J., Mansour, H.M., Telko, M.J., Xu, Z., Smyth, H.D.C., Mulder, T., McLean, R., Langridge, J., Papadopoulos, D., 2007b. Physical Characterization of Component Particles Included in Dry Powder Inhalers. Ii. Dynamic Characteristics. *Journal of Pharmaceutical Sciences* 96, 1302-1319.

Hoe, S., Ivey, J.W., Boraey, M.A., Shamsaddini-Shahrbabak, A., Javaheri, E., Matinkhoo, S., Finlay, W.H., Vehring, R., 2014. Use of a Fundamental Approach to Spray-Drying Formulation Design to Facilitate the Development of Multi-Component Dry Powder Aerosols for Respiratory Drug Delivery. *Pharmaceutical Research* 31, 449-465.

Hoskins, L.C., 1975. Pure Rotational Raman Spectroscopy of Diatomic Molecules. *Journal of Chemical Education* 52, 568-572.

Huang, L.F., Tong, W.Q.T., 2004. Impact of Solid State Properties on Developability Assessment of Drug Candidates. *Advanced Drug Delivery Reviews* 56(3), 321-334.

Hubert, S., Briancon, S., Hedoux, A., Guinet, Y., Paccou, L., Fessi, H., Puel, F., 2011. Process Induced Transformations During Tablet Manufacturing: Phase Transition Analysis of Caffeine Using Dsc and Low Frequency Micro-Raman Spectroscopy. *International Journal of Pharmaceutics* 420, 76-83.

Hutsebaut, D., Vandenabeele, P., Moens, L., 2005. Evaluation of an Accurate Calibration and Spectral Standardization Procedure for Raman Spectroscopy. *Analyst* 130, 1204-1214.

Ivanda, M., Furić, K., Musić, S., Ristić, M., Gotić, M., Ristić, D., Gonçalves, R.R., 2007. Low Wavenumber Raman Scattering of Nanoparticles and Nanocomposite Materials. *Journal of Raman Spectroscopy* 38(6), 647-659.

Jackson, K., Young, D., Pant, S., 2000. Drug-Excipient Interactions and Their Affect on Absorption. *Pharmaceutical Science & Technology Today* 3, 336-345.

Kelesidis, T., Kelesidis, I., Rafailidis, P.I., Falagas, M.E., 2007. Counterfeit or Substandard Antimicrobial Drugs: A Review of the Scientific Evidence. *Journal of Antimicrobial Chemotherapy* 60, 214-236.

Li, X., Vogt, F.G., Hayes Jr, D., Mansour, H.M., 2014. Design, Characterization, and Aerosol Dispersion Performance Modeling of Advanced Spray-Dried Microparticulate /Nanoparticulate Mannitol Powders for Targeted Pulmonary Delivery as Dry Powder Inhalers. *Journal of Aerosol Medicine and Pulmonary Drug Delivery* 27, 81-93.

Lofthus, A., Krupenie, P. H. (1977). The spectrum of molecular nitrogen. *Journal of Physical and Chemical Reference Data*, 6(1), 113-307.

Mackin, L., Zanon, R., Park, J.M., Foster, K., Opalenik, H., Demonte, M., 2002. Quantification of Low Levels (< 10%) of Amorphous Content in Micronised Active Batches Using Dynamic Vapour Sorption and Isothermal Microcalorimetry. *International Journal of Pharmaceutics* 231(2), 227-236.

Martino, R., Malet-Martino, M., Gilard, V., Balayssac, S., 2010. Counterfeit Drugs: Analytical Techniques for Their Identification. *Analytical and Bioanalytical Chemistry* 398, 77-92.

Masuda, T., Yoshihashi, Y., Yonemochi, E., K., F., Uekusa, H., Terada, K., 2012. Cocrystallization and Amorphization Induced by Drug-Excipient Interaction Improves the Physical Properties of Acyclovir. *International Journal of Pharmaceutics* 422, 160-169.

McCreery, R.L., 2005. Raman Spectroscopy for Chemical Analysis. John Wiley & Sons.

Mendes, L.S., Oliveira, F.C., Suarez, P.A., Rubim, J.C., 2003. Determination of Ethanol in Fuel Ethanol and Beverages by Fourier Transform (Ft)-near Infrared and Ft-Raman Spectrometries. *Analytica Chimica Acta* 493, 219-231.

Moser, C., Havermeyer, F., 2009. Ultra-Narrow-Band Tunable Laserline Notch Filter. *Applied Physics B* 95(3), 597-601.

Newman, A.W., Byrn, S.R., 2003. Solid-State Analysis of the Active Pharmaceutical Ingredient in Drug Products. *Drug Discovery Today* 8, 898-905.

Newton, P.N., Green, M.D., Fernández, F.M., Day, N.P., White, N.J., 2006. Counterfeit Anti-Infective Drugs. *The Lancet Infectious Diseases* 6, 602-613.

O'Neill, M.A., Gaisford, S., 2011. Application and Use of Isothermal Calorimetry in Pharmaceutical Development. *International Journal of Pharmaceutics* 417, 83-93.

Ray, K.G., McCreery, R.L., 1997. Simplified Calibration of Instrument Response Function for Raman Spectrometers Based on Luminescent Intensity Standards. *Applied Spectroscopy* 51, 108-116.

Reidenberg, M.M., Conner, B.A., 2001. Counterfeit and Substandard Drugs. *Clinical Pharmacology and Therapeutics* 69, 189-193.

Robinson, M., Daviskas, E., Eberl, S., Baker, J., Chan, H.K., Anderson, S., Bye, P., 1999. The Effect of Inhaled Mannitol on Bronchial Mucus Clearance in Cystic Fibrosis Patients: A Pilot Study. *European Respiratory Journal* 14, 678-685.

Rogueda, P.G., Price, R., Smith, T., Young, P.M., Traini, D., 2011. Particle Synergy and Aerosol Performance in Non-Aqueous Liquid of Two Combinations Metered Dose Inhalation Formulations: An Afm and Raman Investigation. *Journal of Colloid and Interface Science* 361(2), 649-655.

Schweiger, G., 1990. Raman Scattering on Single Aerosol Particles and on Flowing Aerosols: A Review. *Journal of Aerosol Science* 21, 483-509.

Schweiger, G., 1991. Raman Scattering on Microparticles: Size Dependence. *Journal of the Optical Society of America B* 8, 1770-1778.

Strachan, C.J., Rades, T., Newnham, D.A., Gordon, K.C., Pepper, M., Taday, P.F., 2004. Using Terahertz Pulsed Spectroscopy to Study Crystallinity of Pharmaceutical Materials. *Chemical Physics Letters* 390, 20-24.

Taday, P.F., Newnham, D.A., 2004. Technological Advances in Terahertz Pulsed Systems Bring Far Infrared Spectroscopy into the Spotlight. *Spectroscopy Europe* 16, 20-25.

Tandon, P., Förster, G., Neubert, R., Wartewig, S., 2000. Phase Transitions in Oleic Acid as Studied by X-Ray Diffraction and Ft-Raman Spectroscopy. *Journal of Molecular Structure* 524, 201-215.

Tedesco, J.M., Davis, K.L., 1999. Calibration of Dispersive Raman Process Analyzers, Photonics East (ISAM, VVDC, IEMB). International Society for Optics and Photonics, pp. 200-212.

Vankeirsbilck, T., Vercauteren, A., Baeyens, W., Van der Weken, G., Verpoort, F., Vergote, G., Remon, J.P., 2002a. Applications of Raman Spectroscopy in Pharmaceutical Analysis. *Trends in Analytical Chemistry* 21, 869-877.

Vehring, R., 2005. Red-Excitation Dispersive Raman Spectroscopy Is a Suitable Technique for Solid-State Analysis of Respirable Pharmaceutical Powders. *Applied Spectroscopy* 59, 286-292.

Vehring, R., Aardahl, C.L., Schweiger, G., Davis, E.J., 1998. The Characterization of Fine Particles Originating from an Uncharged Aerosol: Size Dependence and Detection Limits for Raman Analysis. *Journal of Aerosol Science* 29, 1045-1061.

Vippagunta, S.R., Brittain, H.G., Grant, D.J., 2001b. Crystalline Solids. *Advanced Drug Delivery Reviews* 48, 3-26.

Wartewig, S., Neubert, R.H.H., 2005b. Pharmaceutical Applications of Mid-Ir and Raman Spectroscopy. *Advanced Drug Delivery Reviews* 57, 1144-1170.

Willart, J., Descamps, M., 2008. Solid State Amorphization of Pharmaceuticals. *Molecular Pharmaceutics* 5, 905-920.

Witkowski, M.R., 2005. The Use of Raman Spectroscopy in the Detection of Counterfeit and Adulterated Pharmaceutical Products. *American Pharmaceutical Review* 8, 56.

Wunderlich, B., 1999. A Classification of Molecules, Phases, and Transitions as Recognized by Thermal Analysis. *Thermochimica Acta* 340, 37-52.

Xie, Y., Cao, W., Krishnan, S., Lin, H., Cauchon, N., 2008. Characterization of Mannitol Polymorphic Forms in Lyophilized Protein Formulations Using a Multivariate Curve Resolution (Mcr)-Based Raman Spectroscopic Method. *Pharmaceutical Research* 25, 2292-2301.

York, P., 1983. Solid-State Properties of Powders in the Formulation and Processing of Solid Dosage Forms. *International Journal of Pharmaceutics* 14, 1-28.

Zeitler, J.A., Taday, P.F., Newnham, D.A., Pepper, M., Gordon, K.C., Rades, T., 2007. Terahertz Pulsed Spectroscopy and Imaging in the Pharmaceutical Setting-a Review. *Journal of Pharmacy and Pharmacology* 59, 209-223.

Zhang, G.G.Z., Law, D., Schmitt, E.A., Qiu, Y., 2004. Phase Transformation Considerations During Process Development and Manufacture of Solid Oral Dosage Forms. *Advanced Drug Delivery Reviews* 56, 371-390.

Chapter 3: Quantitative Macro-Raman Spectroscopy on Microparticle-based Pharmaceutical Dosage Forms

A similar version of this chapter is a submitted paper manuscript as "Quantitative Macro-Raman Spectroscopy on Microparticle-based Pharmaceutical Dosage Forms" in the name of Hui Wang, Lisa Williams, Susan Hoe, David Lechuga Ballesteros, and Reinhard Vehring.

3.1. Introduction

Microparticle-based dosage forms are commonly used for drug delivery purposes, often in the form of respirable particulate powders contained in delivery devices like pressurized meter dose inhalers (Newman, 2005) or dry powder inhalers (Chougule et al., 2007; Prime et al., 1997). The properties of these respirable pharmaceutical powders, such as particle sizes, chemical and physical stability, or dispersibility, must be accurately investigated and controlled to achieve the desired performance (Chow et al., 2007; Smyth, 2003). In these dosage forms the concentrations and the solid phases of all active pharmaceutical ingredients and excipients must be precisely controlled. Due to the potential for chemical or physical changes, including solid state transitions between amorphous and crystalline phases (Willart and Descamps, 2008; Yu, 2001), polymorphic inter-conversions (Hilfiker, 2006; Vippagunta et al., 2001a), or minor conformational adjustment (Cruz-Cabeza and Bernstein, 2013; Nangia, 2008), which can occur on storage or during patient use, a sensitive technique is required for qualitative and quantitative detection of these changes. Amongst all applicable techniques, Raman spectroscopy has gained particular popularity.

The applications of Raman spectroscopy in pharmaceutical areas have been greatly extended over the past decades (Vankeirsbilck et al., 2002b; Wartewig and Neubert, 2005a). Thanks to its rapidity, non-invasiveness, straightforward sampling, compatibility with aqueous systems, and most importantly, its sensitivity to subtle structural changes, Raman spectroscopy has already been widely employed as a standard method for routine pharmaceutical and chemical analysis. Basic applications of Raman spectroscopy include the study of molecular structure(Lin-Vien et al., 1991) and conformation (Blanpain-Avet et al., 2012), identification of unknown formulations(Wang et al., 2014), and analysis of solid phases(Newman and Byrn, 2003; Taylor and Langkilde, 2000). Also because of the rich molecular information contained in Raman spectra and the sensitivity of Raman signals to minor structure changes, Raman spectroscopy has been found suitable for quantitative analysis of pharmaceutical samples (Vehring, 2005).

The basic theory of quantitative Raman analysis states that Raman signal intensities are linearly proportional to the number of Raman scatterers (McCreery, 2005). The most commonly used quantitative approaches can be categorized into two types: uni- or bi-variate and multivariate analysis. Uni- or bi-variate methods use one or two variables, *e.g.,* peak intensities or ratios of two characteristic peaks (Taylor and Zografi, 1998; Voutsas et al., 1995), or peak areas (Al-Zoubi et al., 2002; Hédoux et al., 2011), to quantify the analytes of interests. Usually, several cases with known formulations need to be measured to generate a calibration curve to correlate spectral information with composition information. This method is straightforward but mainly applicable to simple formulations with undisturbed well-defined characteristic peaks. Multivariate methods use comprehensive spectral information for quantification and are applicable to multi-

component samples, which also make these methods more complex (Strachan et al., 2007). The quantitative method used in this paper is also a multivariate method. Since the details of these different data processing methods have already been described elsewhere (Strachan et al., 2007), they are no longer introduced here.

Like with any other quantitative technique, the error sources affecting Raman quantification are an important concern for practical applications. This topic has already been extensively discussed and many error sources were identified and even quantified (Campbell Roberts et al., 2002). The various sources of errors can be classified into three types: instrument variations, errors introduced by the quantification methodology, and sample heterogeneity. Instrument variations include effects from laser power fluctuation, detector response variation, alignment errors, etc. Many of these effects can be reduced by repeated measurements. The overall quantification methodology errors of uni-variate and multivariate methods have been compared and no significant differences were observed between them (Rantanen et al., 2005). For cases with relatively small sampling volume, the error originated from using either of the methods is usually less significant than the variation caused by sample inhomogeneity (Campbell Roberts et al., 2002; Rantanen et al., 2005). For powder samples consisting of two or more components the major source of error has been reported to arise from the inhomogeneous mixing of powder blends(Taylor and Zografi, 1998) , which, upon sampling into a finite sample volume, can lead to a sample composition which is not representative of the bulk powder.

This is a common problem encountered in measuring the composition of bulk samples: the measured Raman signal may not be representative of the average signal from the whole sample. To overcome the quantification error caused by sample

inhomogeneity, different methods have been proposed, such as enlarging the illuminated area(Johansson et al., 2005), *i.e.,* sample volume, increasing the length of the beam path through the sample(Schwab and McCreery, 1987), increasing sample homogeneity (Bugay et al., 1996), averaging multiple spectra recorded from multiple sampling locations(Bell et al., 2004), rotating or moving the sample holder (Langkilde et al., 1997; Szostak and Mazurek, 2002), or dynamically mixing the sample (Rantanen et al., 2005). With the exception of the method of increasing the degree of homogeneity, which has the potential to introduce modifications to the analyte, all other methods intend to increase the number of particles that can be illuminated and monitored by the detector during a Raman measurement. However, while many authors have suggested increasing the sample volume to reduce errors introduced by non-representative sampling of heterogeneous powders, no quantitative information about the required sample volume as a function of powder characteristics is available.

In this paper this issue has been addressed by using a Monte-Carlo simulation to predict the minimum sample volume required for representative sampling. A corresponding macro-Raman system is presented that allows efficient signal collection from sample volumes that are large enough for representative analysis of typical respirable dosage forms. The error sources for quantitative Raman measurements with controlled sample inhomogeneity are also discussed.

3.2. Materials and Methods

3.2.1. Materials

Commercial pharmaceutical respirable dosage forms for the treatment of asthma and chronic obstructive pulmonary disease were measured with Raman spectroscopy in this study (Table 3.1). Three inhaler products were chosen to assess the quantification capabilities of macro-Raman spectroscopy for formulations with single, dual, and triple components.

Two dry powder inhaler products, Flixotide® Accuhaler® (fluticasone propionate; FP) 50, 100, 250, 500, and Seretide® Accuhaler® (FP and salmeterol xinafoate; SX) 100, 250, 500, were measured by disassembling the inhaler devices and extracting powders from the foil blister strips. Both Flixotide® and Seretide® contained the excipient lactose monohydrate as a carrier and bulking agent. The formulation and component information of pressurized metered dose inhaler Seretide® 50 Evohaler® was used as a simulation input. All samples were measured multiple times to reduce random error of measurement and instrument variation.

Table 3.1 Composition of commercial double- and triple-component inhalers tested

Product	Device	Formulation (μg)			Measured lactose particle size distribution		Raman Measurement Replicates
		FP	SX	Lactose	VMD (μm)	GSD	
Flixotide® 50	Accuhaler®	50	NA	Up to total mass of 12.5mg per blister	81.2	2.3	10
Flixotide® 100		100	NA		80.6	2.4	10
Flixotide® 250		250	NA		80.2	2.3	10
Flixotide® 500		500	NA		75.1	2.6	10
Seretide® 100	Accuhaler®	100	50		77.7	2.2	5
Seretide® 250		250	50		81.6	2.1	5
Seretide® 500		500	50		74.9	2.6	5
Seretide® 50	Evohaler®	50	25	NA	NA		5

3.2.2. Particle Size Measurements

The equivalent optical diameter of the lactose carrier particles in the tested dry powder inhaler formulations was determined using a Laser diffraction system (HELOS BF, Sympatec GmbH, Clausthal-Zellerfeld, Germany) with an attached disperser (OASIS/M, Sympatec GmbH, Clausthal-Zellerfeld, Germany). The particle sizer was set up with an optical module for the diameter range 4.5 to 875 μm. For each measurement the powder from nine foil blisters was loaded into a sample tube and fed into the particle sizer using a micro-dosing device (ASPIROS, Sympatec GmbH, Clausthal-Zellerfeld, Germany) using 300 kPa of dispersion pressure and 50 mm/s feeder speed. Measurements were triggered on a single channel, #23, starting at higher than 0.5 % signal level and ending 1 s after falling to less than 0.5 %. Volume median diameter (VMD) and geometric standard deviation (GSD) of the mean particle size distribution of triplicate measurements were reported and listed in Table 3.1.

3.2.3. Macro-Raman Measurements

The custom designed and assembled Raman instrument used in this study is a linear dispersive Raman system, using a 514.5 nm argon ion laser as excitation source, with laser power up to 1700 mW. A detailed description of the Raman system has been provided in the previous chapter (Wang et al., 2014). Here, the aspects of the system that pertain to the macro mode will be discussed:

For linear Raman spectroscopy the total radiant flux, Φ_t, of the signal from a component with molar concentration, c, in the sample volume, V, can be described by (Vehring, 1998).

$$\Phi_t = \varphi_0 c N_A \sigma V \quad (3.1)$$

where N_A is the Avogadro constant and σ is the Raman scattering cross section for this component. φ_0 denotes the average radiant flux density of the excitation radiation interacting with the Raman scatterers.

Applied to a powder sample with bulk density, ρ_s, we can rewrite this equation for a component with molar mass, *M*, and mass fraction, *Y*, in the sample as

$$\Phi_t = \varphi_0 a^3 \cdot Y \rho_s \cdot \frac{N_A \sigma}{M} \quad (3.2)$$

assuming for the sake of simplicity a cubic sample volume with edge length, *a*. If we further assume that one face of the sample volume is illuminated by a laser with power, $P_{max} = \varphi_{0,max} a^2$, such that the sample is irradiated with the highest possible radiant flux density that does not cause undue sample heating or degradation, the signal intensity at the detector can be written as

$$I = a P_{max} E t_E \cdot Y \rho_S \cdot k \quad (3.3)$$

Equation 3.3 shows that the signal intensity increases linearly with the characteristic length of the sample volume and with the maximum tolerated laser power, which increases with the square of the characteristic length. t_E is the exposure time and *k* is a constant summarizing the fraction in Equation (3.2). *E* is the overall efficiency of signal collection and detection. In micro-Raman applications with typically high magnification the sample volume is one particle, or even a fraction of a particle, which is equivalent to a characteristic dimension on the order of 1 μm. In the current setup the characteristic dimension of the sample volume is on the order of 100 μm or more, which explains why a much higher laser power can be applied in macro-Raman mode. The sample volume can be increased by using collection optics with low magnification factor which results in

a large field of view and large depth of field. The collection optics of the instrument had an overall magnification of only 2.5× and a numerical aperture of 0.25. The unexpanded laser beam was focused using a separate lens producing a large focal spot with a diameter of approximately 25 μm, corresponding to radiant flux densities on the order of 1 GW/m^2, which were tolerated well by the samples. The beam was directed into a conical aluminum cavity, which acted as a multi-pass cell to homogeneously illuminate powder samples with a volume of 0.16μL. The sample volume defined by the collection optics was approximately 0.0035 μL. It constituted a fraction of the sample holder volume, determined primarily by the selected entrance slit width, *i.e.*, spectral resolution, of the spectrograph. However, the effective scattering volume was between 0.0035μL and 0.16 μL because the multi-pass sample cavity allowed multiple reflections of both excitation light source and Raman signals. Therefore, signals were further averaged before being scattered out of the cavity. Initial spectral resolution was about 1 cm^{-1}/pixel, and was artificially increased for data processing purposes to 0.1cm^{-1}/pixel by a linear interpolation process. Samples were measured at room temperature and under dry air conditions, *i.e.*, RH < 3%. Sample pre-conditioning was conducted after loading the powder sample by gradually increasing the laser power to bleach out any fluorescence background, if present. Exposure times ranged from several seconds to 5 minutes.

3.2.4. Stochastic Model

A Monte-Carlo model was developed to predict the minimum sample volume required for a representative composition measurement of microparticle-based powder samples. Illustrated in the Figure 3.1 is a brief flowchart of the simulation. Basic assumptions of the simulation included: lognormal particle size distributions for each

component; single component per particle; and a random polydisperse particles packing efficiency of 60% for simulated sample volumes (Al-Raoush and Alsaleh, 2007).

The sample properties required as input values for the simulation were the number of components in the sample, the descriptors of the particle size distribution, *i.e.*, median diameter and geometric standard deviation for each component; the true density of each component; and the nominal mass fractions of the components in the sample. Other simulation parameters that needed to be specified were the relative error tolerance, the initial sample volume to start with the simulation, the value used to decide whether a simulated composition of a specific simulated volume can be treated as representative of the bulk material, and the number of simulation runs for each sample volume used to calculate the average simulated composition and relative error. The number of simulation for each sample volume represents the number of repeated measurements for quantification in practical cases.

According to the chosen sample properties, the average number of particles of each component can be contained in the simulated sample volume was calculated by using the diameter of average volume and also taking the packing efficiency into account. This amount of virtual particles were randomly generated and placed into the sample volume. After executing the chosen number of simulation runs, the average simulated mass fraction and its relative error with respect to the nominal mass fraction of each component were calculated. The error was compared with the target error tolerance to decide if the chosen sample volume was sufficiently large. If so, the simulation was repeated with a smaller sample volume. The minimum sample volume was determined by successive iterations of the simulated sample volume. Each sample was simulated at least

100 times ($m \geq 100$) to get the distribution of minimum sample volumes, and the obtained m minimum sample volume data points were then fitted using least squares methods, as described in the following detailed logic flow chart of the simulation.

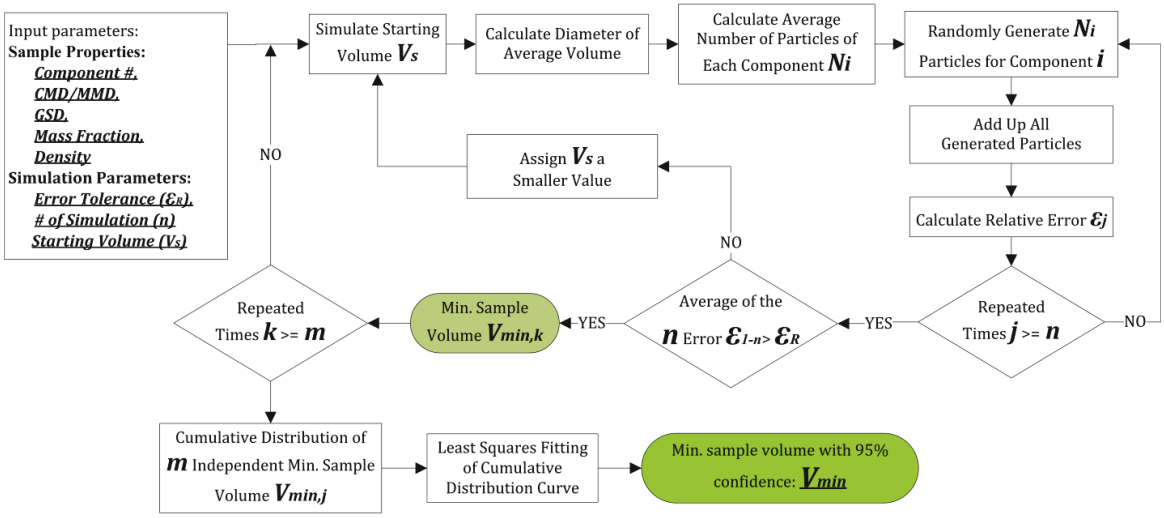

Figure 3.1. Flow chart of the Monte-Carlo simulation

3.2.5. Raman Quantification

Quantification of a multi-component sample is a process to convert measured Raman spectral intensities to sample composition information. The first step in this process is to identify the signal from the components in the spectrum from the powder sample. A deconvolution process was used to extract the spectral contributions of each component from the raw spectra of mixtures according to:

$$S = B + \sum I_i S_{i,N} \quad \Delta\nu + b_i \qquad (3.4)$$

The background signal, B, was mainly caused by fluorescence. It was subtracted in most cases as a linear function of Raman shift before determining the spectral contribution of each component $I_i S_{i,N}$. The intensity factor, I_i, was determined by

subtracting the reference spectrum of each pure component, $S_{i,N}$, until the residual spectrum was minimized. The reference spectra were also adjusted, if necessary, by a small frequency shift, b_i, to correct for instrumental errors affecting the wavenumber calibration, *e.g.*, grating repositioning errors. . The intensity factors can be correlated to the mass fractions of the components, Y_i, by calibration factors, c, according to the following equation.

$$\frac{Y_i}{Y_j} = c_{i/j}\frac{I_i}{I_j} \quad (3.5)$$

Taking component j as internal standard, calibration factor of component *i* relative to *j* is denoted as $c_{i/j}$.

3.2.5.1. Principal component analysis for reference spectra

A typical way of deriving the reference spectra mentioned above is by directly measuring spectra of representative pure components (Vehring, 2005; Wang et al., 2014). However, it may be difficult to find reference materials with exactly the same spectra as the components in the sample mixture. Since Raman spectroscopy is sensitive not only to molecular structures, but to a lesser extent also to solid phases, amount of residual solvents, and impurities, etc., factors like the source and production process of the reference material, and its storage conditions or chemical history may have noticeable impact on the final spectrum. In particular when it comes to analyzing components with very low concentration in the sample a reference spectrum which is not entirely representative of the component spectrum in the sample will give rise to artifacts during deconvolution and potentially increase the limit of quantification.

An alternative to the use of reference materials, derivation of reference spectra by a simplified version of principal component analysis method, was used in this study. For the SX-FP-lactose triple component mixtures used, general spectral information, *e.g.* characteristic peak positions, of individual components were obtained from measurements of pure components. The information could also be directly obtained by simple literature search. Peaks exclusively contributed by one of the components were used as markers for that component during mixture spectra cross-subtraction. As described, reference of FP ($S_{\mathrm{FP,N}}$) was firstly obtained by subtracting the spectrum of 25µg SX+50µg FP mixture from that of 25µg SX+250µg FP mixture until the marker peak of SX was completely subtracted. Reference spectra of SX ($S_{\mathrm{SX,N}}$), and lactose ($S_{\mathrm{Lac,N}}$) were derived subsequently in a similar way as described in Equation (3.7) and (3.8).

$$S_{\mathrm{FP,N}} = S_{25\mu\mathrm{g\ SX}+250\mu\mathrm{g\ FP}} - I_{\mathrm{a}} \bullet S_{25\mu\mathrm{g\ SX}+50\mu\mathrm{g\ FP}} \quad (3.6)$$

$$S_{\mathrm{SX,N}} = S_{25\mu\mathrm{g\ SX}+50\mu\mathrm{g\ FP}} - I_{\mathrm{b}} \bullet S_{\mathrm{FP,N}} \quad (3.7)$$

$$S_{\mathrm{Lac,N}} = S_{50\mu\mathrm{g\ FP}+\mathrm{Lactose}} - I_{\mathrm{c}} \bullet S_{\mathrm{FP,N}} \quad (3.8)$$

where integers I_{a}, I_{b}, and I_{c} are intensity factors of the corresponding elements similar to the intensity factors mentioned in the deconvolution process. Five independent derivations on independently measured spectra were performed for each reference spectrum and the average of the five achieved reference spectra was used as the final reference.

To verify the reproducibility of this reference derivation method, the five derived lactose references were plotted together with their average spectrum in Figure 3.2, and good consistency was found. The spectral differences relative to the average spectrum

were also plotted, expressed as percentage of the highest peak. Signal differences for all independently derived lactose reference spectra were below 1.0 % for the whole spectral range, except for the low frequency shift range (0-75 cm^{-1}). The relatively higher signal difference is likely due to the sensitivity of low frequency shift Raman spectroscopy to temperature (Achibat et al., 1993), which is difficult to control exactly because of possible laser heating of the sample. Reference spectra derivations for SX and FP follow the same processes and also showed high repeatability.

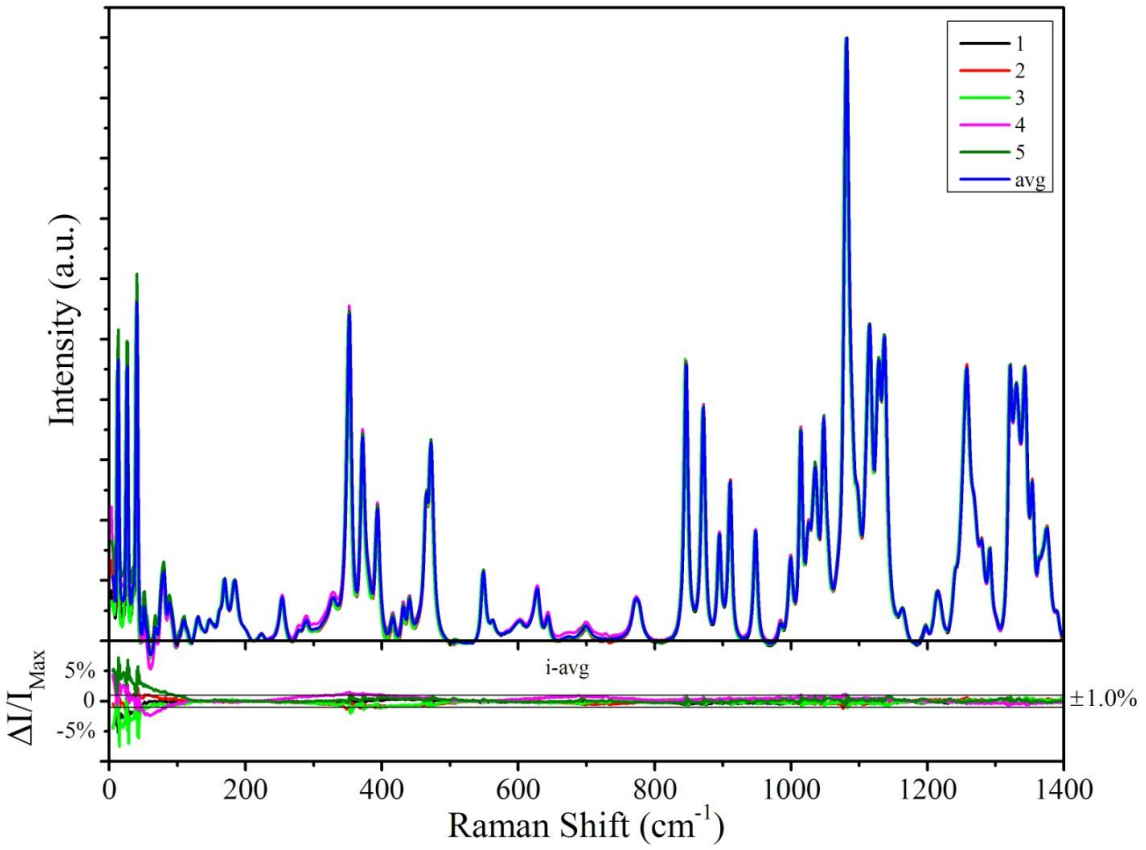

Figure 3.2. Derived lactose reference spectra and spectral differences ($\Delta I/I_{Max}$) of independently derived lactose references in percentage of the highest peak intensity

3.2.5.2. Calibration factors

In the absence of an internal standard, concentrations of sample components can only be determined relative to another component. For example calibration factors of FP relative to lactose can be used to determine the FP – lactose ratio. Measuring and analyzing samples with known composition was used to derive the relative calibration factors. Figure 3.3 shows the linear calibration curve of FP relative to lactose with each data point originated from ten independent measurements and deconvolutions. The calibration factor, $c_{FP/Lac} = 0.781$, can then be used to quantify FP relative to lactose in formulations with unknown composition.

$$\frac{Y_{FP}}{Y_{Lac}} = c_{FP/Lac} \bullet \frac{I_{FP}}{I_{Lac}} \quad (3.9)$$

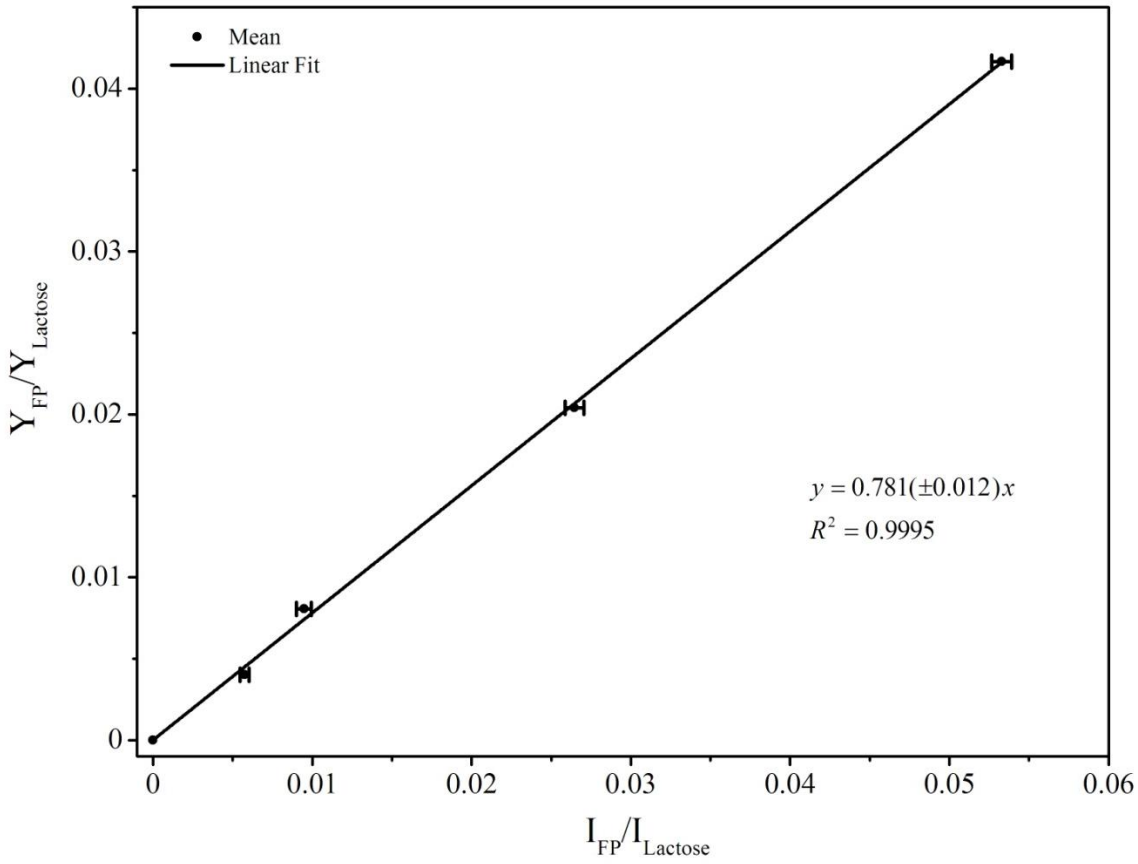

Figure 3.3. Calibration curve of FP relative to lactose

3.3. Results and Discussion

3.3.1. Minimum sample volume

The minimum sample volume is a function of multiple parameters *i.e.*, the number of components in the sample, the MMD and GSD of their particle size distributions, the component mass fractions, their true densities, the relative error tolerance, and also the replicates of simulation for each sample volume prior to the calculation of relative error. Several cases were simulated to study the dependence of the minimum sample volume on these parameters. Besides, the Monte-Carlo simulation results for two commercial products: Seretide® 50 Evohaler® and Seretide® 100 Accuhaler® were also presented in

Figure 3.4 to show the typical minimum sample volume required for carrier-free dosage forms samples with respirable particles and dosage forms containing non-respirable particles like lactose carriers. As demonstrated in Figure 3.4 and Table 3.2 and 3.3, the probability that the average composition of serveral simulations for samples contained in a simulated sample volume is within the chosen relative error tolerance can be described by a lognormal distribution. Components with larger median diameters, broader distributions, lower mass fractions, lower densities, a lower relative error tolerances, and less replicates of simulations required larger sample volumes to achieve representative sample composition. Especially in cases when some components had a very low mass fraction while other components had large particle sizes, the minimum sample volume was significantly larger. This explains the comparatively large minimum sample volume required for Seretide® 100 Accuhaler® products which not only contain low concentration actives SX and FP but also have non-respirable large lactose carriers.

The trend of decreasing sample volume with increasing number of simulation replicates is instructive that the requirement for large sample volume can be greatly reduced by averaging multiple independent measurements. This is the underlying reason that the method of combining multiple micro-Raman measurements on various areas to give averaged spectrum can be used for the quantification of bulk composition.

The black square data points are the simulation results for the Seretide® 50 Evohaler® product containing 2 components: 25μg SX and 50μg FP. Literure values(Hoe et al., 2009; Taki et al., 2011) for the particle size distribution were averaged and used as simulation input parameters for the two components. The relative error tolerance was set to 3%. A confidence coefficient of 95% gave a sample volume of about 1.50×10^{-3}μL for

this specific sample. Based on their particle size distribution, average particle volumes of SX and FP were calculated to be 1.37μm^3 and 0.48 μm^3 respectively. Thus, considering an assumed packing ratio of 60%, the minimum sample volume corresponds to an average number of 245,000 SX and 1,183,000 FP particles. In contrast, the sample volume required for representative quantification of Seretide® 100 Accuhaler® is approxiamately 3000 times larger mainly due to the large lactose carrier particles and low concentration of actives.

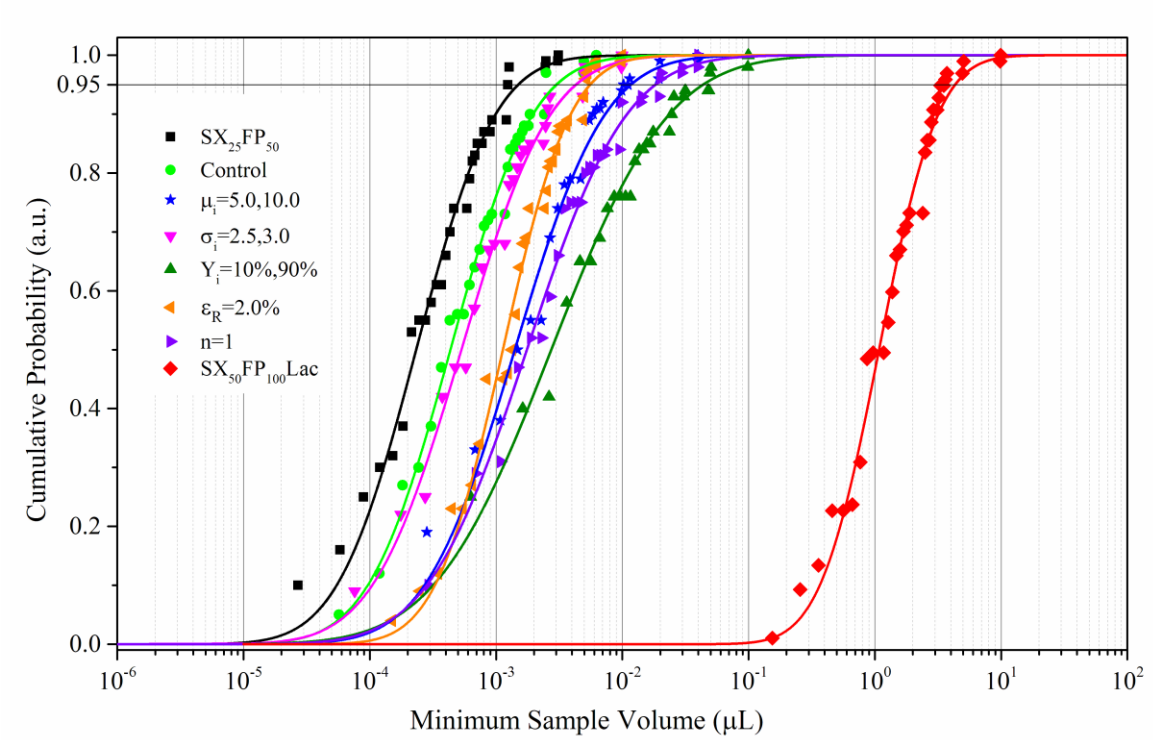

Figure 3.4. Minimum sample volume for microparticle-based powders with controlled simulation parameters

Table 3.2 Monte-Carlo simulation input parameters and output results of Seretide® 50 Evohaler® and Seretide® 100 Accuhaler®

	Formulation / Parameters	25μgSX+50μgFP		50μgSX+100μgFP+Lactose		
		SX	FP	SX	FP	Lactose
	Legend of Plot	$SX_{25}FP_{50}$		$SX_{50}FP_{100}Lac$		
INPUT	MMD: μ_i (μm)	4.03	3.53	4.03	3.53	77.7
	GSD: σ_i	2.33	2.53	2.33	2.53	2.2
	Mass Fraction: Y_i (%)	33.33	66.67	0.40	0.80	98.80
	Density: ρ_i (g/cm^3)	1.11	1.32	1.11	1.32	1.54
	Error Tolerance: ε_R (%)	3.0		3.0		
	Simulation Replicates (n)	5		5		
OUTPUT	Mean of V_{min} : μ (μL)	2.33×10^{-4}		1.08		
	Standard Deviation of V_{min} : σ	3.10		2.32		
	V_{min} with 95% Confidence (μL)	1.50×10^{-3}		4.33		

Table 3.3 Results of using control variable method to study the dependence of minimum sample volume on multiple parameters

	Formulation / Parameters	Double Component Formulation											
		A	B	A	B	A	B	A	B	A	B	A	B
	Legend of Plot	Control		μ_i=5.0,10.0		σ_i=2.5,3.0		Y_i=10%,90%		ε_R =2.0%		n=1	
INPUT	MMD: μ_i (μm)	5.0	5.0	**5.0**	**10.0**	5.0	5.0	5.0	5.0	5.0	5.0	5.0	5.0
	GSD: σ_i	2.5		2.5		**2.5**	**3.0**	2.5		2.5		2.5	
	Mass Fraction: Y_i (%)	50	50	50	50	50	50	**10**	**90**	50	50	50	50
	Density: ρ_i (g/cm^3)	1.0		1.0		1.0		1.0		1.0		1.0	
	Error Tolerance: ε_R (%)	3.0		3.0		3.0		3.0		**2.0**		3.0	
	Simulation Replicates (n)	5		5		5		5		5		**1**	
OUTPUT	Mean of V_{min} : μ ($\times10^{-4}$μL)	4.35		14.08		5.32		27.38		11.32		17.55	
	Standard Deviation of V_{min} : σ	3.24		3.62		3.56		5.38		2.64		4.16	
	V_{min} with 95% Confidence ($\times10^{-3}$μL)	3.01		11.68		4.30		43.60		5.55		18.33	

For the Seretide® 50 Evohaler® sample, the real time relative error of FP mass fraction with respect to its nominal fraction after placing each randomly generated particle into the virtual sample volume is shown in Figure 3.5. The simulation was repeated 100 times to reveal the convergence-in-error consistency. The errors for all simulations have clear converging trends towards zero during the process of generating and placing more particles. Typical micro-Raman systems usually have lateral spatial resolution in the micrometer or even sub-micrometer range, and the maximum area that can be simultaneously measured is usually smaller than 100 μm^2. A typical depth of focus for micro-Raman systems is less than 10μm. Thus, the number of particles that can be measured simultaneously by micro-Raman spectrosocpy is about 100 to 1000 microparticles (see dashed seperation lines in Figure 3.5). The results in Figure 3.5 show that such small sample volumes will likely lead to large errors in measured sample composition. For this paticular sample, more than 1,400,000 particles were required to achieve a relative error lower than 3% with 95% probability. As a result, micro-Raman with high resolution is better suited for local component distribution analysis, instead of bulk composition analysis. However, with an increasing number of particles that can be sampled in macro-Raman systems, the measured composition converges to its true value.

Another limitation of micro-Raman is the slow rate of data acquisition due to the low tolerable laser power and small number of Raman scatterers. Equations (3.2) and (3.3) show that the Raman signal is proportional to the sample volume, if sufficient laser power is available to operate close to the maximum tolerated radiant flux density for the sample material. By comparing the maximum sample volume of typical micro-Raman systems with the lower limit of 0.0035 μL-sample volume used in this study, it follows

that the macro-Raman system collects signal at a rate that is already more than 1000 times faster than that of micro-Raman systems. Thus, regardless of the composition variation, to achieve the same spectral quality from a sample of sufficient size to produce representative results, the acquisition time of micro-Raman spectroscopy would have to be impractically long.

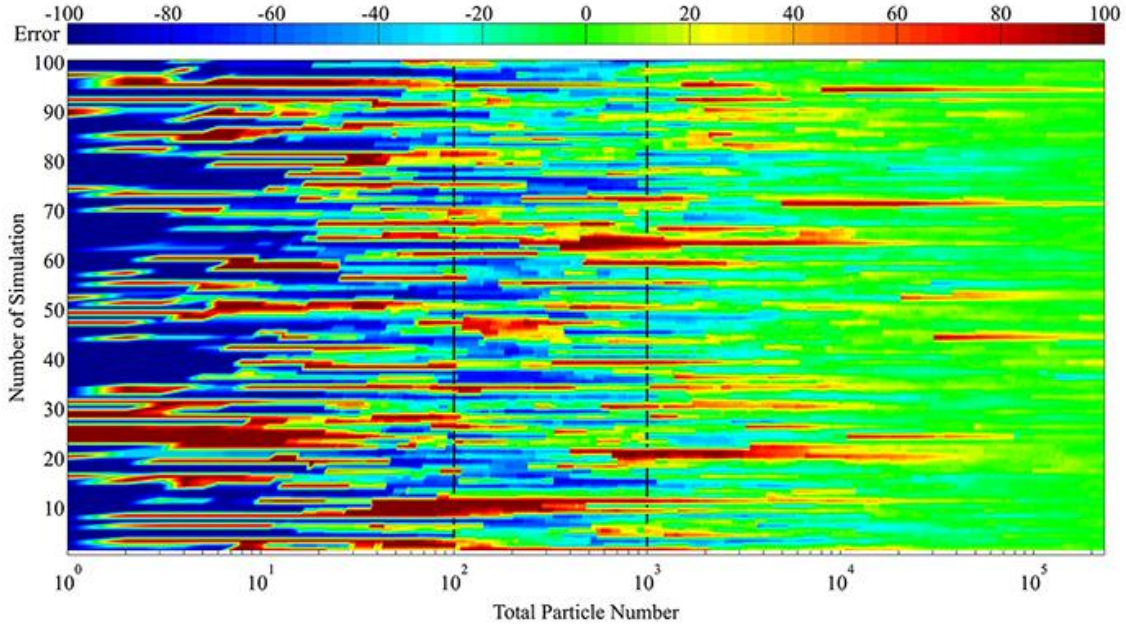

Figure 3.5. 100 simulated sample compositions of powder from the commercial product Seretide® 50 Evohaler® converging to nominal values.

3.3.2. Quantitative powder measurements

The derived calibration factor of FP relative to lactose was applied to analyze the mass fraction of FP in different Seretide® Accuhaler® dry powder inhaler formulations listed in Table 3.4: 25µgSX+50µgFP+Lactose, 25µgSX+125µgFP+Lactose, and 25µgSX+250µgFP+Lactose. Each formulation was measured five times. Results of the application in comparison with the nominal mass fraction are plotted below in Figure 3.6.

The measured FP mass fractions show good agreement with the nominal values even for the case with an FP fraction lower than 1%.

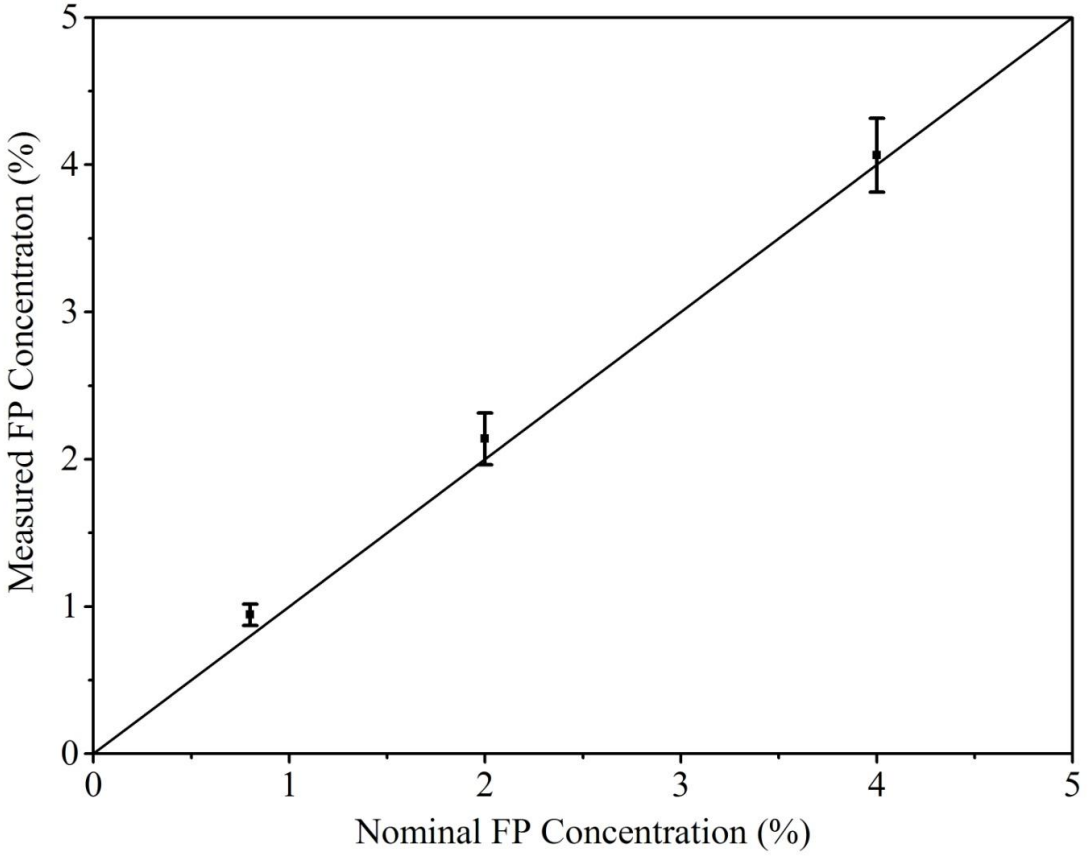

Figure 3.6. Application of FP calibration factors

As described in the introduction section, three error types can be identified in quantitative Raman analysis: the noise of the measurement that is caused by instrument variations, the overall quantification method error, and sample composition deviations due to sampling heterogeneity. A number of noise sources can contribute to the signal-to-noise level in the final Raman spectrum including signal shot noise, background shot noise, detector dark noise, and readout noise. Signal shot noise and background shot noise are the two dominant contributors of the Raman instrument used in this study.

Signal shot noise is fundamental to spectroscopy and originates from the Poisson statistical distribution of photons (McCreery, 2005). Background shot noise arises mainly because of the fluorescence induced by the green excitation source in the instrument used. Noise of the background was greatly reduced by subtracting the fluorescence of all measurements as linear function of Raman shift. Since both types of the noise source are governed by shot noise and follow square root relation, SNR is proportional to the square root of the peak intensity of a specific Raman band. For all measurements conducted in this study, accumulation time was set to have characteristic peak intensity to be at least 250,000 counts after background subtraction.

Taking one of the quantified formulations: 50μgSX+100μgFP+Lactose for demonstration, the propagation of noise-originated error was calculated and shown schematically in Figure 3.7. S_{FP} and S_{Lac} represent the spectral contributions of corresponding components in the mixture spectrum. The strongest peak intensity of S_{FP} for this specific formulation is about 2,500 counts for all repeated measurement which gives the relative shot noise of about 2%. Since both the reference spectra of FP ($S_{FP,N}$) and lactose ($S_{Lac,N}$) are derived from principal component analysis and the relative spectral differences of the derived spectra were shown to be within 1.0% along the whole fingerprint range in Figure 3.2, so here a reasonable 1.0% relative error is assigned to be the difference between the characteristic peak intensities of derived references ($S_{FP,N}$, $S_{Lac,N}$) and that of the ideal references. The rules of random error propagation were used to calculate the resultant relative errors. It can be seen that the maximum relative error caused by shot noise and imperfect references is about 2.4%.

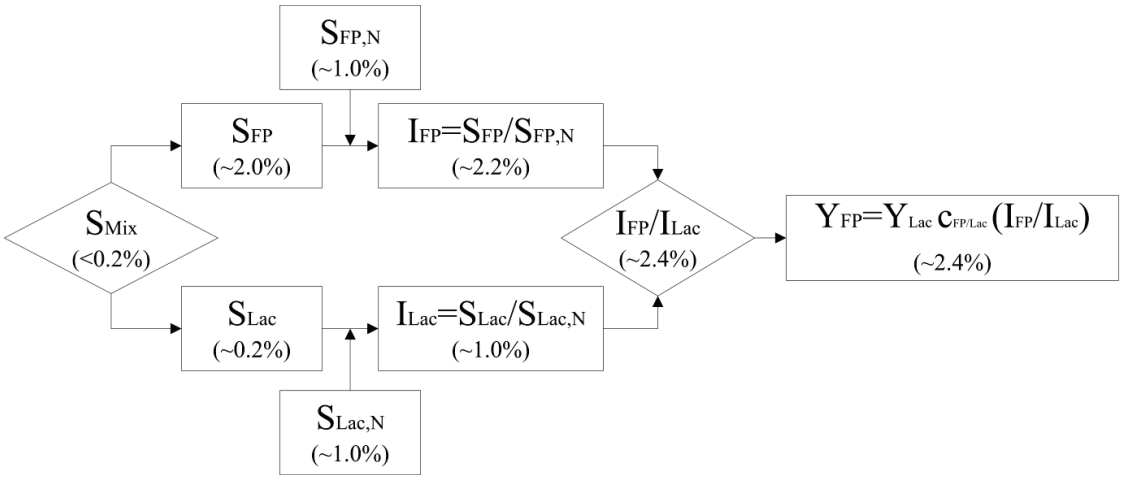

Figure 3.7. Propagation of shot noise error and reference deviation error for Seretide® 100 Accuhaler®: 50μgSX+100μgFP+Lactose

Errors originated from the overall quantification method arise during the deconvolution process. When subtracting a component spectrum from that of the mixture, the exact point of complete subtraction is ambiguous. Thus, an error bar for the factor I_i can be defined as the range between over- and under-subtraction. Since every data point in the FP calibration factor curve was derived from ten independent measurements, variations of intensity ratios for the same formulation from multiple results were also incorporated into the calculation of correct peak intensity ratios. So both the error bar and variations between measurements were used to calculate the acceptable range of peak intensity ratios of FP to lactose, as the error bars of each composition displayed in Figure 3.3. For the same reason, each Seretide® Accuhaler® sample used for quantitative analysis was measured five times and given an error bar to the FP-lactose intensity ratio, which is then converted to FP mass fraction by using the calibration factor just derived. The error bars of the calibration factor and FP-lactose intensity ratio were all incorporated into the final results of composition. The propagated error was calculated and shown as error bars in the Figure 3.6 and also listed in Table 3.4.

Table 3.4 Error estimation of Raman quantification

Formulation	Actual FP mass fraction %	Measured FP mass fraction (±S.D.) %	Relative Error %		
			Spectral noise and imperfect reference(±)	Sample heterogeneity 0.16μL (±S.D.)	Quantification method(±)
50μg SX + 100μg FP + Lactose	0.8	0.94(±0.07)	2.4	4.7(±4.6)	7.4
50μg SX + 250μg FP + Lactose	2.0	2.14(±0.18)	2.0	4.3(±3.8)	8.4
50μg SX + 500μg FP + Lactose	4.0	4.07(±0.25)	1.8	6.0(±5.6)	6.1

Lastly, as discussed above, the amount of sampled powder for quantitative analysis must be large enough to be representative of the bulk composition. For the quantitatively analyzed triple-component sample, the minimum sample volume to achieve less than 3% composition deviation after five independent sampling with 95% probability was determined by simulation to be 4.33 μL. However, the actual measurements were conducted with a true scattering volume between 0.0035 and 0.16μL, which is at least 27 times smaller than the volume required. By setting the simulated volume to the upper limit of 0.16μL, the relative composition error of every five independent measurements can be predicted, as listed in Table 3.4. It means that based on the maximum possible scattering volume, FP composition of every five repeated measurements will have approximately 5% relative error from its nominal value caused by non-representative sampling. Larger errors were observed because of the smaller true scattering volume than 0.16μL. For the three cases quantified above, the maximum relative errors are 26.3%, 16.0% and 8.0% respectively, and they are significantly smaller than the simulated

relative errors for a 0.0035μL-sample volume (40±30%). This indicates that the multi-pass sample holder is useful for increasing the effective scattering volume.

3.4. Conclusions

It was demonstrated that macro-Raman spectroscopy is a suitable method for quantitatively measuring bulk composition of microparticle-based multi-component pharmaceutical dosage forms. Micro-Raman spectroscopy was found to be unsuitable for this application, because the sample composition within its small detection area or volume is likely to be unrepresentative of the bulk composition.

There exists a minimum sample volume for representative quantitative macro-Raman analysis, which can be determined by the Monte-Carlo simulation introduced in this paper for a particular application. In general, the minimum sample volume is a function of the properties of each component in the sample, number of repeated measurements and the tolerable composition error. For double-component microparticle-based samples with relatively small particle size (MMD=3~5 μm, GSD=2~3) and similar mass fraction of each component, the minimum sample volume for 3% error tolerance with high confidence is on the order of 10^{-3} μL, a volume that typically contains more than 10^{6} particles. For dosage forms containing non-respirable components with larger particle size, *e.g.* lactose carriers, sample volumes need to be increased to the order of 1 μL to allow a representative measurement.

Due to the greater number of Raman scatterers that can be illuminated simultaneously, macro-Raman spectroscopy can greatly shorten typical measurement time to minutes, and even seconds, without compromising spectral quality, which makes it a suitable technique for routine analysis in the pharmaceutical industry. Applications of

quantitative analysis for multi-component respirable dosage forms have shown that a multi-pass sample holder was helpful in increasing the effective scattering volume to reduce the composition error. Even for the macro-Raman system used in this study, sample heterogeneity could still contribute to quantification errors, especially when measuring samples containing large carrier particles. The results of simulation also implied that averaging multiple independent measurements could be used to compensate for insufficient scattering volume. For macro-Raman measurements, though higher laser power for macro-Raman will result in shorter acquisition time and faster measurement, the applied power density still has to be kept below the overheating limit to prevent molecular structural damage. Also the Monte-Carlo simulation introduced is based on the assumption that there are no agglomerates present in the simulated sample powder which is often not the case (Huck-Jones et al., 2014).

3.5. References

Achibat, T., Boukenter, A., Duval, E., 1993. Correlation Effects on Raman Scattering from Low-Energy Vibrational Modes in Glasses. Ii. Experimental Results. *The Journal of Chemical Physics* 99, 2046-2051.

Al-Raoush, R., Alsaleh, M., 2007. Simulation of Random Packing of Polydisperse Particles. *Powder Technology* 176, 47-55.

Al-Zoubi, N., Koundourellis, J., Malamataris, S., 2002. Ft-Ir and Raman Spectroscopic Methods for Identification and Quantitation of Orthorhombic and Monoclinic Paracetamol in Powder Mixes. *Journal of Pharmaceutical and Biomedical Analysis* 29, 459-467.

Bell, S.E., Beattie, J.R., McGarvey, J.J., Peters, K.L., Sirimuthu, N., Speers, S.J., 2004. Development of Sampling Methods for Raman Analysis of Solid Dosage Forms of Therapeutic and Illicit Drugs. *Journal of Raman Spectroscopy* 35, 409-417.

Blanpain-Avet, P., Hédoux, A., Guinet, Y., Paccou, L., Petit, J., Six, T., Delaplace, G., 2012. Analysis by Raman Spectroscopy of the Conformational Structure of Whey Proteins Constituting Fouling Deposits During the Processing in a Heat Exchanger. *Journal of Food Engineering* 110, 86-94.

Bugay, D.E., Newman, A.W., Findlay, W.P., 1996. Quantitation of Cefepime· 2hcl Dihydrate in Cefepime· 2hcl Monohydrate by Diffuse Reflectance Ir and Powder X-Ray Diffraction Techniques. *Journal of Pharmaceutical and Biomedical Analysis* 15, 49-61.

Campbell Roberts, S.N., Williams, A.C., Grimsey, I.M., Booth, S.W., 2002. Quantitative Analysis of Mannitol Polymorphs. Ft-Raman Spectroscopy. *Journal of Pharmaceutical and Biomedical Analysis* 28, 1135-1147.

Chougule, M.B., Padhi, B.K., Jinturkar, K.A., Misra, A., 2007. Development of Dry Powder Inhalers. *Recent Patents on Drug Delivery & Formulation* 1, 11-21.

Chow, A.H., Tong, H.H., Chattopadhyay, P., Shekunov, B.Y., 2007. Particle Engineering for Pulmonary Drug Delivery. *Pharmaceutical Research* 24, 411-437.

Cruz-Cabeza, A.J., Bernstein, J., 2013. Conformational Polymorphism. *Chemical Reviews* 114, 2170-2191.

Hédoux, A., Guinet, Y., Descamps, M., 2011. The Contribution of Raman Spectroscopy to the Analysis of Phase Transformations in Pharmaceutical Compounds. *International Journal of Pharmaceutics* 417, 17-31.

Hilfiker, R., 2006. Polymorphism: In the Pharmaceutical Industry. John Wiley & Sons.

Hoe, S., Young, P.M., Chan, H.-K., Traini, D., 2009. Introduction of the Electrical Next Generation Impactor (Engi) and Investigation of Its Capabilities for the Study of Pressurized Metered Dose Inhalers. *Pharmaceutical Research* 26, 431-437.

Huck-Jones, D., Jones, C., Castillio, J., Wolfgang, J., 2014. Combining Morphologically Directed Raman Spectroscopy with Next Generation Impactor Analysis to Improve the Understanding of Particle Properties of Dry Powder Inhalation Formulations. *Respiratory Drug Delivery 2014* 2, 481-484.

Johansson, J., Pettersson, S., Folestad, S., 2005. Characterization of Different Laser Irradiation Methods for Quantitative Raman Tablet Assessment. *Journal of Pharmaceutical and Biomedical Analysis* 39, 510-516.

Langkilde, F.W., Sjöblom, J., Tekenbergs-Hjelte, L., Mrak, J., 1997. Quantitative Ft-Raman Analysis of Two Crystal Forms of a Pharmaceutical Compound. *Journal of Pharmaceutical and Biomedical Analysis* 15, 687-696.

Lin-Vien, D., Colthup, N.B., Fateley, W.G., Grasselli, J.G., 1991. The Handbook of Infrared and Raman Characteristic Frequencies of Organic Molecules. Elsevier.

McCreery, R.L., 2005. Raman Spectroscopy for Chemical Analysis. John Wiley & Sons.

Nangia, A., 2008. Conformational Polymorphism in Organic Crystals. *Accounts of Chemical Research* 41, 595-604.

Newman, A.W., Byrn, S.R., 2003. Solid-State Analysis of the Active Pharmaceutical Ingredient in Drug Products. *Drug Discovery Today* 8, 898-905.

Newman, S.P., 2005. Principles of Metered-Dose Inhaler Design. *Respiratory Care* 50, 1177-1190.

Prime, D., Atkins, P.J., Slater, A., Sumby, B., 1997. Review of Dry Powder Inhalers. *Advanced Drug Delivery Reviews* 26, 51-58.

Rantanen, J., Wikström, H., Rhea, F.E., Taylor, L.S., 2005. Improved Understanding of Factors Contributing to Quantification of Anhydrate/Hydrate Powder Mixtures. *Applied Spectroscopy* 59, 942-951.

Schwab, S.D., McCreery, R.L., 1987. Remote, Long-Pathlength Cell for High-Sensitivity Raman Spectroscopy. *Applied Spectroscopy* 41, 126-130.

Smyth, H.D., 2003. The Influence of Formulation Variables on the Performance of Alternative Propellant-Driven Metered Dose Inhalers. *Advanced Drug Delivery Reviews* 55, 807-828.

Strachan, C.J., Rades, T., Gordon, K.C., Rantanen, J., 2007. Raman Spectroscopy for Quantitative Analysis of Pharmaceutical Solids. *Journal of Pharmacy and Pharmacology* 59, 179-192.

Szostak, R., Mazurek, S., 2002. Quantitative Determination of Acetylsalicylic Acid and Acetaminophen in Tablets by Ft-Raman Spectroscopy. *Analyst* 127, 144-148.

Taki, M., Ahmed, S., Marriott, C., Zeng, X.-M., Martin, G.P., 2011. The 'Stage-by-Stage'deposition of Drugs from Commercial Single-Active and Combination Dry Powder Inhaler Formulations. *European Journal of Pharmaceutical Sciences* 43, 225-235.

Taylor, L.S., Langkilde, F.W., 2000. Evaluation of Solid-State Forms Present in Tablets by Raman Spectroscopy. *Journal of Pharmaceutical Sciences* 89, 1342-1353.

Taylor, L.S., Zografi, G., 1998. The Quantitative Analysis of Crystallinity Using Ft-Raman Spectroscopy. *Pharmaceutical Research* 15, 755-761.

Vankeirsbilck, T., Vercauteren, A., Baeyens, W., Van der Weken, G., Verpoort, F., Vergote, G., Remon, J.P., 2002b. Applications of Raman Spectroscopy in Pharmaceutical Analysis. *TrAC Trends in Analytical Chemistry* 21, 869-877.

Vehring, R., 1998. Linear Raman Spectroscopy on Aqueous Aerosols: Influence of Nonlinear Effects on Detection Limits. *Journal of Aerosol Science* 29, 65-79.

Vehring, R., 2005. Red-Excitation Dispersive Raman Spectroscopy Is a Suitable Technique for Solid-State Analysis of Respirable Pharmaceutical Powders. *Applied Spectroscopy* 59, 286-292.

Vippagunta, S.R., Brittain, H.G., Grant, D.J., 2001a. Crystalline Solids. *Advanced Drug Delivery Reviews* 48, 3-26.

Voutsas, A., Hatalis, M., Boyce, J., Chiang, A., 1995. Raman Spectroscopy of Amorphous and Microcrystalline Silicon Films Deposited by Low-Pressure Chemical Vapor Deposition. *Journal of Applied Physics* 78, 6999-7006.

Wang, H., Boraey, M.A., Williams, L., Lechuga-Ballesteros, D., Vehring, R., 2014. Low-Frequency Shift Dispersive Raman Spectroscopy for the Analysis of Respirable Dosage Forms. *International Journal of Pharmaceutics* 469, 197-205.

Wartewig, S., Neubert, R.H., 2005a. Pharmaceutical Applications of Mid-Ir and Raman Spectroscopy. *Advanced Drug Delivery Reviews* 57, 1144-1170.

Willart, J., Descamps, M., 2008. Solid State Amorphization of Pharmaceuticals. *Molecular Pharmaceutics* 5, 905-920.

Yu, L., 2001. Amorphous Pharmaceutical Solids: Preparation, Characterization and Stabilization. *Advanced Drug Delivery Reviews* 48, 27-42.

Chapter 4: Aerosol sampling for macro-Raman analysis using a low flow rate single-nozzle cascade impactor

4.1. Introduction

Respirable dosage forms are the preferred medication form for treatment of asthma and chronic obstructive pulmonary diseases. The drugs are typically delivered from devices like pressurized metered dose inhalers or dry powder inhalers. Since pulmonary drug delivery efficiency is determined to a large extent by the physical properties of the aerosolized particles, the stability of drugs in these devices needs to be maintained during shelf life and usage. Especially during usage, it is the property of the actuated particles that are directly related to patients. Since inhalation devices produce millions of micro-particles in the aerosol state when actuated, bulk characterization of a single dose may be difficult. Moreover, the relatively large amount of sample for representative quantitative analysis imposed by composition heterogeneity, as introduced in Chapter 3, requires good sampling techniques. Also, Raman spectroscopy as a routine characterization technique in pharmaceutical areas (Buckley and Matousek, 2011; Vankeirsbilck et al., 2002c) is typically for the testing of drugs in forms of tablets (de Veij et al., 2007) and bulk powders (Wang et al., 2014). Therefore, a good sampling technique is required to enable representative sampling of the millions of respirable particles for subsequent Raman analysis.

As previously introduced, one method of extracting powders from pressurized metered dose inhalers involves immersing the canisters into liquid nitrogen, which has temperature of -195.8 °C, to freeze the propellant. The boiling point of the most

commonly used propellant, HFA 134a (1,1,1,2-Tetrafluoroethane), is -26.3°C. When the propellant is frozen, canisters can be safely opened with minimal propellant evaporation. Cut canisters were put into dry box with low humidity at room temperature to avoid moisture condensation, which may potentially modify the substances contained because moisture have already been proved to be able to significantly affect the physical and chemical stability of drugs (Ahlneck and Zografi, 1990). Propellant evaporation proceeds slowly at room temperature. Powders can be transferred to glass vials once the propellant is completely evaporated.

There are several disadvantages to this method. Firstly, the extremely low temperature of liquid nitrogen has the potential to introduce modifications to the contained drugs (Qiu and Park, 2001). Also, powders extracted from the slow evaporation process are different from residual dry powders from actuation, which is of more interests to us because it is in the same state as the drug powders inhaled by patients. This is because in suspension formulations, suspended drugs are in equilibrium with the low-concentration but saturated drug solution in propellant. Freezing and evaporation will cause the solutes to recrystallize and precipitate, resulting in higher fraction of crystalline phase in the extracted powder. For solution formulations, this drug extraction method is not even applicable because of the recrystallization process during slow evaporation. Lastly, the method is a destructive test, with at least one canister required per measurement. Thus even a very common stability study with 30 time points requires at least 30 identical canisters. Regardless of the high cost caused by the large number of canisters, measurements are then conducted on different canisters, which will introduce errors because of inter-canister sample variation.

In light of these drawbacks, an efficient and appropriate way of sampling drugs contained in metered dose inhalers or any other respirable aerosols for subsequent characterization, especially Raman measurement, is desired. Inspired by the traditional Anderson cascade impactor, a new low flow rate single-nozzle impactor is designed and described in this chapter.

4.2. Theory

Nomenclature:

d_a : Aerodynamic diameter

$d_{a,50}$: Cutoff aerodynamic diameter

d_j : Jet diameter, treated equal to nozzle diameter

u_0 : Undisturbed flow velocity in the nozzle

T : Nozzle throat length

S : Jet-to-plate distance

E : Collection efficiency by mass

τ : Particle relaxation time

s : Stopping distance

Re : Reynolds number, particle or flow

ρ_g : Density of gas

ρ_p : Particle density

ρ_0 : Unit density, 1000 kg/m^3

μ : Dynamic viscosity

Stk_{50} : Stokes number for 50% mass collection efficiency

Cc : Cunningham correction factor

C_d : Discharge coefficient

n : Number of jets

Q : Volume flow rate

λ : Mean free path of gas molecules

ΔP : Pressure drop

Two key features of all inertial impactors are the nozzle, which accelerates the gas flow, and the collection plate, which separates aerosol particles from the gas flow. A schematic of an inertial impactor nozzle with diameter d_j and throat length T and collection plate is shown in Figure 4.1. Most inertial impactors have multiple nozzles on each stage to accommodate high volume flow rate or higher aerosol load. Airflow coming from previous stage or outside is treated as laminar at the nozzle inlet with flow velocity u_0. The impaction plate is placed beneath the nozzle with separation distance S. As the gas approaches the impaction plate, the flow tends to turn and bend 90^o as depicted in the streamlines in Figure 4.1. If particles are present in the airflow, they will either follow the curved streamlines or diverge from the streamlines depending on the relative importance of particle inertia and drag forces.

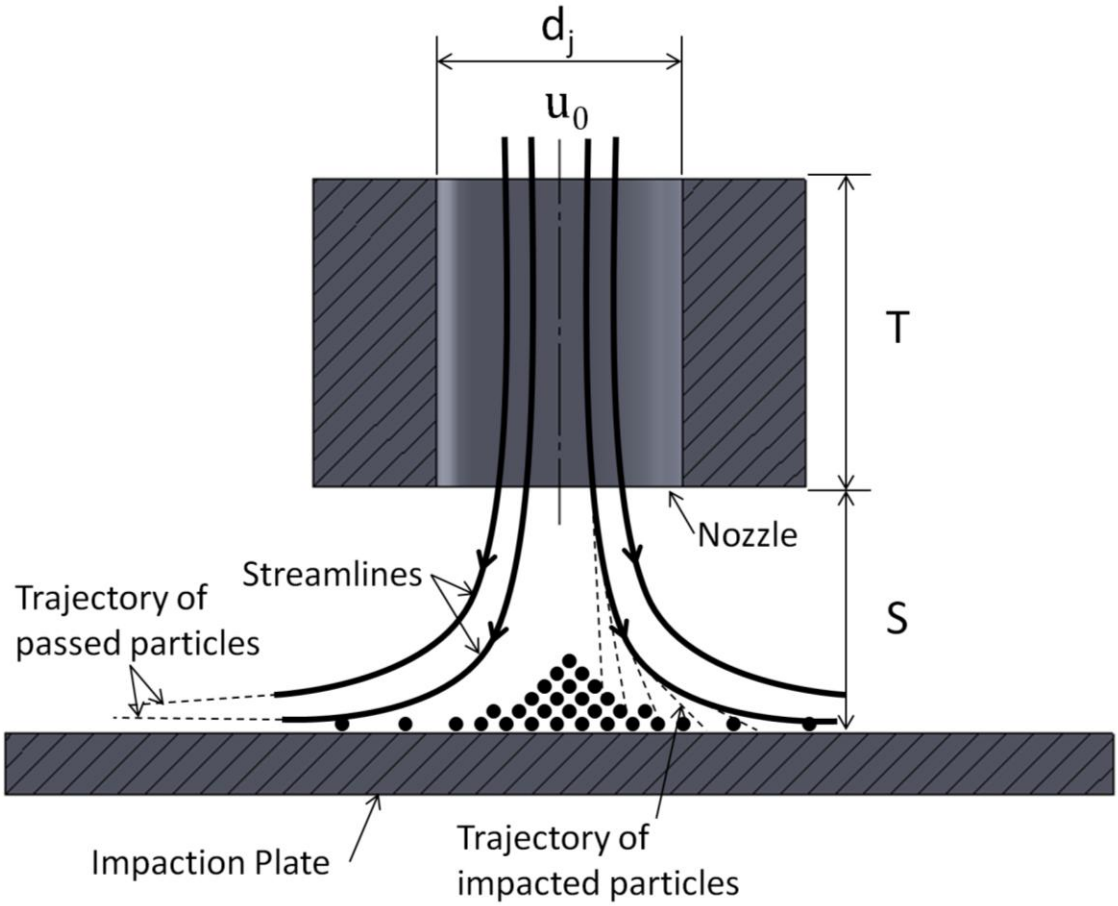

Figure 4.1. Schematic cross-sectional view of streamlines and particle trajectories of an circular impaction nozzle

Briefly speaking, the general principle of all inertial impactors is using the inertia of aerosols in curvilinear motion for collection or separation. Ideal impactors can collect particles larger than a specific aerodynamic diameter and let the others pass through. This critical aerodynamic diameter is usually referred to as cutoff size or cutoff diameter and is traditionally denoted as $d_{a,50}$. However for real cases, the collection efficiency (E) is not exactly a step-function of particle diameter, which means particles larger than the cutoff size are not collected with 100 percent efficiency, and also some undersized

particles will be trapped on the collection plate. As it is the most important characteristic of an impactor stage, determination of the impactor collection efficiency curve is critical.

The following theoretical discussion is limited to impactors operating with gas as the continuous phase. When airflow interacts with an obstacle, streamlines curve around the obstacle. Very small aerosol particles will follow the curved streamlines while very large particles tend to go in straight lines. The dimensionless Stokes number (*Stk*) is traditionally used to characterize curvilinear motion in this situation (Israel and Rosner, 1982).

$$Stk = \frac{Stopping\ Distance(s)}{Characteristic\ Dimention} = \frac{\tau u_0}{D}, \quad Re < 1 \quad (4.1)$$

$$Re = \frac{\rho_g u_0 d_P}{\mu} \quad (4.2)$$

$$\tau = \frac{\rho_P d_P^2 C_c(d_p)}{18\mu} = \frac{\rho_0 d_a^2 C_c(d_a)}{18\mu} \quad (4.3)$$

Particles will follow the streamlines perfectly when Stk$\ll$1 while they tend to move in straight lines when Stk$\gg$1. In Equation (4.3), the particle relaxation time τ is a characteristic time for a particle to adjust its velocity into equilibrium with the air flow. It can also be expressed as a function of unit density ρ_0 and its corresponding aerodynamic diameter d_a. The stopping distance of particle *s* is the maximum distance a particle with initial velocity u_0 in still air can travel in the absence of external forces. The characteristic dimension of the flow field may be the diameter of a cylindrical or spherical obstacle, the centerline radius of a curved flow, etc. In the case of an inertial impactor with a circular nozzle it is the radius of the nozzle ($d_j/2$). Particle Reynolds number *Re* is restricted to be smaller than 1 to guarantee Stokes flow around the particle so that Stokes law for drag

forces calculation remains valid. To calculate the stopping distance of particles with very large Reynolds number, which is very rare for respirable particles, some other equations need to be used (Mercer, 1973). It should be noted that Equation (4.2) also applies to flow in tube with the particle diameter d_{P} replaced by tube diameter, or nozzle diameter d_{j} for impactors.

Substituting the expression for τ in Equation (4.3) into Equation (4.1) yields the relationships between *Stk* and d_{p}, given in Equations (4.4) and (4.5). For particle collection applications, it is the relationship between collection efficiency and particle diameter that is of most interest. This relationship can be determined both theoretically and experimentally. Due to the linear relation between square root of Stokes number $\sqrt{Stk}$ and particle diameter d_{p} in Equation (4.5), collection efficiency curves may also be plotted against $\sqrt{Stk}$.

$$Stk = \frac{\rho_0 d_{\mathrm{a}}^2 u_0 C_{\mathrm{c}}(d_a)}{9\mu d_{\mathrm{j}}} \quad (4.4)$$

$$d_a = \sqrt{\frac{9\mu d_{\mathrm{j}} Stk}{\rho_0 u_0 C_{\mathrm{c}}(d_a)}} \quad (4.5)$$

Unfortunately, there is no analytical way of deriving the function of impactor collection efficiency. The theoretical determination of the relation between the collection efficiency and Stokes number requires complex simulations of airflow and a large number of particle trajectories to generate sufficient particle impaction data (Arffman et al., 2011). The general approach is to vary the particle aerodynamic diameter and injection location, and evaluate the simulated impaction probability for each aerodynamic diameter. According to the statistical impaction results of series of different

monodisperse aerosols, the collection efficiency can thus be calculated. The results of such simulations are dependent on the impactor geometry (Marple and Willeke, 1976a). For experimental determination, usually a series of monodisperse aerosols is measured to generate the efficiency curve for each impactor design. Fortunately, provided that the impactor is designed within certain guidelines, the collection efficiency curve versus Stokes number is the same when operated at the same Stokes number (Hinds, 2012).

The certain impactor design criteria to achieve invariant collection efficiency have already been well studied (Marple and Willeke, 1976a; Marple and Willeke, 1976b; Newton et al., 1977). The collection efficiency is affected by multiple parameters, including nozzle Reynolds number *Re*, jet-to-plate distance *S*, and nozzle throat length *T*. For round impactors, when nozzle Reynolds number, jet-plate distance to nozzle diameter ratio, and nozzle length to nozzle diameter ratio meet the requirement listed in Equations (4.6) – (4.8), the maximal sharpness of collection efficiency function can be achieved (Marple and Willeke, 1976a; Newton et al., 1977). Also, when these design criteria are met, Stk_{50} becomes a weak function of *Re*, *S* and *T*. Typical values of $\sqrt{Stk_{50}}$ ranges from 0.47 to 0.51 for various proven impactor designs (Hinds, 2012; Huang and Tsai, 2002; Marple and Willeke, 1976a; Rader and Marple, 1985). Impactor designs that follow the design guidelines of Equations (4.6) – (4.8) will thus have very predictable and stable efficiency curves, with the resulting collection efficiency or particle size measurements less sensitive to external experimental conditions, fabrication tolerances, or variations in operator procedure.

$$500 \le Re \le 3000 \quad (4.6)$$

$$S / d_j \ge 1 \quad (4.7)$$

$$T / d_j \geq 1 \quad (4.8)$$

Assuming a constant Stk_{50} as in Equation (4.9), the cutoff size can be easily calculated according to Equation (4.10). The equations are valid for both single nozzle impactors (n=1) and multiple nozzle impactors (n>1).

$$\sqrt{Stk_{50}} = 0.49 \text{ for circular nozzle} \quad (4.9)$$

$$d_{a,50} = \sqrt{\frac{9\mu d_j Stk_{50}}{\rho_0 u_0 C_c}} \quad (4.10)$$

Relating mean nozzle inlet gas velocity u_0 to volume flow rate Q as in Equation (4.11) and substituting into Equation (4.10) results in Equation (4.12). The slip correction factor Cc depends on λ, the mean free path of the gas molecules in the continuous phase, as in Equation (4.13) (Hinds, 2012; DeCarlo et al., 2004). Cc is thus a function of gas density and increases with higher temperature and lower pressure. The large correction factor in low-pressure conditions has been used to design low-pressure impactors to extend cutoff sizes to tens of nanometers.

$$u_0 = \frac{4Q}{n\pi d_j^2} \quad (4.11)$$

$$d_{a,50} = \sqrt{\frac{9n\pi\mu d_j^3 Stk_{50}}{4\rho_0 Q C_c}} \quad (4.12)$$

$$C_c = 1 + \frac{\lambda}{d_p}\left(2.34 + 1.05e^{-0.39\frac{d_p}{\lambda}}\right) \quad (4.13)$$

It's worth noting that even in impactors designed for atmospheric operation, low-pressure situations can happen because of the pressure drop across small nozzles. The pressure drop can be calculated according to (4.14) (Pozrikidis, 2009).

$$\Delta P = -\frac{\rho_g u_0^2}{2C_d^2} \quad (4.14)$$

Since Cunningham correction factor is a function of particle diameter d_p, Equation (4.10) or Equation (4.12) must be solved iteratively for the cutoff diameter. An empirical equation for cutoff diameter calculation incorporating the effects of pressure drop is available in Equation (4.15). The accuracy is within 2% for cutoff diameters larger than 0.2μm and operating pressure in the range of 91 to 101kPa (Hinds, 2012). For situations outside of these limits, the empirical relation no long applies and iterative solution of Equation (4.10) or Equation (4.12) is required.

$$d_{a,50} = \sqrt{\frac{9n\pi\mu d_j^3 Stk_{50}}{4\rho_0 Q}} - 0.078(\mu\text{m}) \quad (4.15)$$

4.3. Impactor Design

The major purpose of this impactor is for the collection of respirable aerosol particles for subsequent macro-Raman characterization. From the study discussed in Chapter 3, thousands and even millions of particles are typically required for quantitative composition analysis using Raman spectroscopy, especially for samples with very large non-respirable active carriers, *e.g.* lactose. To collect sufficient quantity of powder for representative Raman measurements, single-nozzle impactor is preferred. Multi-nozzle impactors disperse aerosols onto tens and even hundreds of spots on the collection plate, making it hard to efficiently gather the spread powders into the Raman sample holder cavity. While an alternative is to collect more powders to make each deposited powder spot large enough for Raman measurement, a much larger mass of powder would be

required. Thus, a single-nozzle design is the most efficient both in terms of sample preparation time and powder consumption.

For this application, the ideal case for collection is to have an impactor stage with extremely small cutoff diameter that can guarantee the collection of all passing particles. However, approaching zero cutoff size requires very high flow rate and small jet diameter, which will consequentially result in high local flow velocity. The high local flow velocity can significantly reduce the collection efficiency due to the increased probability of particle bounce and reentrainment.

Shown in Figure 4.2 for illustrative purposes are the cumulative mass distribution curves of four differently distributed particulate samples with different mass median diameters and geometric standard deviations. Assuming an impactor with a cutoff diameter of 3.0 μm and a perfect step collection efficiency function is used to sample the aerosol with MMD=10μm and GSD=2.5, 90% of the total aerosol by mass is expected to be collected on the impaction plate. This collection efficiency is satisfactory for collections of aerosol for most basic characterization purposes with the exception for cases with fractions of ultrafine particles, which will require special concerns. However, the same impactor with 3 μm cutoff diameter can only collect 50% of the aerosol with MMD=3 μm and GSD=2.5. Therefore, for powder samples with large particle sizes, it is unnecessary to use impactors with extremely small cutoff sizes, but also impactors with large cutoff diameter is not suitable for collecting particles with small sizes. Thus, it is desirable to have impactor stages with variable cutoff diameters so that large sized aerosols can be collected without approaching the high flow velocity that will blow off collected particles and also small sized particles can be collected with high efficiency.

But still, it is the collection of small particles that is most challenging so that the local flow velocity must be carefully designed to minimize particle bouncing.

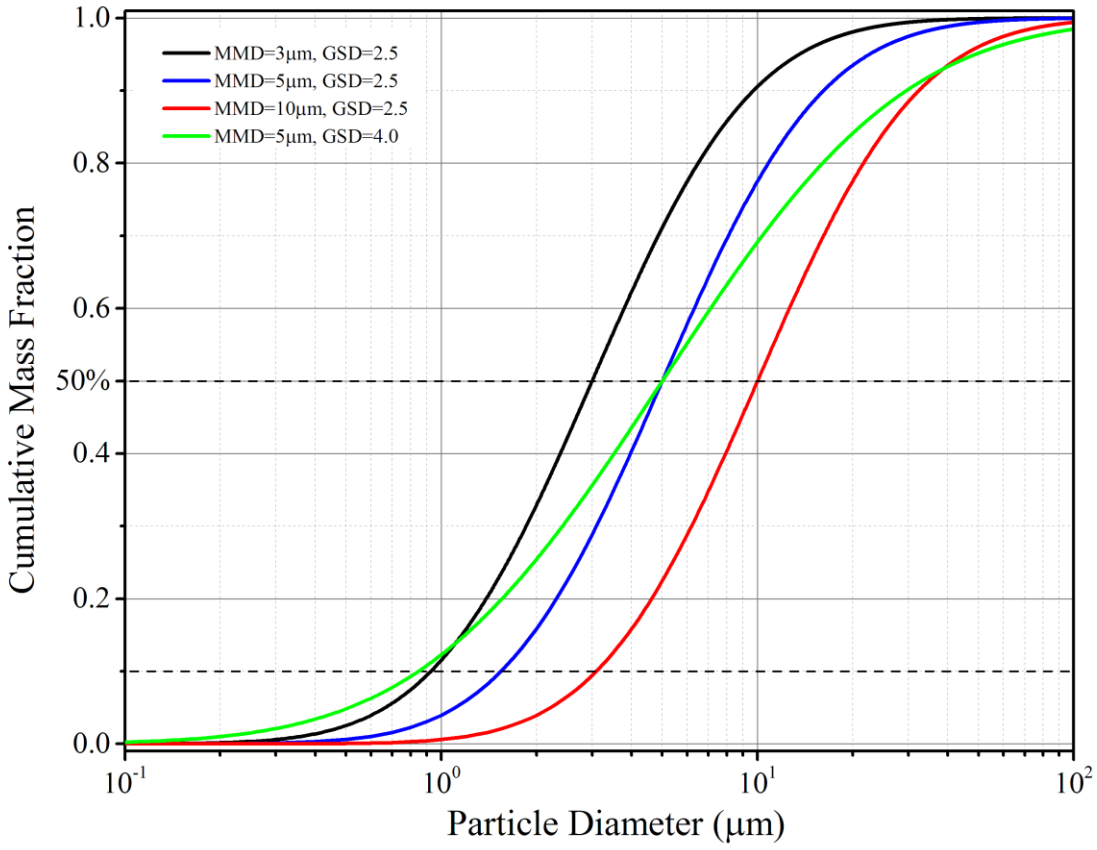

Figure 4.2. Cumulative mass fraction of three different particle size distributions

These considerations provide a justification for designing collection stages with different cutoff diameters. Moreover, by assembling the stages, particle sizing becomes one potential application requiring very small amount of particles. Before using the impactors for collection, roughly estimated cumulative mass distribution curves of the to-be-collected aerosol in the same style as Figure 4.2 can be used to decide the cutoff diameter, thus the collection stage, to be used.

To develop appropriate design criteria, mechanisms resulting in less than ideal collection efficiency require consideration. Particle loss from stages caused by particle bounce or reentrainment are usually referred to as particle bounce in general, and may become more likely as particles pile up in the impaction spot (Dunbar et al., 2005). It is a very common problem encountered in inertial impactors. As a result, these mechanisms may cause low collection efficiency compared to the theoretical expectation, shifting collection efficiency curves toward large particle sizes. The extent of particle bounce has been found to be dependent on the nature of collected particles *e.g.* solid or liquid, rigid or soft, properties of the impaction plate *e.g.* geometry, material, nature of the coating material, load of particles, etc. (Chang et al., 1999; Dzubay et al., 1976; Newton et al., 1990; Pak et al., 1992; Tsai and Cheng, 1995; Turner and Hering, 1987) The most widely used method of improving collection performance is by using a viscous coating material to modify the impaction surface (Pak et al., 1992). The effect of collection plate material also been studied (Chang et al., 1999; Newton et al., 1990). Impaction plates with different geometries such as conical, concave, partially enclosed cavity substrates have also proved to be useful (Kim and Yook, 2011). However for solid particles, another decisive factor is the local air flow velocity (Markowski, 1984). Higher flow velocity results in greater probability of reentrainment or bounce. Since coating materials may introduce contamination to the Raman spectra of samples of interest, a careful consideration of design factors enabling efficient collection without coating is required.

To provide design guidance, simple experiments were conducted to qualitatively explore the effect of flow velocity on plate deposition. Shown in Figure 4.3 was the collection result of a trial test conducted on a traditional Anderson cascade impactor. The

4^{th} stage of an Anderson cascade impactor with 400 0.53mm-diameter nozzles was modified by leaving two of the nozzles open and blocking all the remaining 398 ones. Air flow rate was controlled with an adjustable valve and measured with a flow meter. Commercial metered dose inhalers were actuated five times to generate aerosols for each case. Variable volume flow rates ranging from 0.2 L/min to 10.0 L/min was tested in order to find the upper limit of local flow velocity. Significant particle bounce was observed when the flow velocity was increased above 40 m/s. The two panels in Figure 4.3 correspond to collections with volume flow rate of 0.5 L/min (a) and 1.5 L/min (b) respectively. Local flow velocities and theoretical cutoff diameter were calculated to be 18.9 m/s and 0.97 μm for the lower flow rate case and 56.7 m/s, 0.53 μm for the higher flow case. In panel (b), at the higher flow rate, a dispersed ring of particles can be seen spread around the periphery of the mostly bare central jet zone. In panel (a), even though lower volume flow led to higher cutoff diameter, two distinct piles of particles could still be collected. Thus, assuming flow velocity is the main factor resulting in particle bounce and reentrainment, a rough design guideline for efficient particle collection can be developed.

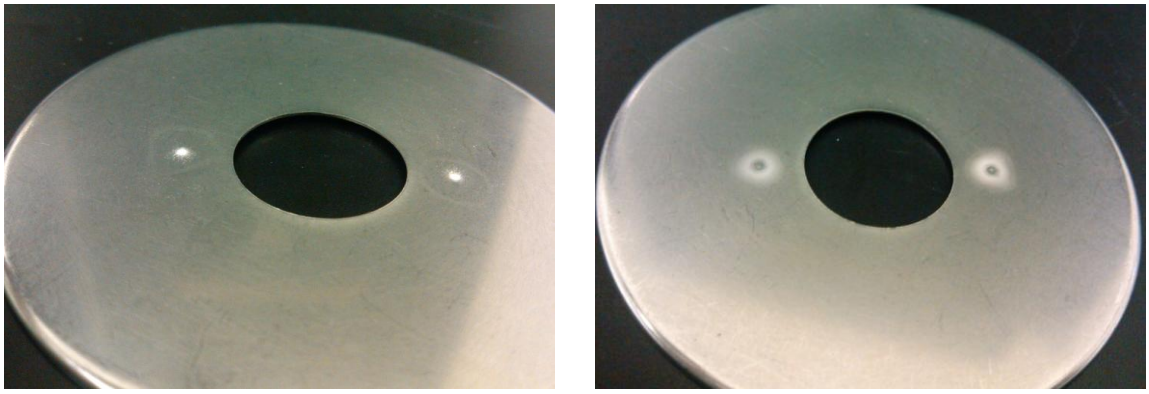

(a) (b)

Figure 4.3. Collected pharmaceutical powders using modified Anderson cascade impactor stage 4 with 0.53mm nozzle diameter: (a) Q=0.5L/min, u_0 =18.9m/s, $d_{a,50}$ =0.97μm; (b) Q=1.5L/min, u_0=56.7m/s, $d_{a,50}$=0.53μm

Rearranging the above Equation (4.11) and (4.15) and assuming constant correction factor, unit particle density, standard atmospheric pressure, and environmental temperature, we get the following relations:

$$d_{a,50} = k_1\sqrt{\frac{d_j^3}{Q}} - 0.078(\mu m) \quad (4.16)$$

$$u_0 = k_2\frac{Q}{d_j^2} \quad (4.17)$$

with k_1 and k_2 are constants calculated as:

$$k_1 = \sqrt{\frac{9n\pi\mu Stk_{50}}{4\rho_0}} = 1.76\times10^{-4}(m/s^{0.5}) \quad (4.18)$$

$$k_2 = \frac{4}{n\pi} = 1.27(s/m) \quad (4.19)$$

The dilemma here according to Equation (4.16) and (4.17) is that to have small enough cutoff diameters, d_j^3/Q should be small. Relatively high volume flow rate is preferred

also to prevent impactor internal wall deposition. However, small value of Q/d_j^2 is desired to avoid high local flow velocity. These two concerns impose restrictions on the selection of appropriate volume flow rate and nozzle diameters. Combining equations (4.16) and (4.17), we can also get the following relation between $d_{a,50}$, d_j and u_0.

$$d_{a,50} = k_1\sqrt{k_2}\sqrt{\frac{d_j}{u_0}} - 0.078(\mu m) = k_3\sqrt{\frac{d_j}{u_0}} - 0.078(\mu m) \quad (4.20)$$

$$k_3 = 1.98\times10^{-4}\ (m^{0.5}) \quad (4.21)$$

The interrelationships of Equations (4.16) - (4.21) are explored in Table 4.1. Considering the extreme cases for aerosol collection as a starting point, the concerns and restrictions include: Firstly, the minimum cutoff diameter should be at least smaller than 1μm with smaller values preferred because most respirable particles are in the range of 1-5 μm, which is the optimal size range for most oral inhalation products (Chow et al., 2007; Shekunov et al., 2007). Also, due to the increasing difficulties of machining nozzles with decreasing diameter (Zhao et al., 2002; Lorincz, 2013), minimum jet diameter is to be better kept larger than 0.2mm. Concerns regarding volume flow rate are mainly about having high volume flow to avoid internal wall deposition and in the meantime limiting the related local flow velocity within 40 m/s for all stages.

Table 4.1 Correlated values between jet flow velocity, cutoff diameter, nozzle diameter, and volume flow rate

u_0 (m/s)	d_j (mm)	$d_{a,50}$ (μm)	Q (L/min)
40	0.2	0.36	0.08
	0.5	**0.62**	**0.47**
	1.0	0.91	1.89
	2.0	1.32	7.56
	3.0	1.64	17.01
30	0.2	0.43	0.06
	0.5	0.73	0.35
	1.0	1.07	1.42
	2.0	1.54	5.67
	3.0	1.90	12.76
20	0.2	0.55	0.04
	0.5	0.91	0.24
	1.0	1.32	0.94
	2.0	1.90	3.78
	3.0	2.35	8.50

Comparing the listed values above, 0.5 L/min was selected as the designed volume flow rate, with a minimum cutoff diameter of about 0.62μm at local flow velocity of 40m/s with a 0.5mm nozzle diameter. Based on the 0.5 L/min volume flow rate, jet diameters for the other stages can be determined according to the desired cutoff diameter.

The collection plate is designed as shown in Figure 4.4(a). Multiple circular through holes allow gas flow to pass through. The mounting hole in the middle of the plate was designed to be compatible with standard scanning electron microscope (SEM) stub geometry. It makes the center of the stub surface the place where particle impactions happen. This removable impaction stub not only makes the transportation of collected particles much easier, but also further extends the application of this impactor such that the collected sample can be directly analyzed by SEM without further sample handling.

For Raman sampling, the collected powder pile can be directly pressed into the cavity of the sample holder, as shown in Figure 4.4(b).

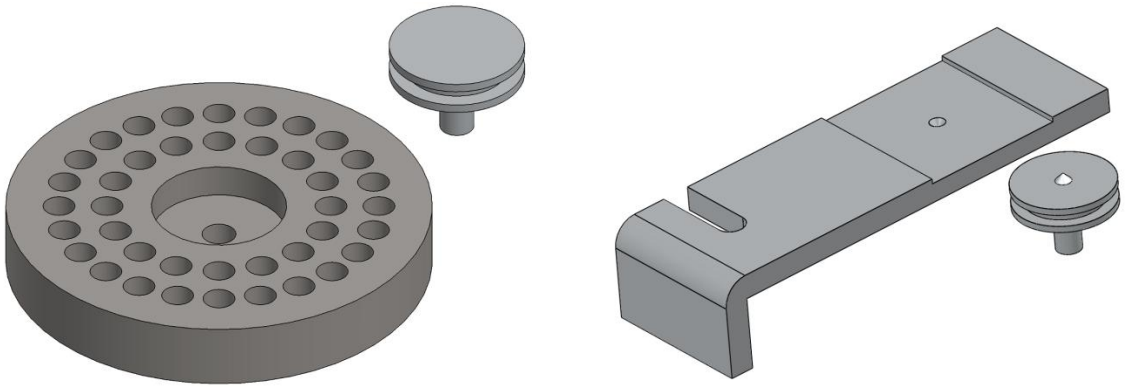

(a) (b)

Figure 4.4. Collection plate (a) and collected powder on SEM stub ready for transferring to Raman sample holder (b)

Shown in Figure 4.5 is a cross section view of the impactor assembled with four-stages. The impactor stages and collection plates were made of the pharmaceutical industry's preferred material 316-stainless steel because of its superior corrosion resistance imposed by possibilities of collecting chemically corrosive materials and subsequent cleaning with organic solvents, and excellent durability that will help maintain accuracy and extend impactor service life. 1060 aluminum alloy was used to make the SEM stubs, which can also be directly purchased from the market. All stages have the same outer diameter of 47 mm. The height of the individual stages varies from 23.5 mm to 27.7 mm with the first stage being the shortest and the final stage being the highest. The first stage is designed to interface with a standardized United States Pharmacopeia (USP) induction port, allowing sampling of the fraction of aerosol which passes through a model throat. Specifications of different stages are shown in the Table 4.2. The total height of the four assembled stages is slightly shorter than 10 centimeters.

In cases where efficient collection of most of an aerosol is desired, the combination of one middle stage that has desired cutoff diameter with the first and bottom stages is typically used, making the fist-sized setup very compact and mobile. Details and SolidWorks Drawings of the impactor design are available in Appendix A.

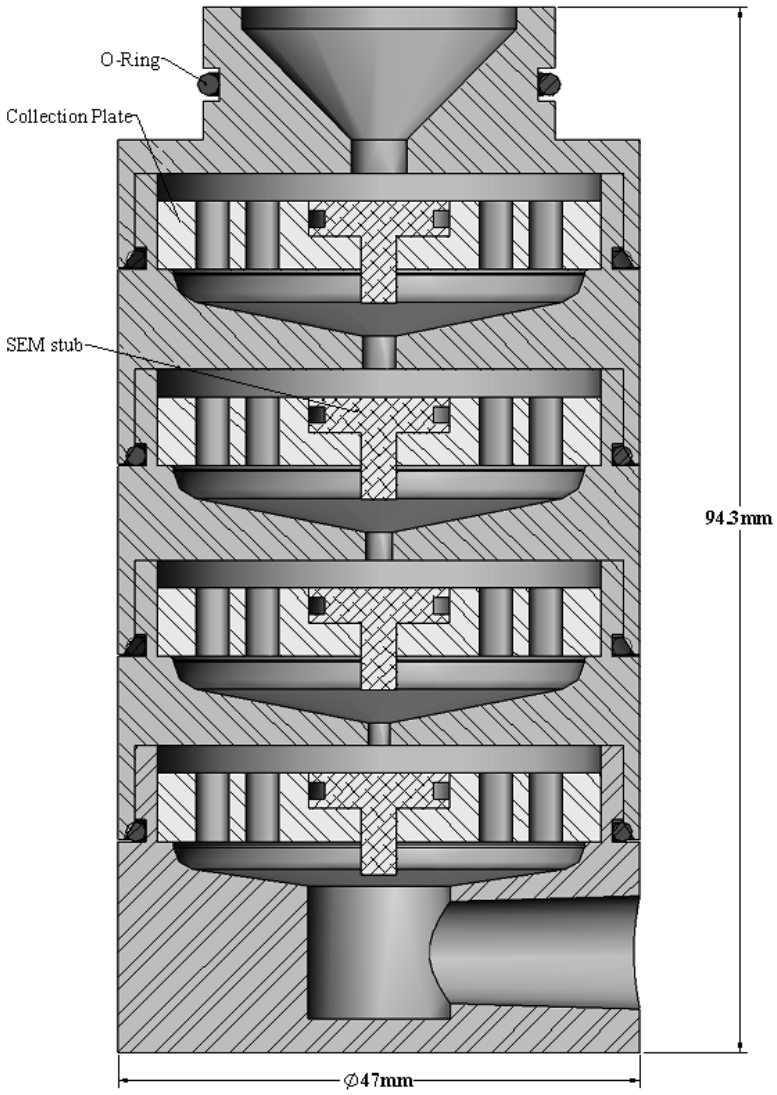

Figure 4.5. Cross section view of designed new impactor with 3 intermediate stages

Stage 0 is the first stage with a theoretical cutoff diameter of 21.12μm, which works as a pre-separator to exclude very large particles that may cause bouncing and reentrainment errors and even potentially block the nozzles in the following stages. Other

than the first stage, ten intermediate stages with various cutoff diameters covering the cutoff diameter range from 0.60μm to 9.92μm were manufactured to provide versatile sampling of a variety of aerosols. Different stage combinations can be used for different samples and different purposes. It should be noted that even with all stages assembled, the total pressure drop is only about 2kPa and 6kPa incorporating the discharge coefficient, which is well below the validity limit of empirical Equation (4.15) for the calculation of cutoff diameters.

Table 4.2 Specifications of designed impactor

Stage	Q (L/min)	d_j (mm)	$d_{a,50}$ (μm)	u_0 (m/s)	T (mm)	S (mm)	Re	S/d_j	T/d_j	ΔP (Pa)
0	0.5	4.95	**21.12**	0.43	3.00	2.5	141.73	0.51	0.61	0.11
1		3.00	**9.922**	1.18	3.00		233.86	0.83	1.00	0.84
2		2.40	**7.076**	1.84	2.50		292.33	1.04	1.04	2.04
3		1.90	**4.96**	2.94	2.00		369.26	1.32	1.05	5.20
4		1.65	**4.00**	3.90	2.00		425.20	1.52	1.21	9.14
5		1.40	**3.12**	5.41	1.50		501.13	1.79	1.07	17.64
6		1.20	**2.45**	7.37	1.50		584.66	2.08	1.25	32.69
7		1.00	**1.84**	10.61	1.00		701.59	2.50	1.00	67.78
8		0.85	**1.43**	14.69	1.00		825.40	2.94	1.18	129.84
9		0.70	**1.05**	21.65	1.00		1002.27	3.57	1.43	282.29
10		0.60	**0.82**	29.47	1.00		1169.31	4.17	1.67	522.98
11		0.50	**0.60**	42.44	1.00		1403.17	5.00	2.00	1084.45

Sealing of assembled stages is very important during aerosol collection to ensure a constant flow rate though the impactor. Buna-N O-rings were used to achieve seals at each stage. The compression springs used in traditional Anderson cascade impactors to seal the stages are not suitable for the newly designed impactor because these springs work only for fixed number of stages. A clamping device which is compatible with variable stack height was designed, and is shown in Figure 4.6. The clamp consists of three parts: bottom base, fully threaded sleeve, and an external-threaded compression plate. The assembled impactor can be sealed by inserting the compression plate into the

sleeve, adjusting its position in the sleeve according to the height of assembled stages to be sealed, loading the impactor stages, screwing the sleeve onto the base, and then compressing by tightening the sleeve.

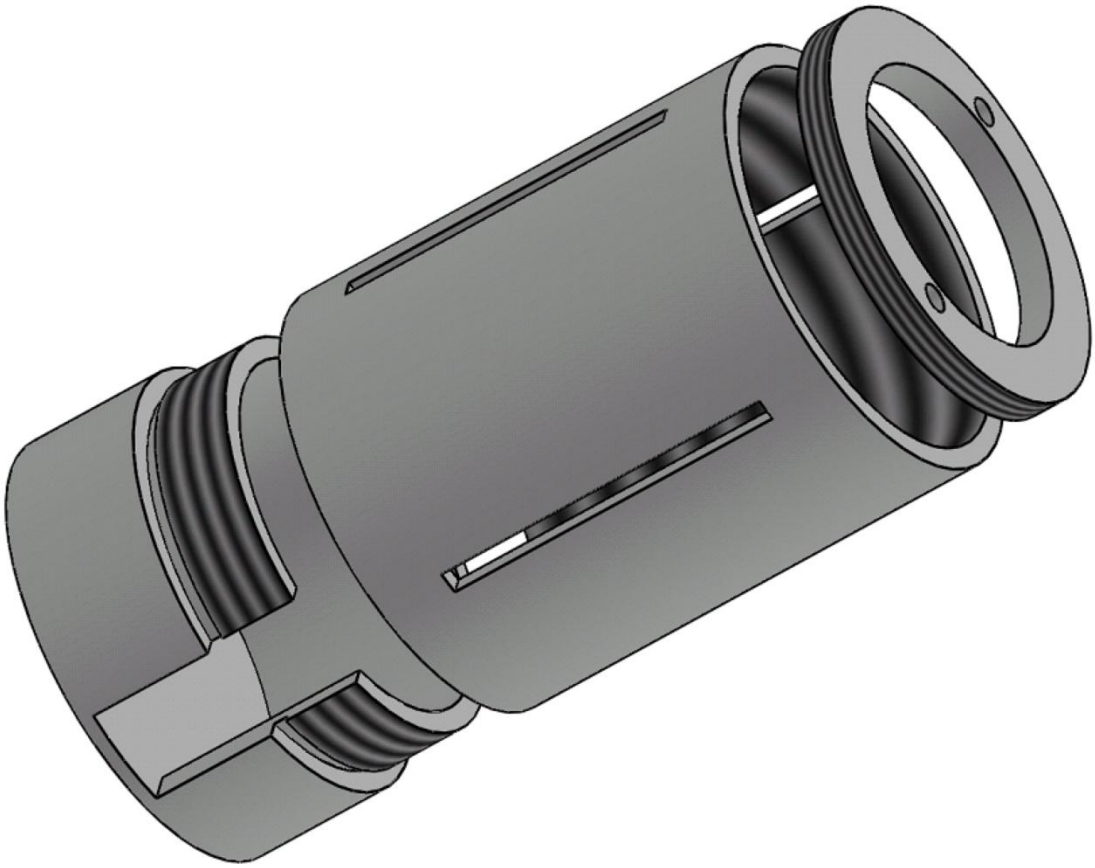

Figure 4.6. Sleeve clamp for sealing of stacked stages

4.4. Results and Discussion

The performance of the single nozzle cascade impactor was preliminarily evaluated by collecting aerosol doses from a commercial pressurized meter dose inhaler product. Seretide® 250 Evohaler® contains two active pharmaceutical ingredients: 25µg salmeterol xinafoate (SX) and 250µg fluticasone propionate (FP). Approximate literure values for the particle size distribution of the two components are MMD_{SX}=4.03, GSD_{SX}=2.33 and MMD_{FP}=3.53, GSD_{SX}=2.53 (Hoe et al., 2009; Taki et al., 2011). Hypothetical log-normal

cumulative mass distributions of both components were plotted in Figure 4.7 to assist the selection of collection plate. With 1µm cutoff diameter, more than 90% of the mixture of particles will be collected. Standard flow rate 0.5L/min and single middle stage with jet diameter of 0.70 mm was then selected based on Table 4.2. The chosen operating parameters correspond to a theoretical cutoff diameter of 1.05µm. One single dose was actuated into the USP induction port. The sampled particles piled up on the SEM stub as shown in Figure 4.8. The collected amount of sample was sufficient to fill the cavity of a Raman sample holder for subsequent analysis.

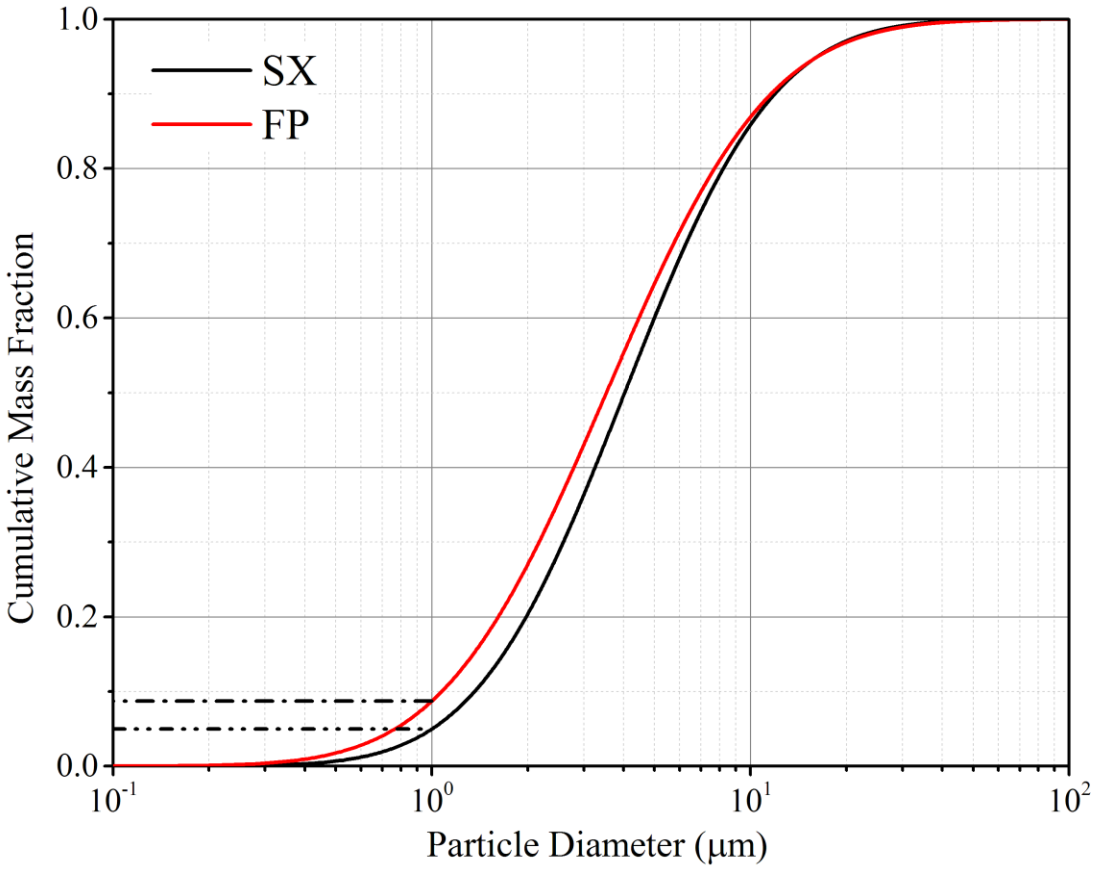

Figure 4.7. Cumulative mass distribution of salmeterol xinafoate and fluticasone propionate

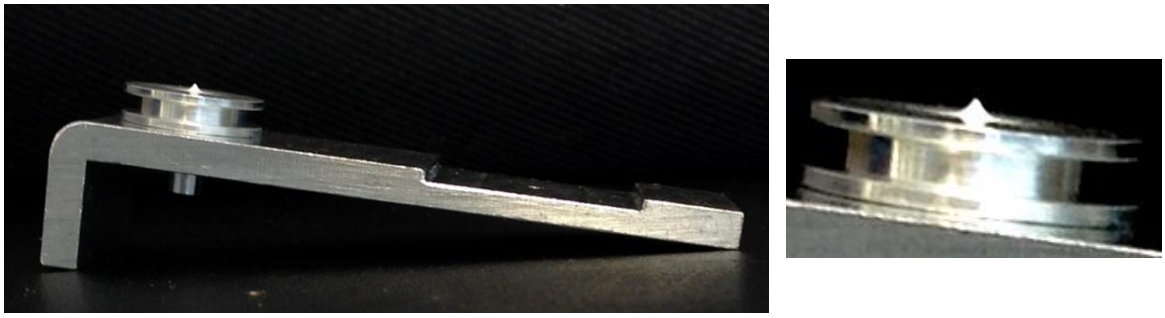

Figure 4.8. Collected pharmaceutical particles from one single pMDI actuation containing 300μg actives

4.5. Conclusion

A novel low flow rate single-nozzle impactor was designed to enable aerosol sampling from inhalation devices and subsequent Raman, SEM, or other characterization. The new impactor concentrates the powder of a single dose from a typical commercial meter dose inhaler onto a sample holder, enabling subsequent characterization, *e.g.* Raman, SEM. Using a removable stub as the collection plate makes the transfer of powders much easier for Raman measurement, SEM imaging, etc. Additionally, particle sizing over diameter range of 0.6 μm to 10 μm is possible by using the multi-stage configuration. Further, the unique design of the impactors should allow particle sizing based on very small sample mass.

4.6. References

Arffman, A., Marjamäki, M., Keskinen, J., 2011. Simulation of Low Pressure Impactor Collection Efficiency Curves. *Journal of Aerosol Science* 42, 329-340.

Buckley, K., Matousek, P., 2011. Recent Advances in the Application of Transmission Raman Spectroscopy to Pharmaceutical Analysis. *Journal of Pharmaceutical and Biomedical Analysis* 55, 645-652.

Chang, M., Kim, S., Sioutas, C., 1999. Experimental Studies on Particle Impaction and Bounce: Effects of Substrate Design and Material. *Atmospheric Environment* 33, 2313-2322.

Chow, A.H., Tong, H.H., Chattopadhyay, P., Shekunov, B.Y., 2007. Particle Engineering for Pulmonary Drug Delivery. *Pharmaceutical Research* 24, 411-437.

DeCarlo, P.F., Slowik, J.G., Worsnop, D.R., Davidovits, P., Jimenez, J.L., 2004. Particle Morphology and Density Characterization by Combined Mobility and Aerodynamic Diameter Measurements. Part 1: Theory. *Aerosol Science and Technology* 38, 1185-1205.

de Veij, M., Vandenabeele, P., Hall, K.A., Fernandez, F.M., Green, M.D., White, N.J., Dondorp, A.M., Newton, P.N., Moens, L., 2007. Fast Detection and Identification of Counterfeit Antimalarial Tablets by Raman Spectroscopy. *Journal of Raman Spectroscopy* 38, 181-187.

Dunbar, C., Kataya, A., Tiangbe, T., 2005. Reducing Bounce Effects in the Andersen Cascade Impactor. *International Journal of Pharmaceutics* 301, 25-32.

Dzubay, T., Hines, L., Stevens, R., 1976. Particle Bounce Errors in Cascade Impactors. *Atmospheric Environment (1967)* 10, 229-234.

Hinds, W.C., 2012. Aerosol Technology: Properties, Behavior, and Measurement of Airborne Particles. John Wiley & Sons.

Hoe, S., Young, P.M., Chan, H.-K., Traini, D., 2009. Introduction of the Electrical Next Generation Impactor (Engi) and Investigation of Its Capabilities for the Study of Pressurized Metered Dose Inhalers. *Pharmaceutical Research* 26, 431-437.

Huang, C.-H., Tsai, C.-J., 2002. Influence of Impaction Plate Diameter and Particle Density on the Collection Efficiency of Round-Nozzle Inertial Impactors. *Aerosol Science & Technology* 36, 714-720.

Israel, R., Rosner, D., 1982. Use of a Generalized Stokes Number to Determine the Aerodynamic Capture Efficiency of Non-Stokesian Particles from a Compressible Gas Flow. *Aerosol Science and Technology* 2, 45-51.

Kim, Y.-J., Yook, S.-J., 2011. Enhancement of Collection Efficiency of Inertial Impactors Using Elliptical Concave Impaction Plates. *Journal of Aerosol Science* 42, 898-908.

Lorincz, J., 2013. Drilling Small, Deep Holes with Precision: Quality Production Results for Aircraft, Medical Applications. *Manufacturing Engineering*, 79-86.

Markowski, G.R., 1984. Reducing Blowoff in Cascade Impactor Measurements. *Aerosol Science and Technology* 3, 431-439.

Marple, V.A., Willeke, K., 1976a. Impactor Design. *Atmospheric Environment (1967)* 10, 891-896.

Marple, V.A., Willeke, K., 1976b. Inertial Impactors: Theory, Design and Use, Fine Particles: Aerosol Generation, Measurement, Sampling, and Analysis, pp. 412-446.

Mercer, T., 1973. Aerosol Technology in Hazard Evaluation. Elsevier.

Newton, G., Raabe, O., Mokler, B., 1977. Cascade Impactor Design and Performance. *Journal of Aerosol Science* 8, 339-347.

Newton, G.J., Cheng, Y.S., Barr, E.B., Yeh, H.C., 1990. Effects of Collection Substrates on Performance and Wall Losses in Cascade Impactors. *Journal of Aerosol Science* 21, 467-470.

Pak, S.S., Liu, B.Y., Rubow, K.L., 1992. Effect of Coating Thickness on Particle Bounce in Inertial Impactors. *Aerosol Science and Technology* 16, 141-150.

Pozrikidis, C., 2009. Fluid Dynamics: Theory, Computation, and Numerical Simulation. Springer.

Qiu, Y., Park, K., 2001. Environment-Sensitive Hydrogels for Drug Delivery. *Advanced Drug Delivery Reviews* 53, 321-339.

Rader, D.J., Marple, V.A., 1985. Effect of Ultra-Stokesian Drag and Particle Interception on Impaction Characteristics. *Aerosol Science and Technology* 4, 141-156.

Shekunov, B.Y., Chattopadhyay, P., Tong, H.H., Chow, A.H., 2007. Particle Size Analysis in Pharmaceutics: Principles, Methods and Applications. *Pharmaceutical Research* 24, 203-227.

Taki, M., Ahmed, S., Marriott, C., Zeng, X.-M., Martin, G.P., 2011. The 'Stage-by-Stage'deposition of Drugs from Commercial Single-Active and Combination Dry Powder Inhaler Formulations. *European Journal of Pharmaceutical Sciences* 43, 225-235.

Tsai, C.-J., Cheng, Y.-H., 1995. Solid Particle Collection Characteristics on Impaction Surfaces of Different Designs. *Aerosol Science and Technology* 23, 96-106.

Turner, J.R., Hering, S.V., 1987. Greased and Oiled Substrates as Bounce-Free Impaction Surfaces. *Journal of Aerosol Science* 18, 215-224.

Vankeirsbilck, T., Vercauteren, A., Baeyens, W., Van der Weken, G., Verpoort, F., Vergote, G., Remon, J.P., 2002c. Applications of Raman Spectroscopy in Pharmaceutical Analysis. *TRAC Trends in Analytical Chemistry* 21, 869-877.

Wang, H., Boraey, M.A., Williams, L., Lechuga-Ballesteros, D., Vehring, R., 2014. Low-Frequency Shift Dispersive Raman Spectroscopy for the Analysis of Respirable Dosage Forms. *International Journal of Pharmaceutics* 469, 197-205.

Zhao, W., Wang, Z., Di, S., Chi, G., Wei, H., 2002. Ultrasonic and Electric Discharge Machining to Deep and Small Hole on Titanium Alloy. *Journal of Materials Processing Technology* 120, 101-106.

Chapter 5: Conclusions and Future Work

The applications of Raman spectroscopy to the analysis of respirable pharmaceutical dosage forms are explored in this thesis, including qualitative analysis using low-frequency signals, quantitative analysis of bulk compositions. As the first stage of testing particulate aerosols, a novel aerosol collection and sampling technique was developed by using a low flow rate single nozzle impactor.

Qualitative assessment of respirable pharmaceutical dosage forms using low-frequency Raman spectroscopy is investigated, and is proven to be very suitable and powerful for this application. Compared to traditional Raman analysis, low-frequency Raman is even more sensitive to the subtle changes of solid states because of its direct relation to the modes of inter-molecular vibrations. The applications include amorphous-crystalline phase differentiation, solid phase identification of multi-component systems, and also polymorph differentiation. Since inhalation drug products may involve amorphous or crystalline drugs and also combination products are becoming more prevalent, the technique is especially suited to stability analysis of respirable dosage forms. Low-frequency Raman thus has the potential to become a routinely employed analysis in stability studies.

The suitability of macro-Raman for quantitative analysis of bulk compositions of multi-component samples is discussed in Chapter 3. It is shown that Raman scattering volume is the key variable which influences the reliability of quantification results. A Monte-Carlo simulation was developed to determine the minimum sample volume required for representative sampling based on the particle size distributions and mass fractions of each component. Results indicate that sample volumes for representative

sampling of typical respirable dosage forms are on the order of 10^{-3} μL. However, this volume increases rapidly up to the order of 1 μL once non-respirable large carrier particles and low concentration actives are present. The scattering volume of the Raman setup used in the study varies between 0.0035 μL and 0.16 μL. Thus, for more challenging compositions, measurement replication and averaging or alternate sample presentation may be required to achieve suitable results with the current setup. The results of this chapter will be useful when building new Raman systems for quantifications of bulk compositions.

A novel single-nozzle cascade impactor for direct Raman sampling is introduced in Chapter 4. Proof-of-concept was demonstrated by sampling a single actuated dose from a pressurized metered dose inhaler containing 300 μg powders. However, more work needs to be done with the new impactor. To enable reliable collection or particle sizing with the appropriate stage(s), the collection efficiency curve of each impactor stage needs to be determined. This could be done by using a series of monodisperse aerosols or by measuring the size distribution of the collected or emitted fraction from a polydisperse feed aerosol with known size distribution (Hoffmann and Stein, 2002). Furthermore, the maximum powder load on each stage and its dependence on different factors, *e.g.* nozzle diameter and impaction surface should also be studied. The impactor shows promise in enabling evaluation of size dependent composition of multi-component respirable dosage forms by fractionating the respirable aerosols onto multiple stages and quantifying the size-dependent composition with the macro-Raman setup described in Chapter 2 and methodology described in Chapter 3. This would enable an unprecedented degree of scrutiny of the solid-state of aerosolized drugs.

References

Aardahl, C.L., Foss, W.R., Davis, E.J., 1996. The Effects of Optical Resonances on Raman Analysis of Liquid Aerosols. *Journal of Aerosol Science* 27, 1015-1033.

Achibat, T., Boukenter, A., Duval, E., 1993. Correlation Effects on Raman Scattering from Low-Energy Vibrational Modes in Glasses. Ii. Experimental Results. *The Journal of Chemical Physics* 99, 2046-2051.

Ahlneck, C., Zografi, G., 1990. The Molecular Basis of Moisture Effects on the Physical and Chemical Stability of Drugs in the Solid State. *International Journal of Pharmaceutics* 62, 87-95.

Al-Raoush, R., Alsaleh, M., 2007. Simulation of Random Packing of Polydisperse Particles. *Powder Technology* 176, 47-55.

Al-Zoubi, N., Koundourellis, J., Malamataris, S., 2002. Ft-Ir and Raman Spectroscopic Methods for Identification and Quantitation of Orthorhombic and Monoclinic Paracetamol in Powder Mixes. *Journal of Pharmaceutical and Biomedical Analysis* 29, 459-467.

Aldhous, P., 2005. Counterfeit Pharmaceuticals: Murder by Medicine. *Nature* 434, 132-136.

Andrew, J.J., 2006. Raman Microscopy and Imaging. *Encyclopedia of Analytical Chemistry*.

Arffman, A., Marjamäki, M., Keskinen, J., 2011. Simulation of Low Pressure Impactor Collection Efficiency Curves. *Journal of Aerosol Science* 42, 329-340.

Ayala, A.P., 2007. Polymorphism in Drugs Investigated by Low Wavenumber Raman Scattering. *Vibrational Spectroscopy* 45, 112-116.

Beard, M.C., Turner, G.M., Schmuttenmaer, C.A., 2002. Terahertz Spectroscopy. *Journal of Physical Chemistry B* 106, 7146-7159.

Bell, S.E., Beattie, J.R., McGarvey, J.J., Peters, K.L., Sirimuthu, N., Speers, S.J., 2004. Development of Sampling Methods for Raman Analysis of Solid Dosage Forms of Therapeutic and Illicit Drugs. *Journal of Raman Spectroscopy* 35, 409-417.

Blanpain-Avet, P., Hédoux, A., Guinet, Y., Paccou, L., Petit, J., Six, T., Delaplace, G., 2012. Analysis by Raman Spectroscopy of the Conformational Structure of Whey Proteins Constituting Fouling Deposits During the Processing in a Heat Exchanger. *Journal of Food Engineering* 110, 86-94.

Bloembergen, N., 1967. The Stimulated Raman Effect. *American Journal of Physics* 35, 989-1023.

Brittain, H.G., 2001. X-Ray Diffraction Iii: Pharmaceutical Applications of X-Ray Powder Diffraction. *Pharmaceutical Technology* 25(3), 142-150.

Brittain, H.G., Morris, K.R., Bugay, D.E., Thakur, A.B., Serajuddin, A., 1993. Solid-State Nmr and Ir for the Analysis of Pharmaceutical Solids: Polymorphs of Fosinopril Sodium. *Journal of Pharmaceutical and Biomedical Analysis* 11, 1063-1069.

Buckley, K., Matousek, P., 2011. Recent Advances in the Application of Transmission Raman Spectroscopy to Pharmaceutical Analysis. *Journal of Pharmaceutical and Biomedical Analysis* 55, 645-652.

Bugay, D.E., 2001. Characterization of the Solid-State: Spectroscopic Techniques. *Advanced Drug Delivery Reviews* 48, 43-65.

Bugay, D.E., Newman, A.W., Findlay, W.P., 1996. Quantitation of Cefepime· 2hcl Dihydrate in Cefepime· 2hcl Monohydrate by Diffuse Reflectance Ir and Powder X-Ray Diffraction Techniques. *Journal of Pharmaceutical and Biomedical Analysis* 15, 49-61.

Burger, A., Henck, J.O., Hetz, S., Rollinger, J.M., Weissnicht, A.A., Stoettner, H., 2000. Energy / Temperature Diagram and Compression Behavior of the Polymorphs of D-Mannitol. *Journal of Pharmaceutical Sciences* 89, 457-468.

Campbell Roberts, S.N., Williams, A.C., Grimsey, I.M., Booth, S.W., 2002. Quantitative Analysis of Mannitol Polymorphs. Ft-Raman Spectroscopy. *Journal of Pharmaceutical and Biomedical Analysis* 28, 1135-1147.

Campion, A., Kambhampati, P., 1998. Surface-Enhanced Raman Scattering. *Chemical Society Reviews* 27, 241-250.

Carey, P., 1982. Biochemical Applications of Raman and Resonance Raman Spectroscopes. Elsevier.

Chan, C.K., Flagan, R.C., Seinfeld, J.H., 1991. Resonance Structures in Elastic and Raman Scattering from Microspheres. *Applied Optics* 30(4), 459-467.

Chan, H.K., Clark, A.R., Feeley, J.C., Kuo, M.-C., Lehrman, S.R., Pikal-Cleland, K., Miller, D.P., Vehring, R., Lechuga-Ballesteros, D., 2004. Physical Stability of Salmon Calcitonin Spray-Dried Powders for Inhalation. *Journal of Pharmaceutical Sciences* 93, 792-804.

Chang, M., Kim, S., Sioutas, C., 1999. Experimental Studies on Particle Impaction and Bounce: Effects of Substrate Design and Material. *Atmospheric Environment* 33, 2313-2322.

Chen, Z.P., Li, L.M., Jin, J.W., Nordon, A., Littlejohn, D., Yang, J., Yu, R.Q., 2012. Quantitative Analysis of Powder Mixtures by Raman Spectrometry: The Influence of Particle Size and Its Correction. *Analytical Chemistry* 84(9), 4088-4094.

Chougule, M.B., Padhi, B.K., Jinturkar, K.A., Misra, A., 2007. Development of Dry Powder Inhalers. *Recent Patents on Drug Delivery & Formulation* 1, 11-21.

Chow, A.H., Tong, H.H., Chattopadhyay, P., Shekunov, B.Y., 2007. Particle Engineering for Pulmonary Drug Delivery. *Pharmaceutical Research* 24, 411-437.

Clas, S.D., Dalton, C.R., Hancock, B.C., 1999. Differential Scanning Calorimetry: Applications in Drug Development. *Pharmaceutical Science & Technology Today* 2, 311-320.

Costantino, H.R., Carrasquillo, K.G., Cordero, R.A., Mumenthaler, M., Hsu, C.C., Griebenow, K., 1998. Effect of Excipients on the Stability and Structure of Lyophilized Recombinant Human Growth Hormone. *Journal of Pharmaceutical Sciences* 87, 1412-1420.

Cruz-Cabeza, A.J., Bernstein, J., 2013. Conformational Polymorphism. *Chemical Reviews* 114, 2170-2191.

Dao, N.Q., 2006. Dispersive Raman Spectroscopy, Current Instrumental Designs. *Encyclopedia of Analytical Chemistry*.

Davis, E.J., Schweiger, G., 2002. The Airborne Microparticle: Its Physics, Chemistry, Optics, and Transport Phenomena. Springer.

Daviskas, E., Anderson, S.D., Gomes, K., Briffa, P., Cochrane, B., Chan, H., Young, I.H., Rubin, B.K., 2005. Inhaled Mannitol for the Treatment of Mucociliary Dysfunction in Patients with Bronchiectasis: Effect on Lung Function, Health Status and Sputum. *Respirology* 10, 46-56.

DeCarlo, P.F., Slowik, J.G., Worsnop, D.R., Davidovits, P., Jimenez, J.L., 2004. Particle Morphology and Density Characterization by Combined Mobility and Aerodynamic Diameter Measurements. Part 1: Theory. *Aerosol Science and Technology* 38, 1185-1205.

De Gelder, J., De Gussem, K., Vandenabeele, P., Moens, L., 2007. Reference Database of Raman Spectra of Biological Molecules. *Journal of Raman Spectroscopy* 38, 1133-1147.

de Veij, M., Vandenabeele, P., Hall, K.A., Fernandez, F.M., Green, M.D., White, N.J., Dondorp, A.M., Newton, P.N., Moens, L., 2007. Fast Detection and Identification of Counterfeit Antimalarial Tablets by Raman Spectroscopy. *Journal of Raman Spectroscopy* 38, 181-187.

De Wolf, I., 1996. Micro-Raman Spectroscopy to Study Local Mechanical Stress in Silicon Integrated Circuits. *Semiconductor Science and Technology* 11, 139.

Deisingh, A.K., 2005. Pharmaceutical Counterfeiting. *Analyst* 130, 271-279.

Deschamps, T., Martinet, C., de Ligny, D., Bruneel, J.L., Champagnon, B., 2012. Low-Frequency Raman Scattering under High Pressure in Diamond Anvil Cell: Experimental Protocol and Application to Geo_2 and Sio_2 Boson Peaks. *Journal of Non-Crystalline Solids* 358, 3156-3160.

Dickey, Fred M., Scott C. Holswade, eds. Laser beam shaping: theory and techniques. CRC Press, 2002.

Dunbar, C., Kataya, A., Tiangbe, T., 2005. Reducing Bounce Effects in the Andersen Cascade Impactor. *International Journal of Pharmaceutics* 301, 25-32.

Dzubay, T., Hines, L., Stevens, R., 1976. Particle Bounce Errors in Cascade Impactors. *Atmospheric Environment (1967)* 10, 229-234.

Ferraro, J.R., Nakamoto, K., 1994. Introductory Raman Spectroscopy. Academic Press, pp. 1-90.

Fini, G., 2004. Applications of Raman Spectroscopy to Pharmacy. *Journal of Raman Spectroscopy* 35, 335-337.

Hancock, B.C., Zografi, G., 1994. The Relationship between the Glass Transition Temperature and the Water Content of Amorphous Pharmaceutical Solids. *Pharmaceutical Research* 11, 471-477.

Hancock, B.C., Zografi, G., 1997. Characteristics and Significance of the Amorphous State in Pharmaceutical Systems. *Journal of Pharmaceutical Sciences* 86, 1-12.

Hedoux, A., Decroix, A.A., Guinet, Y., Paccou, L., Derollez, P., Descamps, M., 2011a. Low-and High-Frequency Raman Investigations on Caffeine: Polymorphism, Disorder and Phase Transformation. *The Journal of Physical Chemistry B* 115, 5746-5753.

Hedoux, A., Guinet, Y., Descamps, M., 2011b. The Contribution of Raman Spectroscopy to the Analysis of Phase Transformations in Pharmaceutical Compounds. *International Journal of Pharmaceutics* 417, 17-31.

Hédoux, A., Guinet, Y., Descamps, M., 2011. The Contribution of Raman Spectroscopy to the Analysis of Phase Transformations in Pharmaceutical Compounds. *International Journal of Pharmaceutics* 417, 17-31.

Hedoux, A., Guinet, Y., Paccou, L., 2011c. Analysis of the Mechanism of Lysozyme Pressure Denaturation from Raman Spectroscopy Investigations, and Comparison with Thermal Denaturation. *The Journal of Physical Chemistry B* 115, 6740-6748.

Hédoux, A., Paccou, L., Guinet, Y., Willart, J.F., Descamps, M., 2009. Using the Low-Frequency Raman Spectroscopy to Analyze the Crystallization of Amorphous Indomethacin. *European Journal of Pharmaceutical Sciences* 38, 156-164.

Heinz, A., Strachan, C.J., Gordon, K.C., Rades, T., 2009. Analysis of Solid-State Transformations of Pharmaceutical Compounds Using Vibrational Spectroscopy. *Journal of Pharmacy and Pharmacology* 61, 971-988.

Hendra, P., Jones, C., Warnes, G., 1991. Fourier Transform Raman Spectroscopy: Instrumentation and Chemical Applications. Ellis Horwood.

Hickey, A.J., Mansour, H.M., Telko, M.J., Xu, Z., Smyth, H.D.C., Mulder, T., McLean, R., Langridge, J., Papadopoulos, D., 2007a. Physical Characterization of Component Particles Included in Dry Powder Inhalers. I. Strategy Review and Static Characteristics. *Journal of Pharmaceutical Sciences* 96, 1282-1301.

Hickey, A.J., Mansour, H.M., Telko, M.J., Xu, Z., Smyth, H.D.C., Mulder, T., McLean, R., Langridge, J., Papadopoulos, D., 2007b. Physical Characterization of Component Particles Included in Dry Powder Inhalers. Ii. Dynamic Characteristics. *Journal of Pharmaceutical Sciences* 96, 1302-1319.

Hilfiker, R., 2006. Polymorphism: In the Pharmaceutical Industry. John Wiley & Sons.

Hinds, W.C., 2012. Aerosol Technology: Properties, Behavior, and Measurement of Airborne Particles. John Wiley & Sons.

Hoe, S., Ivey, J.W., Boraey, M.A., Shamsaddini-Shahrbabak, A., Javaheri, E., Matinkhoo, S., Finlay, W.H., Vehring, R., 2014. Use of a Fundamental Approach to Spray-Drying Formulation Design to Facilitate the Development of Multi-Component Dry Powder Aerosols for Respiratory Drug Delivery. *Pharmaceutical Research* 31, 449-465.

Hoe, S., Young, P.M., Chan, H.-K., Traini, D., 2009. Introduction of the Electrical Next Generation Impactor (Engi) and Investigation of Its Capabilities for the Study of Pressurized Metered Dose Inhalers. *Pharmaceutical Research* 26, 431-437.

Hoffmann, A.C., Stein, L.E., 2002. Gas Cyclones and Swirl Tubes. *Springer-Verlag Berlin Heidelberg* 2008.

Hoskins, L.C., 1975. Pure Rotational Raman Spectroscopy of Diatomic Molecules. *Journal of Chemical Education* 52, 568-572.

Huang, C.-H., Tsai, C.-J., 2002. Influence of Impaction Plate Diameter and Particle Density on the Collection Efficiency of Round-Nozzle Inertial Impactors. *Aerosol Science & Technology* 36, 714-720.

Huang, L.F., Tong, W.Q.T., 2004. Impact of Solid State Properties on Developability Assessment of Drug Candidates. *Advanced Drug Delivery Reviews* 56(3), 321-334.

Hubert, S., Briancon, S., Hedoux, A., Guinet, Y., Paccou, L., Fessi, H., Puel, F., 2011. Process Induced Transformations During Tablet Manufacturing: Phase Transition Analysis of Caffeine Using Dsc and Low Frequency Micro-Raman Spectroscopy. *International Journal of Pharmaceutics* 420, 76-83.

Huck-Jones, D., Jones, C., Castillio, J., Wolfgang, J., 2014. Combining Morphologically Directed Raman Spectroscopy with Next Generation Impactor Analysis to Improve the Understanding of Particle Properties of Dry Powder Inhalation Formulations. *Respiratory Drug Delivery 2014* 2, 481-484.

Hutsebaut, D., Vandenabeele, P., Moens, L., 2005. Evaluation of an Accurate Calibration and Spectral Standardization Procedure for Raman Spectroscopy. *Analyst* 130, 1204-1214.

Israel, R., Rosner, D., 1982. Use of a Generalized Stokes Number to Determine the Aerodynamic Capture Efficiency of Non-Stokesian Particles from a Compressible Gas Flow. *Aerosol Science and Technology* 2, 45-51.

Ivanda, M., Furić, K., Musić, S., Ristić, M., Gotić, M., Ristić, D., Gonçalves, R.R., 2007. Low Wavenumber Raman Scattering of Nanoparticles and Nanocomposite Materials. *Journal of Raman Spectroscopy* 38(6), 647-659.

Jackson, K., Young, D., Pant, S., 2000. Drug-Excipient Interactions and Their Affect on Absorption. *Pharmaceutical Science & Technology Today* 3, 336-345.

Johansson, J., Pettersson, S., Folestad, S., 2005. Characterization of Different Laser Irradiation Methods for Quantitative Raman Tablet Assessment. *Journal of Pharmaceutical and Biomedical Analysis* 39, 510-516.

Kelesidis, T., Kelesidis, I., Rafailidis, P.I., Falagas, M.E., 2007. Counterfeit or Substandard Antimicrobial Drugs: A Review of the Scientific Evidence. *Journal of Antimicrobial Chemotherapy* 60, 214-236.

Kim, Y.-J., Yook, S.-J., 2011. Enhancement of Collection Efficiency of Inertial Impactors Using Elliptical Concave Impaction Plates. *Journal of Aerosol Science* 42, 898-908.

Langkilde, F.W., Sjöblom, J., Tekenbergs-Hjelte, L., Mrak, J., 1997. Quantitative Ft-Raman Analysis of Two Crystal Forms of a Pharmaceutical Compound. *Journal of Pharmaceutical and Biomedical Analysis* 15, 687-696.

Li, X., Vogt, F.G., Hayes Jr, D., Mansour, H.M., 2014. Design, Characterization, and Aerosol Dispersion Performance Modeling of Advanced Spray-Dried Microparticulate/Nanoparticulate Mannitol Powders for Targeted Pulmonary Delivery as Dry Powder Inhalers. *Journal of Aerosol Medicine and Pulmonary Drug Delivery* 27, 81-93.

Lin-Vien, D., Colthup, N.B., Fateley, W.G., Grasselli, J.G., 1991. The Handbook of Infrared and Raman Characteristic Frequencies of Organic Molecules. Elsevier.

Lofthus, A., Krupenie, P. H. (1977). The spectrum of molecular nitrogen. *Journal of Physical and Chemical Reference Data*, 6(1), 113-307.

Lorincz, J., 2013. Drilling Small, Deep Holes with Precision: Quality Production Results for Aircraft, Medical Applications. *Manufacturing Engineering*, 79-86.

Mackin, L., Zanon, R., Park, J.M., Foster, K., Opalenik, H., Demonte, M., 2002. Quantification of Low Levels (< 10%) of Amorphous Content in Micronised Active Batches Using Dynamic Vapour Sorption and Isothermal Microcalorimetry. *International Journal of Pharmaceutics* 231(2), 227-236.

Malard, L., Pimenta, M., Dresselhaus, G., Dresselhaus, M., 2009. Raman Spectroscopy in Graphene. *Physics Reports* 473, 51-87.

Malinovsky, V., Sokolov, A., 1986. The Nature of Boson Peak in Raman Scattering in Glasses. *Solid State Communications* 57, 757-761.

Markowski, G.R., 1984. Reducing Blowoff in Cascade Impactor Measurements. *Aerosol Science and Technology* 3, 431-439.

Marple, V.A., Willeke, K., 1976a. Impactor Design. *Atmospheric Environment (1967)* 10, 891-896.

Marple, V.A., Willeke, K., 1976b. Inertial Impactors: Theory, Design and Use, Fine Particles: Aerosol Generation, Measurement, Sampling, and Analysis, pp. 412-446.

Martino, R., Malet-Martino, M., Gilard, V., Balayssac, S., 2010. Counterfeit Drugs: Analytical Techniques for Their Identification. *Analytical and Bioanalytical Chemistry* 398, 77-92.

Masuda, T., Yoshihashi, Y., Yonemochi, E., K., F., Uekusa, H., Terada, K., 2012. Cocrystallization and Amorphization Induced by Drug-Excipient Interaction Improves the Physical Properties of Acyclovir. *International Journal of Pharmaceutics* 422, 160-169.

McCreery, R.L., 2005. Raman Spectroscopy for Chemical Analysis. John Wiley & Sons.

Mendes, L.S., Oliveira, F.C., Suarez, P.A., Rubim, J.C., 2003. Determination of Ethanol in Fuel Ethanol and Beverages by Fourier Transform (Ft)-near Infrared and Ft-Raman Spectrometries. *Analytica Chimica Acta* 493, 219-231.

Mercer, T., 1973. Aerosol Technology in Hazard Evaluation. Elsevier.

Morris, M.D., Matousek, P., 2010. Emerging Raman Applications and Techniques in Biomedical and Pharmaceutical Fields. Springer.

Moser, C., Havermeyer, F., 2009. Ultra-Narrow-Band Tunable Laserline Notch Filter. *Applied Physics B* 95(3), 597-601.

Nangia, A., 2008. Conformational Polymorphism in Organic Crystals. *Accounts of Chemical Research* 41, 595-604.

Newman, A.W., Byrn, S.R., 2003. Solid-State Analysis of the Active Pharmaceutical Ingredient in Drug Products. *Drug Discovery Today* 8, 898-905.

Newman, S.P., 2005. Principles of Metered-Dose Inhaler Design. *Respiratory Care* 50, 1177-1190.

Newton, G., Raabe, O., Mokler, B., 1977. Cascade Impactor Design and Performance. *Journal of Aerosol Science* 8, 339-347.

Newton, G.J., Cheng, Y.S., Barr, E.B., Yeh, H.C., 1990. Effects of Collection Substrates on Performance and Wall Losses in Cascade Impactors. *Journal of Aerosol Science* 21, 467-470.

Newton, P.N., Green, M.D., Fernández, F.M., Day, N.P., White, N.J., 2006. Counterfeit Anti-Infective Drugs. *The Lancet Infectious Diseases* 6, 602-613.

O'Neill, M.A., Gaisford, S., 2011. Application and Use of Isothermal Calorimetry in Pharmaceutical Development. *International Journal of Pharmaceutics* 417, 83-93.

Pak, S.S., Liu, B.Y., Rubow, K.L., 1992. Effect of Coating Thickness on Particle Bounce in Inertial Impactors. *Aerosol Science and Technology* 16, 141-150.

Parker, F.S., 1983. Applications of Infrared, Raman, and Resonance Raman Spectroscopy in Biochemistry. Springer.

Pelletier, M.J., 1999. Analytical Applications of Raman Spectroscopy. Blackwell Publishing.

Pozrikidis, C., 2009. Fluid Dynamics: Theory, Computation, and Numerical Simulation. Springer.

Prime, D., Atkins, P.J., Slater, A., Sumby, B., 1997. Review of Dry Powder Inhalers. *Advanced Drug Delivery Reviews* 26, 51-58.

Qiu, Y., Park, K., 2001. Environment-Sensitive Hydrogels for Drug Delivery. *Advanced Drug Delivery Reviews* 53, 321-339.

Rader, D.J., Marple, V.A., 1985. Effect of Ultra-Stokesian Drag and Particle Interception on Impaction Characteristics. *Aerosol Science and Technology* 4, 141-156.

Rantanen, J., Wikström, H., Rhea, F.E., Taylor, L.S., 2005. Improved Understanding of Factors Contributing to Quantification of Anhydrate/Hydrate Powder Mixtures. *Applied Spectroscopy* 59, 942-951.

Ray, K.G., McCreery, R.L., 1997. Simplified Calibration of Instrument Response Function for Raman Spectrometers Based on Luminescent Intensity Standards. *Applied Spectroscopy* 51, 108-116.

Reidenberg, M.M., Conner, B.A., 2001. Counterfeit and Substandard Drugs. *Clinical Pharmacology and Therapeutics* 69, 189-193.

Robinson, M., Daviskas, E., Eberl, S., Baker, J., Chan, H.K., Anderson, S., Bye, P., 1999. The Effect of Inhaled Mannitol on Bronchial Mucus Clearance in Cystic Fibrosis Patients: A Pilot Study. *European Respiratory Journal* 14, 678-685.

Rogueda, P.G., Price, R., Smith, T., Young, P.M., Traini, D., 2011. Particle Synergy and Aerosol Performance in Non-Aqueous Liquid of Two Combinations Metered Dose Inhalation Formulations: An Afm and Raman Investigation. *Journal of Colloid and Interface Science* 361(2), 649-655.

Schwab, S.D., McCreery, R.L., 1987. Remote, Long-Pathlength Cell for High-Sensitivity Raman Spectroscopy. *Applied Spectroscopy* 41, 126-130.

Schweiger, G., 1990. Raman Scattering on Single Aerosol Particles and on Flowing Aerosols: A Review. *Journal of Aerosol Science* 21, 483-509.

Schweiger, G., 1991. Raman Scattering on Microparticles: Size Dependence. *Journal of the Optical Society of America B* 8, 1770-1778.

Shekunov, B.Y., Chattopadhyay, P., Tong, H.H., Chow, A.H., 2007. Particle Size Analysis in Pharmaceutics: Principles, Methods and Applications. *Pharmaceutical Research* 24, 203-227.

Smyth, H.D., 2003. The Influence of Formulation Variables on the Performance of Alternative Propellant-Driven Metered Dose Inhalers. *Advanced Drug Delivery Reviews* 55, 807-828.

Stöckle, R.M., Suh, Y.D., Deckert, V., Zenobi, R., 2000. Nanoscale Chemical Analysis by Tip-Enhanced Raman Spectroscopy. *Chemical Physics Letters* 318, 131-136.

Strachan, C.J., Rades, T., Gordon, K.C., Rantanen, J., 2007. Raman Spectroscopy for Quantitative Analysis of Pharmaceutical Solids. *Journal of Pharmacy and Pharmacology* 59, 179-192.

Strachan, C.J., Rades, T., Newnham, D.A., Gordon, K.C., Pepper, M., Taday, P.F., 2004. Using Terahertz Pulsed Spectroscopy to Study Crystallinity of Pharmaceutical Materials. *Chemical Physics Letters* 390, 20-24.

Szostak, R., Mazurek, S., 2002. Quantitative Determination of Acetylsalicylic Acid and Acetaminophen in Tablets by Ft-Raman Spectroscopy. *Analyst* 127, 144-148.

Taday, P.F., Newnham, D.A., 2004. Technological Advances in Terahertz Pulsed Systems Bring Far Infrared Spectroscopy into the Spotlight. *Spectroscopy Europe* 16, 20-25.

Taki, M., Ahmed, S., Marriott, C., Zeng, X.-M., Martin, G.P., 2011. The 'Stage-by-Stage'deposition of Drugs from Commercial Single-Active and Combination Dry Powder Inhaler Formulations. *European Journal of Pharmaceutical Sciences* 43, 225-235.

Tandon, P., Förster, G., Neubert, R., Wartewig, S., 2000. Phase Transitions in Oleic Acid as Studied by X-Ray Diffraction and Ft-Raman Spectroscopy. *Journal of Molecular Structure* 524, 201-215.

Taylor, L.S., Langkilde, F.W., 2000. Evaluation of Solid-State Forms Present in Tablets by Raman Spectroscopy. *Journal of Pharmaceutical Sciences* 89, 1342-1353.

Taylor, L.S., Zografi, G., 1998. The Quantitative Analysis of Crystallinity Using Ft-Raman Spectroscopy. *Pharmaceutical Research* 15, 755-761.

Tedesco, J.M., Davis, K.L., 1999. Calibration of Dispersive Raman Process Analyzers, Photonics East (ISAM, VVDC, IEMB). International Society for Optics and Photonics, pp. 200-212.

Tsai, C.-J., Cheng, Y.-H., 1995. Solid Particle Collection Characteristics on Impaction Surfaces of Different Designs. *Aerosol Science and Technology* 23, 96-106.

Turner, J.R., Hering, S.V., 1987. Greased and Oiled Substrates as Bounce-Free Impaction Surfaces. *Journal of Aerosol Science* 18, 215-224.

Vankeirsbilck, T., Vercauteren, A., Baeyens, W., Van der Weken, G., Verpoort, F., Vergote, G., Remon, J.P., 2002a. Applications of Raman Spectroscopy in Pharmaceutical Analysis. *Trends in Analytical Chemistry* 21, 869-877.

Vankeirsbilck, T., Vercauteren, A., Baeyens, W., Van der Weken, G., Verpoort, F., Vergote, G., Remon, J.P., 2002b. Applications of Raman Spectroscopy in Pharmaceutical Analysis. *TrAC Trends in Analytical Chemistry* 21, 869-877.

Vankeirsbilck, T., Vercauteren, A., Baeyens, W., Van der Weken, G., Verpoort, F., Vergote, G., Remon, J.P., 2002c. Applications of Raman Spectroscopy in Pharmaceutical Analysis. *TRAC Trends in Analytical Chemistry* 21, 869-877.

Vehring, R., 1998. Linear Raman Spectroscopy on Aqueous Aerosols: Influence of Nonlinear Effects on Detection Limits. *Journal of Aerosol Science* 29, 65-79.

Vehring, R., 2005. Red-Excitation Dispersive Raman Spectroscopy Is a Suitable Technique for Solid-State Analysis of Respirable Pharmaceutical Powders. *Applied Spectroscopy* 59, 286-292.

Vehring, R., Aardahl, C.L., Schweiger, G., Davis, E.J., 1998. The Characterization of Fine Particles Originating from an Uncharged Aerosol: Size Dependence and Detection Limits for Raman Analysis. *Journal of Aerosol Science* 29, 1045-1061.

Vippagunta, S.R., Brittain, H.G., Grant, D.J., 2001a. Crystalline Solids. *Advanced Drug Delivery Reviews* 48, 3-26.

Vippagunta, S.R., Brittain, H.G., Grant, D.J., 2001b. Crystalline Solids. *Advanced Drug Delivery Reviews* 48, 3-26.

Voutsas, A., Hatalis, M., Boyce, J., Chiang, A., 1995. Raman Spectroscopy of Amorphous and Microcrystalline Silicon Films Deposited by Low-Pressure Chemical Vapor Deposition. *Journal of Applied Physics* 78, 6999-7006.

Wang, H., Boraey, M.A., Williams, L., Lechuga-Ballesteros, D., Vehring, R., 2014. Low-Frequency Shift Dispersive Raman Spectroscopy for the Analysis of Respirable Dosage Forms. *International Journal of Pharmaceutics* 469, 197-205.

Wartewig, S., Neubert, R.H., 2005a. Pharmaceutical Applications of Mid-Ir and Raman Spectroscopy. *Advanced Drug Delivery Reviews* 57, 1144-1170.

Wartewig, S., Neubert, R.H.H., 2005b. Pharmaceutical Applications of Mid-Ir and Raman Spectroscopy. *Advanced Drug Delivery Reviews* 57, 1144-1170.

Weber, W.H., Merlin, R., 2000. Raman Scattering in Materials Science. Springer.

Willart, J., Descamps, M., 2008. Solid State Amorphization of Pharmaceuticals. *Molecular Pharmaceutics* 5, 905-920.

Witkowski, M.R., 2005. The Use of Raman Spectroscopy in the Detection of Counterfeit and Adulterated Pharmaceutical Products. *American Pharmaceutical Review* 8, 56.

Wunderlich, B., 1999. A Classification of Molecules, Phases, and Transitions as Recognized by Thermal Analysis. *Thermochimica Acta* 340, 37-52.

Xie, Y., Cao, W., Krishnan, S., Lin, H., Cauchon, N., 2008. Characterization of Mannitol Polymorphic Forms in Lyophilized Protein Formulations Using a Multivariate Curve Resolution (Mcr)-Based Raman Spectroscopic Method. *Pharmaceutical Research* 25, 2292-2301.

York, P., 1983. Solid-State Properties of Powders in the Formulation and Processing of Solid Dosage Forms. *International Journal of Pharmaceutics* 14, 1-28.

Yu, L., 2001. Amorphous Pharmaceutical Solids: Preparation, Characterization and Stabilization. *Advanced Drug Delivery Reviews* 48, 27-42.

Zeitler, J.A., Taday, P.F., Newnham, D.A., Pepper, M., Gordon, K.C., Rades, T., 2007. Terahertz Pulsed Spectroscopy and Imaging in the Pharmaceutical Setting-a Review. *Journal of Pharmacy and Pharmacology* 59, 209-223.

Zhang, G.G.Z., Law, D., Schmitt, E.A., Qiu, Y., 2004. Phase Transformation Considerations During Process Development and Manufacture of Solid Oral Dosage Forms. *Advanced Drug Delivery Reviews* 56, 371-390.

Zhao, W., Wang, Z., Di, S., Chi, G., Wei, H., 2002. Ultrasonic and Electric Discharge Machining to Deep and Small Hole on Titanium Alloy. *Journal of Materials Processing Technology* 120, 101-106.

Appendix A

Drawing NO.

HW 001 First Stage

HW 002 Final Stage

HW 003 Collection Plate

HW 004 Middle Stages

HW 101 Bottom Base of Sleeve Clamp

HW 102-01 Sleeve of Sleeve Clamp (1~4 stages)

HW 102-02 Sleeve of Sleeve Clamp (5~7 stages)

HW 103 Compression plate of Sleeve Clamp

NOTES: (UNLESS OTHERWISE SPECIFIED)

1. SURFACE TO CLEAN AND BURR FREE
2. ALL NORMINAL RIGHT ANGLE EDGES CAN HAVE R0.1 MAX FILLET
3. ISO TOLERANCE SYSTEMS (ISO286/ANSI B4.2-1978)ARE USED FOR LIMITS AND FITS

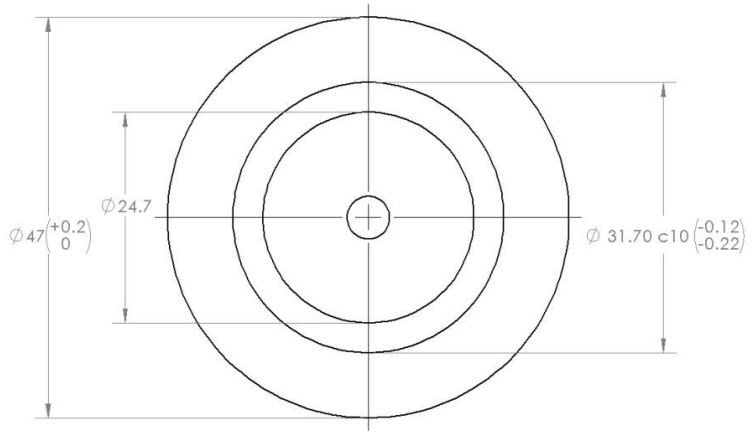

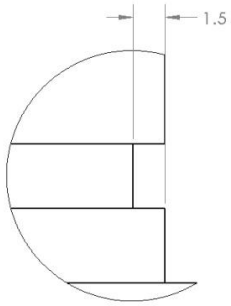

DETAIL B
SCALE 5 : 1

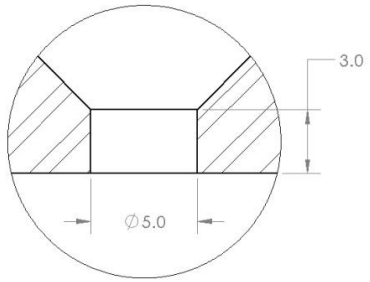

DETAIL C
SCALE 5 : 1

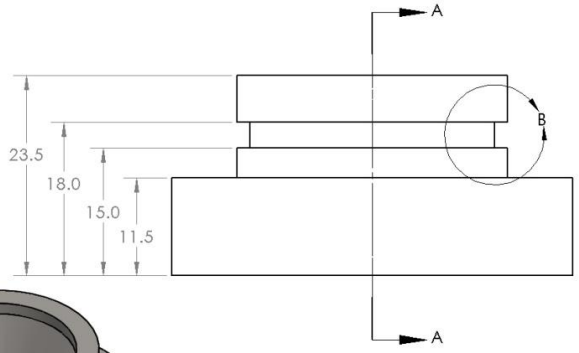

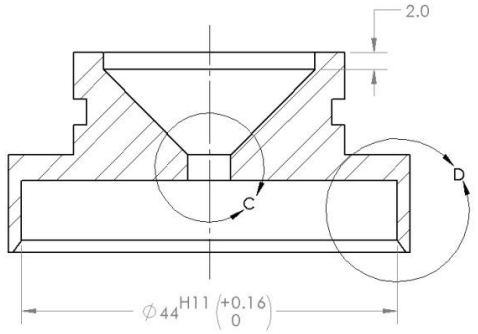

SECTION A-A

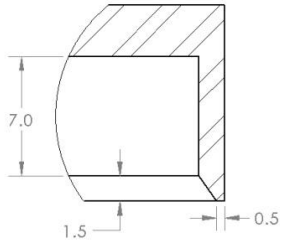

DETAIL D
SCALE 4 : 1

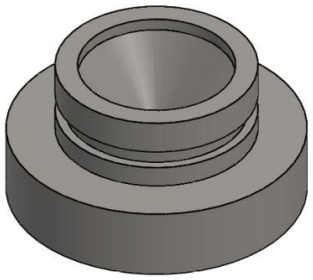

Unless otherwise specified	TITLE: Modified ACI First Stage			UNIVERSITY OF ALBERTA EDMONTON·ALBERTA·CANADA	
DIMENSIONS ARE IN MILIMETERS TOLERANCES: ANGULAR: ± 1° One PLACE DECIMAL: ± 0.1 Two PLACE DECIMAL: ±0.05		Name	Date	MATERIAL: 316 Stainless Steel	DWG NO. HW 001 SIZE A3
Surface Finish: 0.4 or better	Drawn	H.Wang	5/23/2014		
Revision	Checked	J.Ivey	5/27/2014		
	Approved			WEIGHT:	SCALE:2:1 SHEET 1 OF 1

NOTES: (UNLESS OTHERWISE SPEDIFIED)

1. PART TO BE CLEAN AND BURR FREE
2. ALL NOMINAL RIGHT ANGLE EDGES CAN HAVE R0.1 MAX FILLET
3. ISO TOLERANCE SYSTEMS (ISO286/ANSI B4.2-1978)ARE USED FOR LIMITS AND FITS

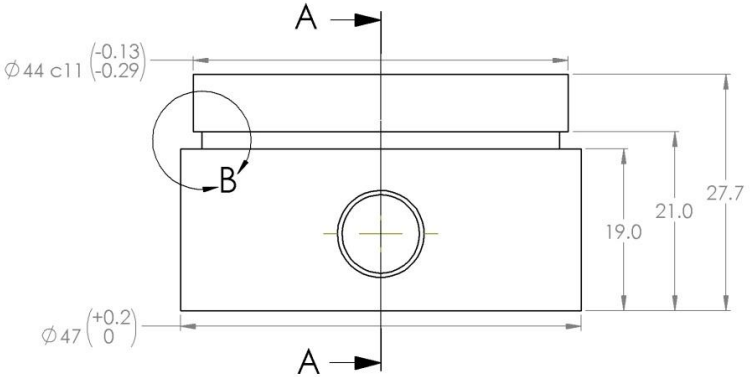

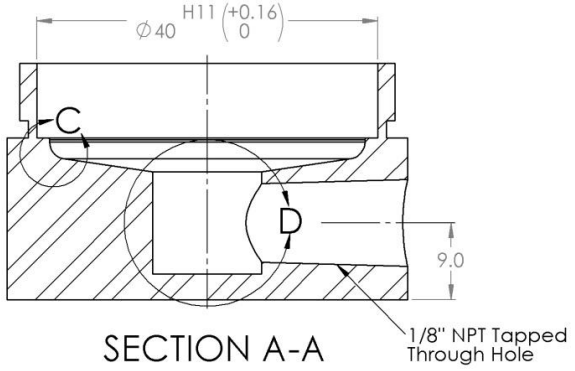

SECTION A-A

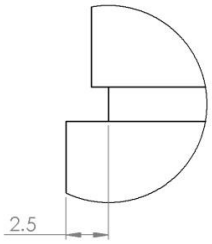

DETAIL B
SCALE 4 : 1

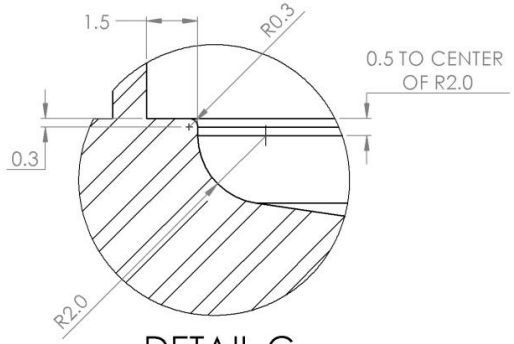

DETAIL C
SCALE 8 : 1

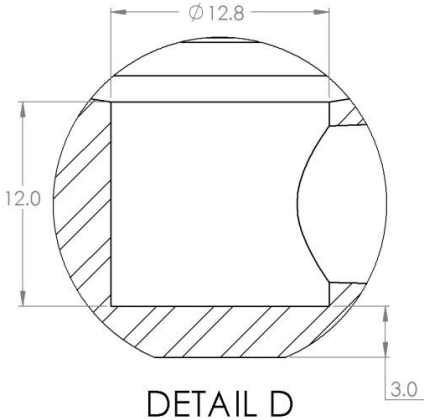

DETAIL D
SCALE 4 : 1

Unless otherwise specified	TITLE: Modified ACI Final Stage			UNIVERSITY OF ALBERTA EDMONTON·ALBERTA·CANADA	
DIMENSIONS ARE IN MILIMETERS TOLERANCES: ANGULAR: ± 1° One PLACE DECIMAL: ± 0.1 Two PLACE DECIMAL: ± 0.05		Name	Date	MATERIAL:	DWG NO.	SIZE
Surface Finish: 0.4 or better	Drawn	H.Wang	5/26/2014	316 Stainless Steel	HW 002	A3
Revision	Checked	J.Ivey	5/27/2014			
	Approved			WEIGHT:	SCALE:2:1	SHEET 1 OF 1

NOTES: (UNLESS OTHERWISE SPEDIFIED)

1. PART TO BE CLEAN AND BURR FREE
2. ALL NOMINAL RIGHT ANGLE EDGES CAN HAVE R0.1 MAX FILLET
3. ISO TOLERANCE SYSTEMS (ISO286/ANSI B4.2-1978)ARE USED FOR LIMITS AND FITS

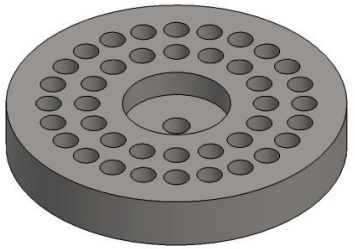

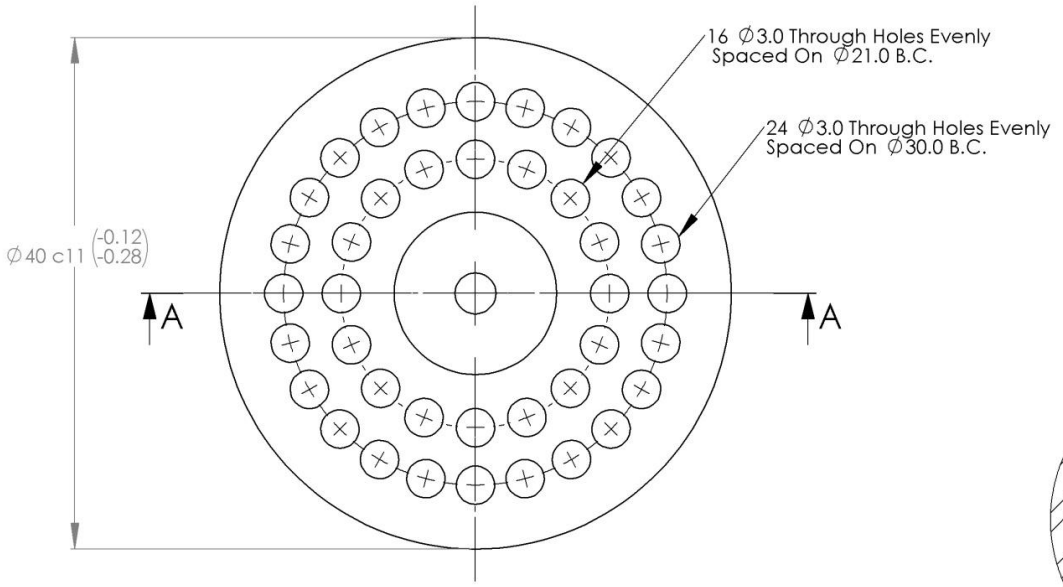

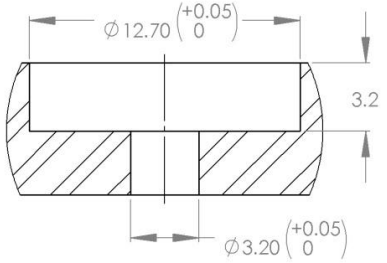

DETAIL B
SCALE 5 : 1

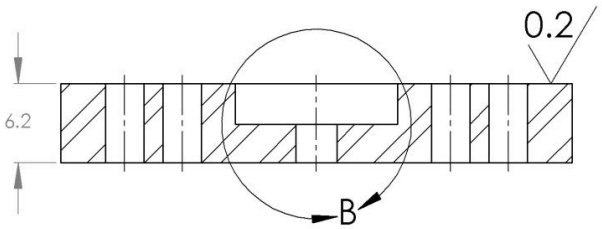

SECTION A-A
SCALE 3 : 1

Unless otherwise specified	TITLE: Modified ACI Collection Plate			UNIVERSITY OF ALBERTA EDMONTON·ALBERTA·CANADA		
DIMENSIONS ARE IN MILLIMETERS TOLERANCES: ANGULAR: ± 1° One PLACE DECIMAL: ± 0.1 Two PLACE DECIMAL: ± 0.05		Name	Date	MATERIAL:	DWG NO.	SIZE
Surface Finish: 0.4 or better	Drawn	H.Wang	5/26/2014	316 Stainless Steel	HW 003	A3
Revision	Checked	J.Vey	5/27/2014			
	Approved			WEIGHT:	SCALE:2:1	SHEET 1 OF 1

NOTES: (UNLESS OTHERWISE SPECIFIED)

1. ALL 11 CONFIGURATIONS ARE TO BE MACHINED
2. VARIABLE DIMENSIONS ARE **dj, T, H** AS INDICATED
3. SURFACE TO BE CLEAN AND BURR FREE
4. ISO TOLERANCE SYSTEMS (ISO286/ANSI B4.2-1978)ARE USED FOR LIMITS AND FITS
5. ALL NOMINAL RIGHT ANGLE EDGES CAN HAVE R0.1 MAX FILLET

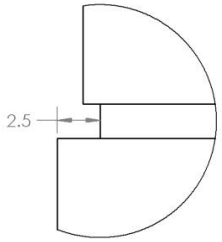

DETAIL B
SCALE 4 : 1

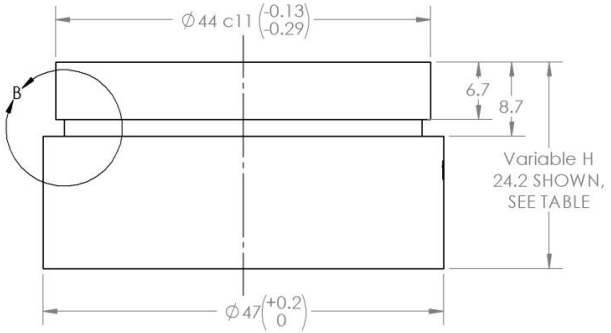

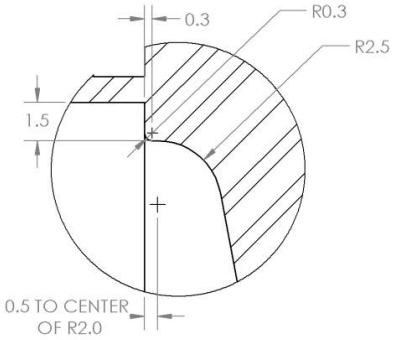

DETAIL C
SCALE 6 : 1

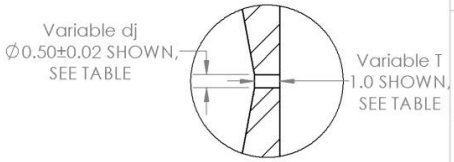

DETAIL E
SCALE 6 : 1

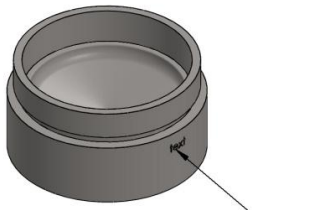

Deboss Feature indicating dj
10.5 ±0.2mm to the baseline
Size: Hight=3mm Depth=0.5mm MAX

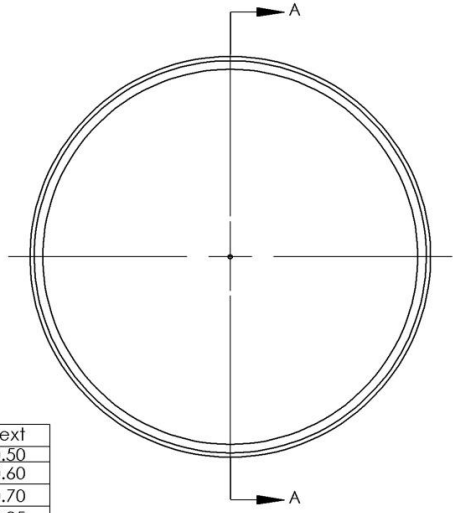

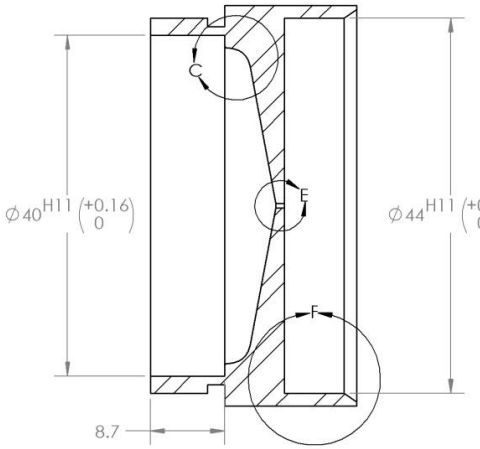

SECTION A-A

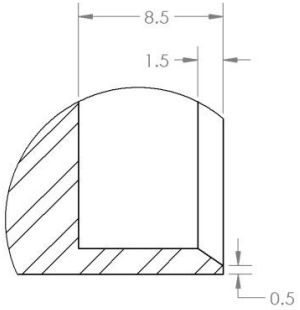

DETAIL F
SCALE 4 : 1

Stage #	dj(mm)	T(mm)	H(mm)	text
1	0.50 ±0.02	1.0	24.2	0.50
2	0.60 ±0.02	1.0	24.2	0.60
3	0.70 ±0.02	1.0	24.2	0.70
4	0.85 ±0.02	1.0	24.2	0.85
5	1.00 ±0.02	1.0	24.2	1.00
6	1.20 ±0.02	1.5	24.7	1.20
7	1.40 ±0.02	1.5	24.7	1.40
8	1.65 ±0.02	2.0	25.2	1.65
9	1.90 ±0.03	2.0	25.2	1.90
10	2.40 ±0.03	2.5	25.7	2.40
11	3.00 ±0.03	3.0	26.2	3.00

Unless otherwise specified
DIMENSIONS ARE IN MILIMETERS
TOLERANCES:
ANGULAR: ± 1 °
One PLACE DECIMAL: ± 0.1
Two PLACE DECIMAL: ± 0.05
Surface Finish: 0.4 or better

TITLE: Modified ACI Middle Stages

	Name	Date
Drawn	H.Wang	5/23/2014
Checked	J.Ivey	5/27/2014

MATERIAL: 316 Stainless Steel

UNIVERSITY OF ALBERTA
EDMONTON·ALBERTA·CANADA

DWG NO. HW - 004

SIZE A3

WEIGHT: SCALE:2:1 SHEET 1 OF 1

NOTES: (UNLESS OTHERWISE SPEDIFIED)

1. PART TO BE CLEAN AND BURR FREE
2. ALL NOMINAL RIGHT ANGLE EDGES CAN HAVE R0.1 MAX FILLET
3. ISO TOLERANCE SYSTEMS (ISO286/ANSI B4.2-1978)ARE USED FOR LIMITS AND FITS

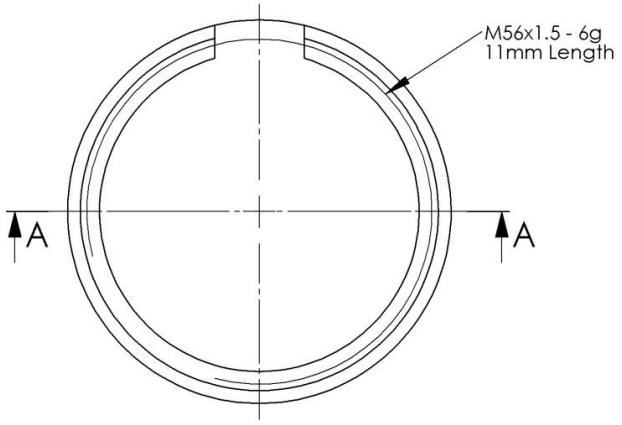

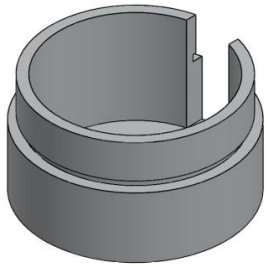

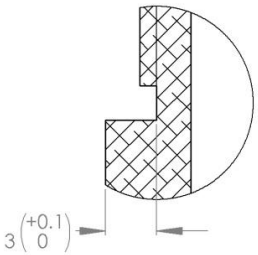

DETAIL B
SCALE 4 : 1

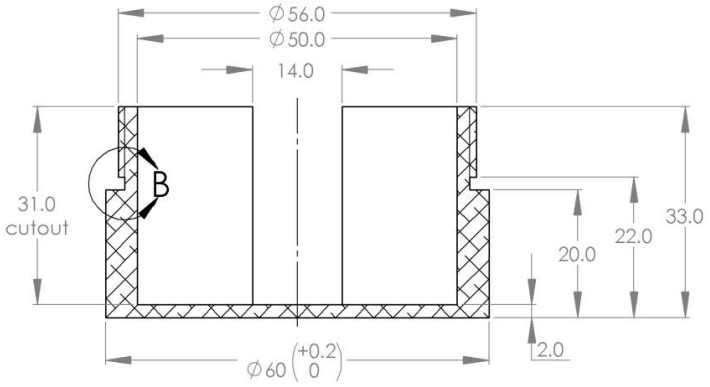

SECTION A-A
SCALE 3 : 2

Unless otherwise specified	TITLE: Sleeve Clamping Bottom Piece			UNIVERSITY OF ALBERTA EDMONTON·ALBERTA·CANADA		
DIMENSIONS ARE IN MILIMETERS TOLERANCES: ANGULAR: ± 1° One PLACE DECIMAL: ± 0.1 Two PLACE DECIMAL: ± 0.05		Name	Date	MATERIAL:	DWG NO.	SIZE
Surface Finish: 0.8 or better	Drawn	H.Wang	5/26/2014	6061 Alloy	HW 101	A3
Revision	Checked	J.Ivey	5/27/2014			
	Approved			WEIGHT:	SCALE:1:1	SHEET 1 OF 1

NOTES: (UNLESS OTHERWISE SPEDIFIED)

1. PART TO BE CLEAN AND BURR FREE
2. ALL NOMINAL RIGHT ANGLE EDGES CAN HAVE R0.1 MAX FILLET
3. ISO TOLERANCE SYSTEMS (ISO286/ANSI B4.2-1978)ARE USED FOR LIMITS AND FITS

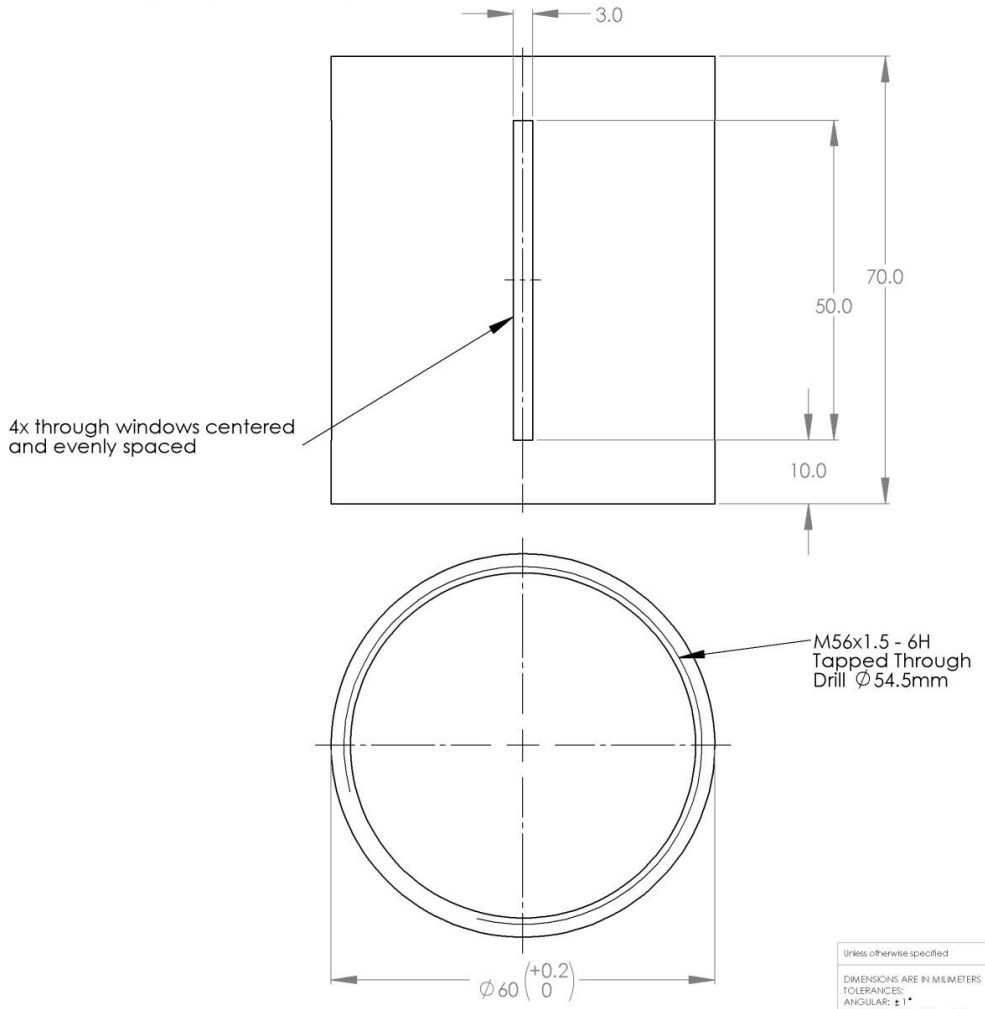

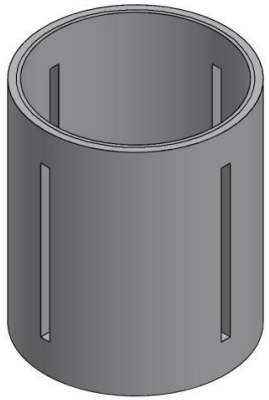

Unless otherwise specified	TITLE: Modified ACI Sleeve Clamping-Short Sleeve			UNIVERSITY OF ALBERTA EDMONTON·ALBERTA·CANADA	
DIMENSIONS ARE IN MILIMETERS TOLERANCES: ANGULAR: ± 1° One PLACE DECIMAL: ± 0.1 Two PLACE DECIMAL: ±0.05		Name	Date	MATERIAL: 6061 Alloy	DWG NO. HW 102-01
Surface Finish: 0.8 or better	Drawn	H.Wang	5/26/2014		SIZE A3
Revision	Checked	J.Ivey	5/27/2014		
	Approved			WEIGHT:	SCALE:1:1 SHEET 1 OF 1

NOTES: (UNLESS OTHERWISE SPEDIFIED)

1. PART TO BE CLEAN AND BURR FREE
2. ALL NOMINAL RIGHT ANGLE EDGES CAN HAVE R0.1 MAX FILLET
3. ISO TOLERANCE SYSTEMS (ISO286/ANSI B4.2-1978)ARE USED FOR LIMITS AND FITS

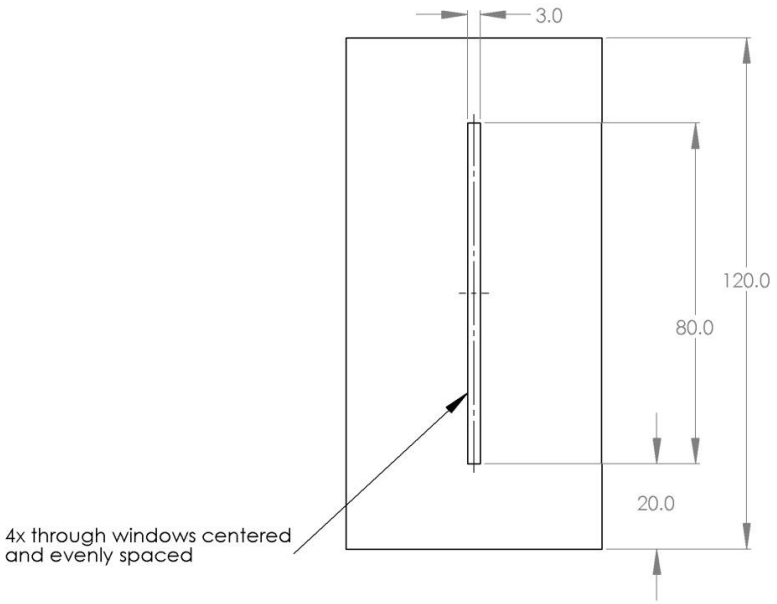

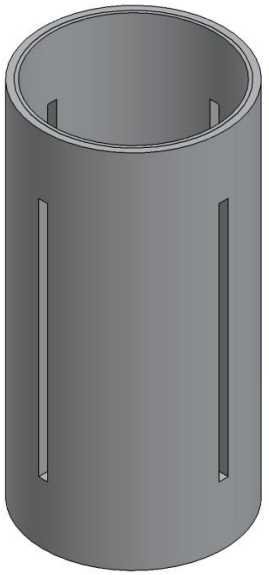

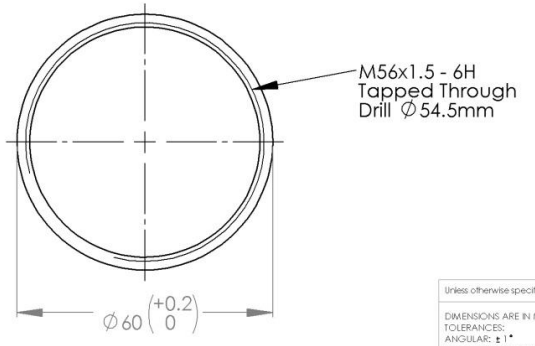

Unless otherwise specified	TITLE: Modified ACI Sleeve Clamping-Long Sleeve			UNIVERSITY OF ALBERTA EDMONTON·ALBERTA·CANADA	
DIMENSIONS ARE IN MILIMETERS TOLERANCES: ANGULAR: ± 1° One PLACE DECIMAL: ± 0.1 Two PLACE DECIMAL: ±0.05		Name	Date	MATERIAL:	DWG NO. HW 102-02	SIZE A3
Surface Finish 0.8 or better	Drawn	H.Wang	5/26/2014	6061 Alloy		
Revision	Checked	J.Jvey	5/27/2014			
	Approved			WEIGHT:	SCALE:1:1	SHEET 1 OF 1

NOTES: (UNLESS OTHERWISE SPEDIFIED)

1. PART TO BE CLEAN AND BURR FREE
2. ALL NOMINAL RIGHT ANGLE EDGES CAN HAVE R0.1 MAX FILLET
3. ISO TOLERANCE SYSTEMS (ISO286/ANSI B4.2-1978)ARE USED FOR LIMITS AND FITS

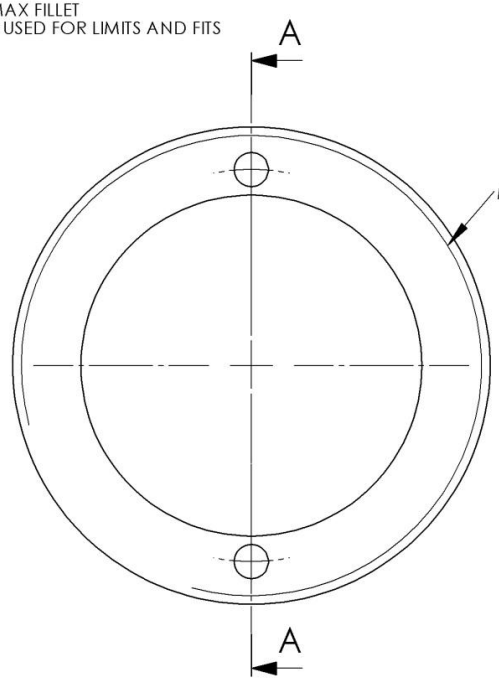

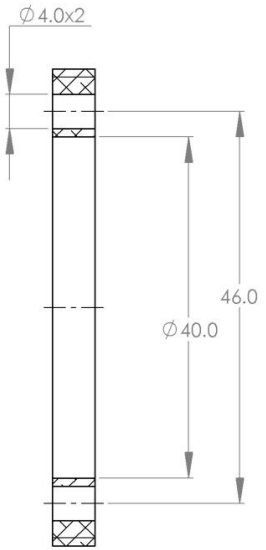

SECTION A-A

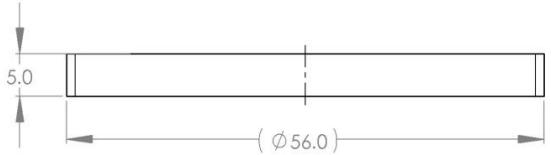

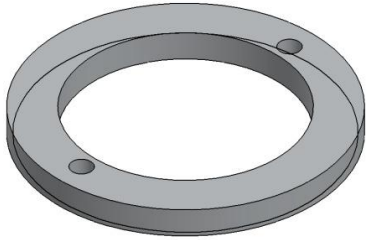

Unless otherwise specified DIMENSIONS ARE IN MILIMETERS TOLERANCES: ANGULAR: ± 1° One PLACE DECIMAL: ± 0.1 Two PLACE DECIMAL: ±0.05	TITLE: Sleeve Clamping Inner Piece			UNIVERSITY OF ALBERTA EDMONTON·ALBERTA·CANADA	
		Name	Date	MATERIAL:	DWG NO.
Surface Finish: 0.8 or better	Drawn	H.Wang	5/26/2014	6061 Alloy	HW 103
Revision	Checked	J.Jvey	5/27/2014		SIZE: A3
	Approved			WEIGHT:	SCALE:2:1 SHEET 1 OF 1